# EXTENDING THE BATTERY-POWERED OPERATING TIME OF A WIRELESS ENVIRONMENTAL MONITORING SYSTEM

by

Ross Matthew Butler

A thesis

submitted in partial fulfillment

of the requirements for the degree of

Master of Science in Computer Engineering

Boise State University

December 2012

BOISE STATE UNIVERSITY GRADUATE COLLEGE

# DEFENSE COMMITTEE AND FINAL READING APPROVALS

of the thesis submitted by

Ross Matthew Butler

Thesis Title: Extending the Battery-Powered Operating Time of a Wireless Environmental Monitoring System

Date of Final Oral Examination: 19 October 2012

The following individuals read and discussed the thesis submitted by student Ross Matthew Butler, and they evaluated his presentation and response to questions during the final oral examination. They found that the student passed the final oral examination.

| | |
|---|---|
| Sin Ming Loo, Ph.D. | Chair, Supervisory Committee |
| Jennifer A. Smith, Ph.D. | Member, Supervisory Committee |
| Vishal Saxena, Ph.D. | Member, Supervisory Committee |

The final reading approval of the thesis was granted by Sin Ming Loo, Ph.D., Chair of the Supervisory Committee. The thesis was approved for the Graduate College by John R. Pelton, Ph.D., Dean of the Graduate College.

# DEDICATION

To my wife, Gay Lynn Anderson, who held up the sky every time it started to fall.

Her belief in me kept me going more times than she'll ever know.

To my grandfather, C. I. Brown, who, when I was a little boy, would always remark after introducing me to someone, "He's going to be an electrical engineer."

# ACKNOWLEDGEMENTS

I would like to thank my thesis advisor, Dr. Sin Ming Loo, for the opportunity to realize my dream of fusing my electrical engineering education with my software development experience. His guidance and mentoring along with the embedded systems experience I gained in his laboratory are invaluable assets as I embark on a new career.

I would also like to thank my committee members, Dr. Jennifer Smith and Dr. Vishal Saxena, for providing their time to facilitate bringing my thesis to completion.

I would like to express gratitude to my lab cohorts for a stimulating and enjoyable working and learning environment. I would especially like to thank Jim Hall for sharing his broad hardware and firmware insight, Vikram Patel for the conversations that inspired new ideas and approaches, Michael Pook for assisting with circuit board layouts and constructively questioning my ideas and methods, Josh Kiepert for sharing his impressive technical knowledge, Brendan Healy for the very cool battery enclosure design, Ali Ibrahim for performing the circuit modifications, and Nick Terrell for his circuit board production assistance and the off-topic conversations that helped keep me sane.

Finally, I would like to thank my family for their support and encouragement as well as their patience all those times I neglected them while doing the school thing. I do not know how to sufficiently express my deepest appreciation and gratitude to my wife, Gay Lynn, for her encouragement, support, and making my academic work possible.

# ABSTRACT

Advances in low-power microelectronics and sensor technologies have enabled the creation of sophisticated environmental monitoring systems capable of operating on battery power. Independence from a power outlet connection opens up many new potential applications, but limited battery life still imposes significant restrictions on a monitoring system's capabilities and the number of systems that can be economically deployed and maintained. These restrictions have motivated much research into reducing monitoring system energy usage, increasing battery capacity, and harnessing alternative energy sources. While most of the research focuses on new system design, there is a need for techniques to extend the battery-powered operating time of existing environmental monitoring systems without compromising their sensor data quality. This thesis explores and develops methods for extending the operating time of an existing air-quality monitoring system. The system contains seven environmental sensors that create a substantial energy demand and make long-term battery operation challenging. The resulting hardware and firmware modifications doubled the system's battery-powered operating time without significantly reducing its environmental measurement data quality. The addition of an external battery sized to match the system's form factor increased operating time well past the goal for the intended application. Although the modifications and results presented in this thesis are specific to one environmental monitoring system, the same techniques could be applied to other monitoring systems and to embedded systems in general.

TABLE OF CONTENTS

LIST OF TABLES

LIST OF FIGURES

# LIST OF ABBREVIATIONS

| | |
|---|---|
| A | Ampere |
| ABC | Automatic Background Calibration |
| AC | Alternating Current |
| ADC | Analog to Digital Converter |
| Ah | Ampere-hour |
| BSU | Boise State University |
| CMOS | Complementary Metal-Oxide Semiconductor |
| DMM | Digital Multi-Meter |
| DSO | Digital Storage Oscilloscope |
| FAA | Federal Aviation Administration |
| GPIO | General-Purpose Input-Output |
| HSIL | Hartman System Integration Laboratory |
| $I^2C$ | Inter-Integrated Circuit |
| IHAQ | In-Home Air Quality |
| Li-ion | Lithium ion |
| LCD | Liquid Crystal Display |
| LED | Light Emitting Diode |
| mA | milliampere |
| µF | microfarad |
| MOSFET | Metal Oxide Semiconductor Field Effect Transistor |
| NCS | National Children's Study |
| NIH | National Institutes of Health |
| NRMSE | Normalized Root Mean Square Error |
| op-amp | operational amplifier |
| PCBC | Primary-Cell Battery Controller |
| PSD | Power Spectral Density |
| SPI | Serial Peripheral Interface |
| SUT | System Under Test |
| UART | Universal Asynchronous Receiver-Transmitter |
| USB | Universal Serial Bus |
| UVLO | Under-Voltage Lock Out |
| V | Volt |
| W | Watt |
| Wh | Watt-hour |

# CHAPTER ONE: INTRODUCTION

## 1.1 Evolution of Battery-Powered Environmental Monitoring Systems

The desire to understand our environment and its effects on us has been manifested throughout history. From early, crude thermoscopes [1] to modern, sophisticated electrochemical sensors, humans have developed tools for measuring environmental factors ranging from temperature to the concentration of specific substances. Our ability to understand our environment and its effects on us is limited by the quality and quantity of data that we can collect, hence the perpetual efforts to increase the accuracy, scope, and availability of environmental measurements.

The development of small, portable, computerized environmental sensor systems has enabled environmental monitoring to an extent hardly imaginable even fifty years ago. Rather than depending on large, expensive sensing devices and manually maintained data logs or cumbersome chart recorders, multiple environmental factors can now be measured and automatically recorded by small, battery-operated sensor systems that operate for long periods of time without attention. Microcontrollers and miniaturized, real-time sensors make possible the design and construction of reliable, relatively inexpensive systems that can measure multiple environmental factors and record the time-series data in a form ready for analysis.

As the size and cost of environmental monitors[1] have decreased and their capabilities have increased, many new applications for the monitors have become feasible. Some of those applications require the deployment of a large number of monitors, placement of monitors in locations that are difficult to access, or unattended operation of monitors for long periods of time. For example, structural health monitoring systems can use sensors embedded throughout a structure to monitor stress, vibration, and other factors [2], [3]. Seismic monitoring in a geologically active region, such as near an active volcano [4] or on a landslide-prone hillside [5], might require the placement of monitors over a large area and in difficult terrain. Monitoring the microclimate conditions experienced by individual organisms over a large habitat area would require the dense deployment of tens to thousands of individual environmental sensors, and the sensors would be expected to be robust, maintenance-free, and able to operate for years [6]. In all these cases, power outlets are likely unavailable, and frequent—if any—battery replacement would not be feasible.

### 1.2 Extending the Operating Time of Environmental Monitors

When placed in a remote or difficult to access location, an environmental monitor may be required to operate on battery power for weeks, months, or possibly years. Even deployments in industrial settings can require the placement of monitors where power or communication wiring cannot be installed economically, and frequent battery replacement, especially with large deployments, would be cost prohibitive. The need for operating environmental monitors for long periods of time independently of a power

[1] Throughout this thesis, an environmental monitoring system may also be referred to as a monitoring system, environmental monitor, or monitor.

outlet connection has led to much research into reducing the energy requirements of processors, sensors, wireless communication modules, and related electronics. The research is often focused on approaches that must be taken from the inception of system or even component design, or that require significant modification to an existing system. Research into methods specifically applicable to existing systems does not seem as prevalent.

Methods for reducing energy usage in environmental monitors can be classified in two broad categories: those that are applied from the beginning of a system design and those that can feasibly be applied to existing designs. The methods that are applied from design inception tend to produce the best results because the designers can select the most effective energy reduction methods for each part of the system and for the system as a whole [7]. Modifying an existing system to reduce energy usage will likely be less effective than a ground-up redesign because of the need to retain system architecture and key system components that are potentially less energy efficient than what would be used in a new design. However, the modifications may achieve significant energy savings quickly and for relatively low cost. In some cases, modifying an existing system can be a more practical approach, especially with modular, flexible systems that facilitate modification at a system and component level and have already been tested and accepted for a particular application.

Often, the goal of reducing energy consumption in an environmental monitor is to extend the operating time of the monitor or to facilitate additional functionality [8]. While reducing energy consumption is the preferred approach for a variety of reasons, it may be possible to meet the goal by increasing the energy available to the monitor.

Energy harvesting, where light, vibration, or heat that are present in the monitor's surroundings are converted to energy, is a promising avenue for powering a monitor for a very long period of time, perhaps indefinitely [9], [10]. However, the amount of energy available through harvesting is usually very small, making energy harvesting feasible only for monitors having very low energy requirements in the first place. Using a higher capacity battery can extend operating time, but size and cost constraints impose limits on the amount of additional energy that can be provided. The most successful approach will combine reducing energy usage with increasing the available energy supply.

### 1.3 Case Study Overview

In 2000, the US Congress authorized the National Institute of Child Health and Human Development "to conduct a national longitudinal study of environmental influences (including physical, chemical, biological and psychosocial) on children's health and development" [11], [12]. Now under the direction of the National Institutes of Health (NIH), the National Children's Study (NCS) is "the largest research study of genetic and environmental influences on children's health ever conducted in the United States" [13]. To support the environmental influences facet of the NCS, the NIH is seeking a compact, low-cost environmental monitoring system that can be placed in a child's home. The system would be required to measure and record environmental factors including airborne particle concentration (PM2.5 and PM10), temperature, humidity, and atmospheric carbon dioxide and carbon monoxide.

In an effort to meet the needs of the NCS, researchers at the Hartman System Integration Laboratory (HSIL) of Boise State University have adapted their airline cabin air quality monitoring system for in-home use. The airline cabin monitor is a portable,

battery-operated system that provides most of the air quality monitoring capability required for the NCS [14]. With the addition of a custom airborne particulate counter and several usability enhancements, the researchers have created an in-home air quality (IHAQ) monitor that inherits the considerable hardware and software features of the airline cabin monitor [15].

Early prototypes of the IHAQ monitor were designed to operate for eight hours using an internal, rechargeable battery. Although efforts to minimize energy usage were made during the design of the monitor, long-term operation using battery power was not a priority; the HSIL researchers assumed that a power outlet would be available because the monitors would be deployed in homes. Hence, very-low-power design techniques were not applied. However, it later became apparent that connecting a monitor to a power outlet in a home is not feasible, and the NCS would require much longer, continuous, unattended environmental monitoring than could be achieved with the monitor's internal battery.

Discussions with collaborators associated with the NIH revealed that the primary in-home monitoring periods would be overnight and weeklong. For an overnight monitoring session, the IHAQ monitor would be required to operate continuously for up to twenty-four hours. A nominally weeklong session would require continuous operation for up to eight days. In both scenarios, the monitor must be capable of operating for the required period of time using only battery power. To minimize intrusions into the home, replacing the battery during the monitoring period is not desirable. It became apparent that the IHAQ monitor's battery-powered operating time would have to be greatly increased in order to meet the requirements of the NCS.

## 1.4 Thesis Objective

The objective of this thesis is to explore practical approaches and methods for extending the battery-powered operating time of an existing environmental monitoring system. The exploration is realized through efforts to extend the operating time of the IHAQ monitor to meet the requirements of the NCS. The operating time goal for the IHAQ monitor is twofold: For ease of deployment and reduced operating cost when single-day environmental monitoring is desired, the monitor should be able to operate for twenty-four hours using only its internal, rechargeable battery. For weeklong monitoring where the monitor is placed in the home, for example, on a Monday and retrieved the following Monday, the monitor should be able to operate for eight days using an optional external battery. The battery must be safe, reliable, and physically consistent with the small, non-intrusive design of the IHAQ monitor.

To meet the operating time goals, energy usage within the IHAQ monitor was measured and analyzed, and modifications to the monitor's hardware and firmware were made to substantially reduce its energy consumption. The modifications were constrained to minor hardware changes that could be made to an existing IHAQ monitor prototype and firmware changes that maintain compatibility with other monitors sharing the same firmware framework. Additionally, the modifications could not be allowed to cause significant degradation in measurement data quality.

Meeting the weeklong operating time goal required the development of an external battery that is compatible with the IHAQ monitor's voltage and current requirements, internal battery, and battery charging circuit. The type, size, and number of cells needed for weeklong operation were determined using estimates and measurements

of the monitor's energy usage and cell capacity information found in manufacturer data sheets. A controller module, referred to elsewhere this thesis as the "primary-cell battery controller" (PCBC), was constructed to prevent the internal battery from being charged by the external battery and to ensure proper monitor shutdown behavior when the external battery reaches the end of its service life.

Numerous tests were performed to evaluate the effectiveness of the energy usage reduction modifications and to measure the operating time provided by the internal and external batteries. Sensor measurement data from modified and unmodified monitors were compared to determine the effects, if any, of the modifications on measurement data quality. Where effects were noted, additional tests and analyses were performed to understand the tradeoffs between energy usage reduction and data quality.

### 1.5 Thesis Outline

Chapter Two describes methods for measuring the energy usage of an environmental monitoring system. Chapter Three presents energy usage reduction techniques and explains their applicability to the IHAQ monitor. Chapter Four discusses battery selection, with focus on an external battery for the IHAQ monitor. Estimates of the monitor's energy usage followed by descriptions of the modifications to extend its operating time are presented in Chapter Five. Chapter Six gives a detailed description of the purpose, design, and energy usage analysis of the PCBC. Chapter Seven describes the operating time tests that were performed on the IHAQ monitor and presents the results. The effects of the modifications on data quality are also discussed. Finally, Chapter Eight briefly summarizes the results and suggests future work that could further extend the monitor's operating time.

# CHAPTER TWO: ENERGY USAGE MEASUREMENT METHODS

There are many methods of estimating the energy usage of an environmental monitoring system. Some methods concentrate on analyzing a system's circuits and components while others utilize simulations of a system's operation. However, actually measuring the energy usage of an environmental monitoring system can provide a more accurate assessment of the system's overall energy usage and allow a better understanding of its energy usage patterns. As with estimation methods, there are many different ways of measuring energy usage. Some are better suited for making very detailed measurements, such as the energy usage associated with specific microprocessor instructions, while others provide a broader view, such as the average power consumption over a long period of time.

In this chapter, four energy usage measurement methods are presented. Each method is described at a high level, and its key advantages and disadvantages are mentioned. For the three methods that were utilized to perform measurements for this work, a brief explanation is given of how the method was applied.

## 2.1 Multimeters

Perhaps the most straightforward method of measuring the input power to an environmental monitoring system is to simultaneously measure the input voltage and current then multiply the measurements together to calculate power [16]. A simple implementation of such a measuring system consists of two digital multimeters (DMMs):

one connected across the power input to the system under test (SUT) to measure voltage, and the other connected in series with the SUT's power input to measure current.

Because the power demand of an environmental monitoring system may not be constant due to the different activities performed by the system and the intermittent operation of its sensors, the system's input current is likely time varying. The input voltage can also be time varying if the power source is a battery or resistance is present in series with the system's power input circuit. For accurate power calculations, it becomes necessary to synchronize the voltage and current measurements so they are taken simultaneously. Synchronization can be accomplished by using DMMs that can record a measurement in response to a triggering pulse. Connecting both DMMs to a common trigger source allows simultaneous measurement of voltage and current, facilitating an accurate calculation of power.

A data acquisition system capable of measuring energy usage over a long period of time can be assembled using DMMs with a measurement data output feature. A variable-frequency triggering source can be used to control the measurement (sampling) rate. Such a system, shown in Figure 1, was used for the operating time tests and some of the energy usage characterization tests performed on the IHAQ monitor.

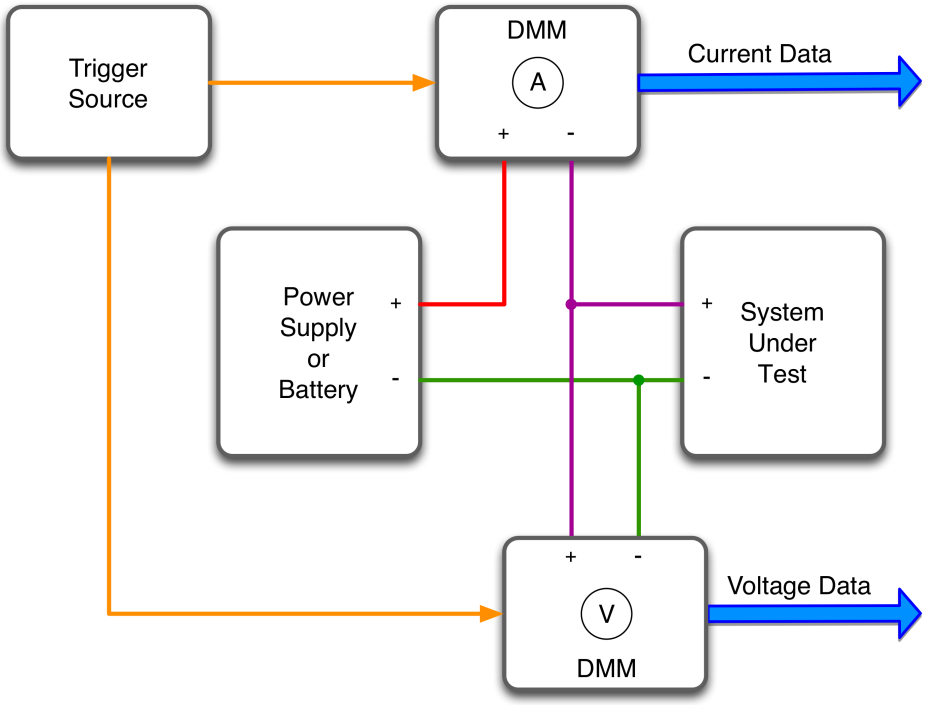


**Figure 1 DMM-Based Measurement Apparatus**

There are two significant concerns that arise when using DMMs to measure the SUT input voltage and current: dynamic range and sampling rate. Dynamic range, which is the ratio between the largest and smallest values being measured, is a concern because the input current to an environmental monitoring system when it is active can be several orders of magnitude higher than the current during a low-power standby mode of operation [17], [18]. This huge difference can easily cause the use of a single DMM measurement range setting to produce inaccurate results—the setting is either too high to accurately measure the low-power mode current or too low to accommodate measuring the active-mode current without overflow. Sampling rate is also a concern because the maximum triggering rate of a DMM can be insufficient to accurately capture the

waveforms resulting from a pulse-type varying load created by the digital circuitry in an environmental monitor [18], [19].

Both concerns were addressed with regard to using a triggered-DMM apparatus to measure IHAQ monitor input power. A single DMM range can accurately measure the monitor's input current because the IHAQ monitor does not have a low-power standby mode, and the ratio of maximum to minimum input current during normal operation is less than an order of magnitude. While monitor's input current has large spikes caused by the $CO_2$ sensor and ripple caused by the particle counter fan, the bypass capacitances present at many points in the IHAQ monitor's circuitry along with the monitor's voltage regulators appear to provide low-pass filtering that suppresses most of the frequency components above the measurement apparatus's Nyquist frequency (20 Hz in most cases). This is similar to the situation described in [17].

Of note is an interesting dynamic range solution provided by the Prospector system presented in [17]. In that measurement system, the DMM is controlled by a computer workstation and triggered by the SUT at predetermined points during specific activities. The computer configures the DMM range setting and acquires measurement data from the DMM. It also coordinates when the triggering signal is enabled via an interface between the computer and the SUT. By telling the SUT the activity for which it should enable the triggering signals, the control program can acquire input current measurements for an activity at different DMM range settings, effectively increasing the dynamic range of the measurement system.

## 2.2 Oscilloscope

A dual-channel digital storage oscilloscope (DSO) can record simultaneous voltage and current measurements at rates up to several gigasamples per second, overcoming the frequency response limitation of a DMM-based measurement system. Because of its fast sampling rate and inherent triggering capability, a DSO is especially effective for measurement of short-term transients and one period of a repeated pattern (e.g., periodic wake from sleep). If the DSO has sufficient memory, it can be used as a data collection device for longer measurements.

To measure current, a DSO differential input can be connected across a resistor that is in series with the SUT's power input [20]. A current-sense amplifier can be used to provide additional gain for measuring small currents, but care must be taken to ensure that the frequency response of the amplifier is sufficiently high. A simplified example of such an apparatus is shown in Figure 2. Alternatively, a clamp-on current probe can be used. A clamp-on probe measures current flowing through a wire by sensing the magnetic field that emanates from the wire, with the strength of the magnetic field being proportional to the current flow. As with a current-sense amplifier, the frequency response of the probe must be considered.

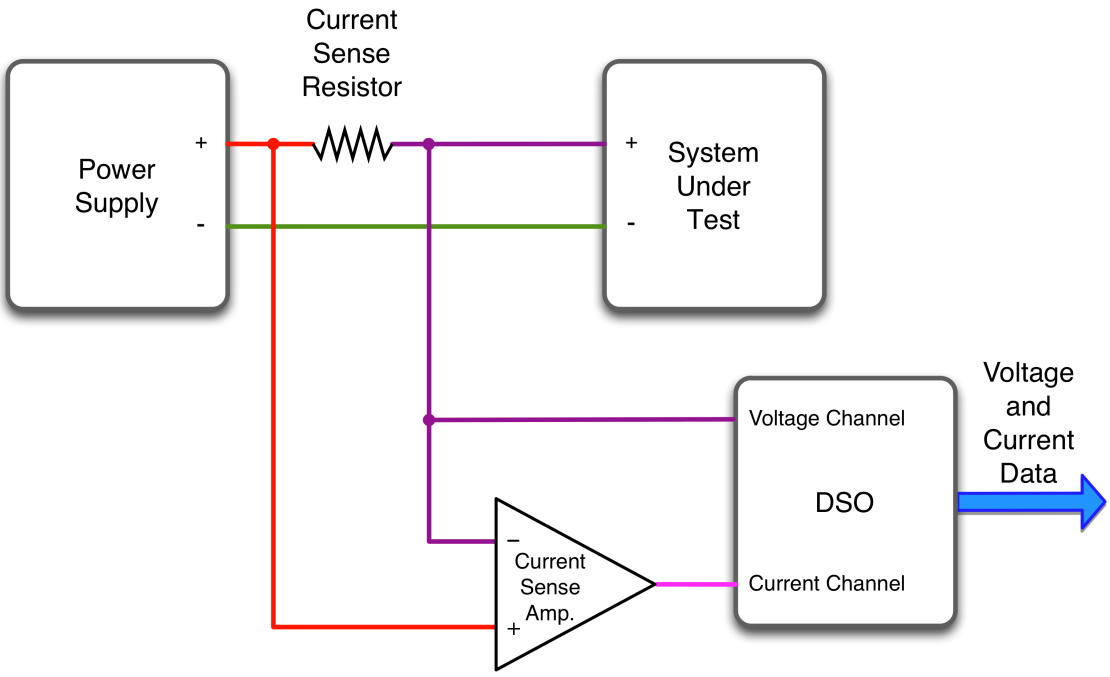


**Figure 2 DSO-Based Measurement Apparatus**

An advantage of a clamp-on current probe is that a series resistance and its associated voltage drop are not introduced into the circuit. However, when measuring small currents, the signal from the probe can have significantly more noise. Figure 3(a) shows a comparison between the zero-current signal output from a clamp-on probe and a current-sense amplifier connected to a series resistor in the same circuit. The large amount of noise from the probe is likely caused by stray magnetic fields near the probe. Also, the probe must be calibrated before each measurement. Strong magnetic fields, such as one caused by high inrush current when a SUT is first turned on, can disturb the calibration. Figure 3(b) shows offset and gain differences between a shunt-based current sensor and a clamp-on current probe.

To avoid the problems associated with a current probe or placing a series resistance in the SUT power supply circuit, [21] proposes using an analog current mirror to supply current to the current-sensing resistor. The advantage of this approach is that resistance is not added in series with the SUT, thus avoiding load-dependent fluctuations of SUT input voltage that would otherwise occur. Discrete bipolar junction transistors are used in order to obtain better high-frequency response than could be obtained with operation amplifiers. Assuming that the power supply is well regulated, the current mirror obviates the need to measure input voltage; a constant voltage value can be used when calculating power.

For IHAQ monitor energy usage analyses, a DSO having both high sampling rate and large data storage capabilities was employed. Its high sampling rate—up to four gigasamples per second—facilitated spectral analysis of the input current and detailed examination of input current spikes. The data storage capabilities allowed moderate-resolution input power measurements lasting over eight minutes, albeit at a relatively low sampling rate.

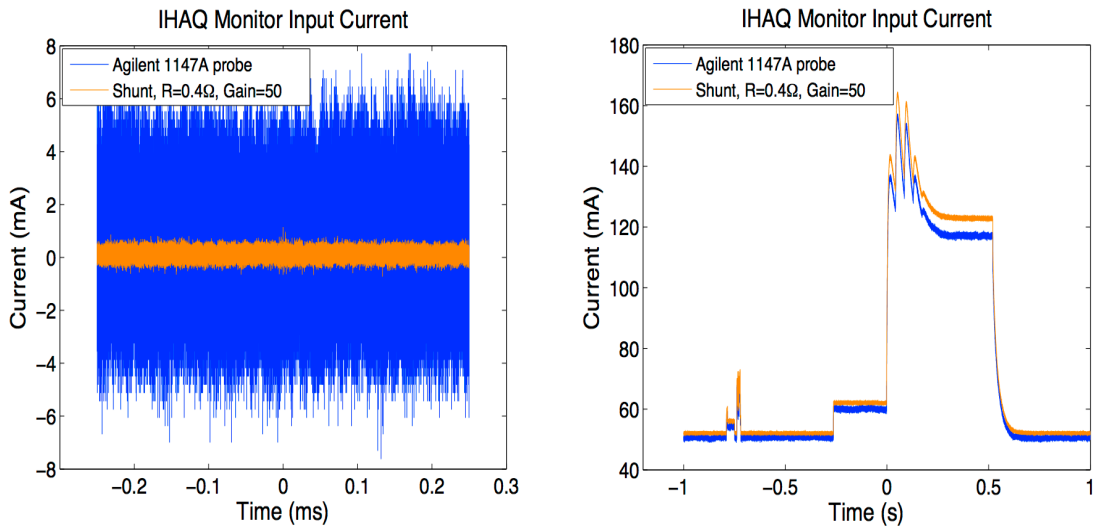


(a) (b)

**Figure 3 Current Probe and Series-Shunt Current Sensor Comparison**

The oscilloscope traces in (a) show the measurement noise when current is not flowing in the circuit. The large current flow increase in (b) is a current spike caused by the $CO_2$ sensor.

### 2.3 Switched Capacitor

An alternative to directly measuring voltage and current to determine power is to measure the voltage change across a capacitor as the capacitor is charged or discharged. In [22], the voltage drop across a resistor in series with the SUT's power input drives a current-sense amplifier. The amplifier's output charges a capacitor of known value. When the voltage across the capacitor reaches a predetermined value, the capacitor is quickly discharged to a lower, predetermined voltage and a counter is incremented. The time-varying voltage across the capacitor appears as a ramp signal, with the amplitude set by the predetermined upper and lower voltage levels. Each charge-discharge cycle then represents a fixed amount of charge supplied to the SUT, which is proportional to the

amount of energy consumed by the SUT. The period of each ramp is inversely proportional to the rate at which the energy is delivered. The counter, which records the number of ramp peaks, can be read to determine the amount of energy used over a period of time.

The measurement system described in [22] still imposes a resistance in series with the SUT to supply the input voltage to the current-sense amplifier, and the system's frequency response is limited by the frequency response of the amplifier. The system described in [23] eliminates the series resistance and the current-sense amplifier by switching between two capacitors that alternately power the SUT. While one capacitor is discharging and supplying current to the SUT, the other is being charged by a power supply. Unfortunately, the voltage supplied to the SUT is not constant, which could alter the SUT's energy usage and thereby distort the measurements. To resolve this problem, [24] combines both approaches and adds a current mirror to isolate the SUT from the capacitors. The current mirror charges one of the capacitors with a current equal to that being supplied to the SUT (similar to [22]) while the other capacitor is discharged. Energy usage can then be determined by counting the charge-discharge cycles.

A switched-capacitor measurement system can provide accurate energy usage measurements even when the input current to the SUT has significant high-frequency components or a large dynamic range. However, a good system, especially one like those described in [24], is much more complex than the DMM or DSO-based systems. Since the IHAQ monitor's input current has a relatively small dynamic range and does not contain significant high-frequency components, the additional complexity of a switched-capacitor system was unwarranted. However, the system may be needed for future work

if the monitor's input current dynamic range is expanded by the implementation of a low-power "sleep" mode of operation to reduce energy consumption.

### 2.4 Capacitor Discharge

The capacitor-discharge method is much simpler than the switched-capacitor method but provides similar high frequency and dynamic range performance. However, it is practical for measuring only very small power consumption, such as that of a system in which the processor spends most of its time in sleep mode [25]. To measure SUT energy usage with this method, a large capacitor of known value is connected to the SUT's power input. A power supply is connected to the capacitor, and capacitor is charged until the voltage across its terminals reaches the upper limit of the SUT's input voltage range. The power supply is then disconnected, and the capacitor is allowed to discharge through the SUT as it supplies the current for SUT operation. Time and voltage are measured until the voltage reaches the lower limit of the SUT's input voltage range. Average current flow and total energy consumed by the SUT can then be calculated using the measurements and the known capacitance value. Figure 4 shows a diagram of the apparatus.

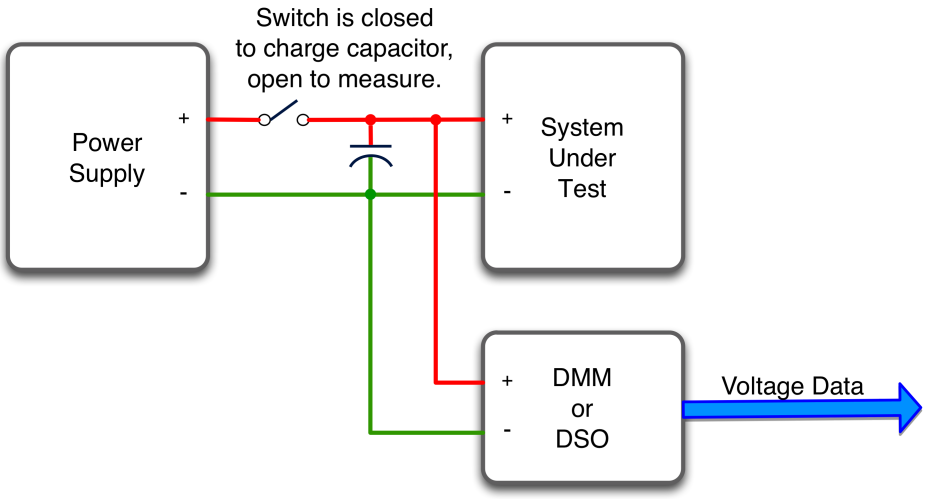


**Figure 4 Capacitor-Discharge Energy Usage Measurement Apparatus**

The capacitor discharge method alleviates the dynamic range and frequency response concerns because the voltage measurements only need to capture the instantaneous voltage across the capacitor. Also, the method can simulate the range of voltages encountered during battery operation but over a much shorter period of time. However, a large capacitor—probably an electrolytic type—is required in order to power the SUT for a reasonable length of time. Electrolytic capacitors are notorious for high internal leakage current [26], and leakage current can make the SUT's energy usage appear greater than it actually is. Also, the actual capacitance of a large electrolytic capacitor can differ greatly from the value marked on the capacitor and can change with temperature [27], so it is necessary to measure the capacitance before each testing session to ensure accuracy of the calculated average current and energy usage.

Because of the IHAQ monitor's relatively large power requirement and the adequacy of the DMM method for determining the monitor's energy usage, the capacitor-

discharge method was not used with the IHAQ monitor. However, the PCBC uses very little energy; its estimated average operating current is only 51 μA. It has a very low full-current duty cycle, so the peak current demands are very brief, and its estimated low-power sleep mode current is over two orders of magnitudes less than the estimated peak current. The capacitor-discharge method, which is well suited for measuring average current and energy usage under these conditions, was used for measuring the PCBC's energy usage.

# CHAPTER THREE: ENERGY USAGE REDUCTION TECHNIQUES

There are myriad ways to reduce energy usage in an environmental monitoring system. Energy reduction can be achieved at the hardware level, the firmware level, or at an overall system design level that encompasses individual monitors as well as data communication and processing. Some approaches to reducing energy usage must be taken during initial system specification and design while others can be applied to existing monitor hardware and firmware. This chapter presents energy reduction methods and techniques that can be used in both circumstances. Although they do not comprise a comprehensive set, they represent what is colloquially deemed "low hanging fruit" due to their relative ease of implementation and high degree of effectiveness. The chapter concludes with a section that addresses how to select the appropriate methods to use.

## 3.1 Processor Voltage and Clock Frequency Scaling

The power dissipated (consumed) by the microprocessor in an environmental monitor has two components: static and dynamic. Static power dissipation is due to leakage currents through the gate dielectric and reverse-biased regions of the processor's metal oxide semiconductor field effect transistors (MOSFETs). It is a function of the physical properties of the MOSFETs and the voltage applied to them. Dynamic power dissipation results from switching the processor's complementary metal oxide semiconductor (CMOS) logic gates between states. Dynamic power is a function of

MOSFET gate capacitance, the square of the voltage applied to the gate, and the switching frequency. A microprocessor's energy consumption is therefore dependent on both the voltage and the clock frequency at which the microprocessor is operated.

The experimental results reported in [28] indicate that leakage current has a larger impact on power consumption, at least in the Texas Instruments OMAP3530 processor used in the experiments. However, this should not be interpreted to mean that clock frequency does not have a large effect also. Figure 5 is a graph of the typical supply currents listed in the data sheet for the Microchip PIC16F506 microcontroller used in the PCBC. The graph shows that the supply current is much higher at the 5.0 V input voltage, and the current increase associated with higher clock frequency is much more pronounced. This behavior does not contradict the findings in [28], but it does suggest that the dependency of switching power on the square of the voltage causes the combination of increased voltage and clock frequency to have a very large effect on energy usage. In any case, reducing the voltage at which a processor operates can provide greater power savings than reducing clock frequency, in part because reducing the supply voltage does not directly affect the amount of work the processor can do in a fixed period of time. If the processor can be placed in a low-power sleep mode when there is no work to do, using a higher clock frequency can actually save energy because the work can be done in less time, thus allowing the processor to spend more time in the low-power mode.

The constraints placed on the hardware and firmware modifications that would be permitted on the IHAQ monitor precluded the consideration of processor voltage or clock frequency changes. However, the PCBC was designed from the ground up, allowing full

flexibility in the selection of the voltage, clock source, and clock frequency for the PCBC's microcontroller. A description of the relevant analyses and the selections is given in subsections 6.5.2 and 6.5.3.

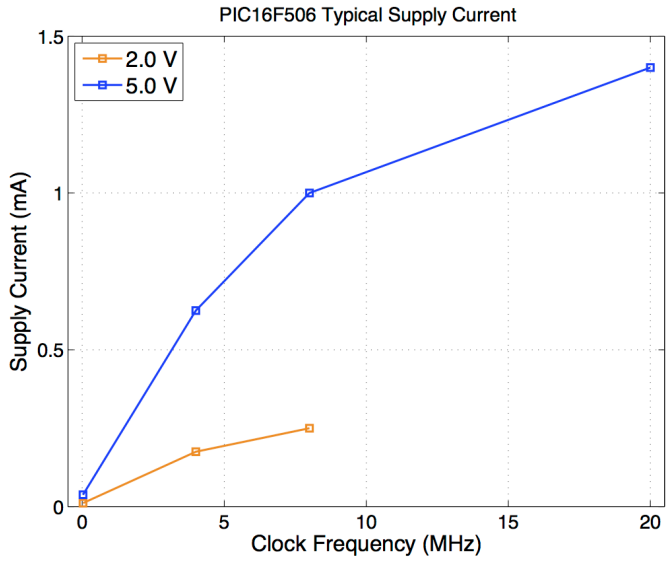


**Figure 5 PIC16F506 Microcontroller Supply Current**

The graph shows the dependency of supply current on voltage and clock frequency. The marked points are the typical values for the industrial version of the device as shown in the manufacturer's data sheet [29]. The frequency of the data points located close to zero on the horizontal axis is 32 kHz. Clock frequencies greater than 8 MHz are not available when operating the device at 2.0 V.

## 3.2 Duty Cycle

Perhaps the most effective way to reduce energy consumption in an environmental monitoring system is to turn on subsystems and components only when they are needed. Reducing the duty cycle (i.e., the on-time to off-time ratio) of a device gives a proportional reduction in the device's energy usage. For example, assume that a sensor uses 10 mW of power while performing measurements but can be turned off

between measurements. Also, assume that the sensor must be turned on for several seconds before taking a measurement in order to stabilize. If only one measurement per minute is made and the sensor is operated for five seconds per measurement, the resulting duty cycle of 5 / 60 = 0.083 reduces the average power to 10 × 0.083 = 0.83 mW—a 91.7% savings. Another good example is found with the light-emitting diodes (LEDs) often used to indicate monitor system status. Continuously illuminating a typical red LED consumes approximately 9 mW. However, if the LED is illuminated for only 25 ms each second, which produces a flash that is easily seen by the human eye, average power consumption is reduced to only 0.225 mW. In other words, the same functionality can be achieved with 97.5% less power.

There are several important considerations with regard to duty cycle. Most importantly, devices that are capable (or at least tolerant) of being cycled on and off must be used. Also important is the wake-up time—the delay between turning a device on or bringing it out of idle mode and when it becomes fully functional. A shorter wake-up time allows a device to remain in the low-power mode longer while still meeting the same operating-time requirement. For example, the MEMSIC MXR2312 thermal accelerometer requires 160 ms to 300 ms for startup while the Analog Devices ADXL212 micro-electro-mechanical system (MEMS) accelerometer requires only 19 ms. This means that the ADXL212 can remain in a low-power state for 141 ms to 281 ms longer each time a measurement is made [30-32]. The extra time spent in a low-power state becomes substantial if several measurements or more are made each second. Finally, the effect of turning a sensor off or putting it in an idle mode may affect the sensor's

precision or accuracy. When determining the duty cycle for a sensor, the effect on its measurement data quality should be evaluated.

## 3.3 Component Selection and Circuit Modifications

When a circuit is initially designed, components that have the needed characteristics, features, and performance are selected. However, continual advancements in active and passive component technologies often make available new components with the same features but superior performance—including reduced energy usage—after the circuit design is complete. In addition, if a circuit was designed without regard for switching it off to conserve energy, integrated circuits that respond to a shutdown signal probably were not used. So, it is not uncommon for later analysis of a circuit to reveal energy savings that can be achieved by updating components and making modifications that facilitate low-power operation. Of course, a new circuit design that emphasizes minimizing energy usage would employ the same ideas from the start.

### 3.3.1 Operational Amplifiers

Operational amplifiers (op-amps) are frequently encountered in the sensor circuits of an environmental monitoring system. Obviously, op-amps designed for low power operation should be selected whenever possible. If a circuit's requirements can be met with a set of op-amps that require only a single supply voltage, the power expense of supplying two voltages (usually positive and negative) can be avoided. When selecting op-amps for a low power design, three additional criteria should also be considered: shutdown capability, high slew rate, and the number of amplifiers in the package [30]. Shutdown capability combined with a high slew rate allows near-zero power

consumption when the amplifier is not needed and quick start-up when it must resume operation. While packages containing multiple amplifiers can simplify circuit layout and reduce part count, the modularity resulting from using a separate package for each system function can facilitate shutting down unneeded circuits without affecting other circuits.

### 3.3.2 Power Switches

Discrete MOSFETs can be used to switch the power to circuits and sensors. MOSFETs having very low on-resistance are preferred as long as they can meet the switching speed requirements. To reduce the number of control signals needed for power switching throughout a system, switching modules that incorporate a serial interface and multiple switches are an attractive solution [30]. For example, the Analog Devices ADG714 and ADG715 feature eight analog switches capable of controlling 30 mA each [33]. The ADG714 has a 3-wire serial interface compatible with the serial peripheral interface bus (SPI), and the ADG715 has a 2-wire serial interface compatible with the inter-integrated circuit bus ($I^2C$). These devices could allow circuit and device-level power switching to be retrofitted into an existing design with relative ease. Regardless of the type of switch used, it should feature fast response and low impedance to minimize the amount of time a switched device or circuit is energized but not ready to perform its function.

### 3.3.3 Voltage References

The need to produce a stable, known reference voltage is frequently encountered in environmental monitoring systems. For example, a comparator that produces a "battery voltage good" signal or an analog-to-digital converter (ADC) connected to a

sensor may require an external reference voltage. Reference voltages can be produced in a variety of ways, including with zener diodes, specialized low-power devices that simulate zener-diode behavior, and resistive voltage dividers. Voltage dividers are also used for level shifting, such as shifting the voltage from a sensor or transducer into the range of an ADC.

Reverse biasing a zener diode is a simple method of producing a stable, known reference voltage. However, to maintain stability, a relatively large current, usually in the milliampere range, must be allowed to flow through the diode. An alternative to a zener diode is a precision shunt regulator, such as the Texas Instruments LMV431 [34]. The LMV431 is available in fixed or adjustable form and requires only 55 μA to achieve voltage regulation, which is two to three orders of magnitude less than the current typically required with a zener diode.

Resistive voltage dividers can be used to provide a reference voltage or to shift a voltage downward to provide compatibility between a voltage source and the input of an ADC. Since the current through (and therefore power dissipated by) a voltage divider is inversely proportional to the divider's total resistance, using higher resistances while maintaining the resistance ratio in the divider will result in reduced energy usage. However, care must be taken to ensure that the Thévenin equivalent resistance of the divider is much less than the input resistance of whatever is connected to the divider's output [27]. Otherwise, the circuit loading imposed on the divider will cause its output voltage to be lower than expected. Similarly, many ADCs require a low impedance input source for proper operation, so it may be necessary to use a buffer amplifier between the voltage divider and the ADC input. The power required by the amplifier should be taken

into consideration when selecting which solution—lower resistances in the divider or higher resistances plus a buffer amplifier—will require the least amount of energy.

### 3.3.4 Diodes

Diodes are often used for reverse-polarity protection, voltage clamping (i.e., preventing the voltage at a particular point in a circuit from exceeding some predetermined value), and analog OR-ing of two or more signals. However, each of these uses has the potential to waste power.

Diodes used for reverse-polarity protection in the power input circuit of an environmental monitor will dissipate power proportional to their forward voltage drop ($V_F$). Using a diode that has the lowest $V_F$ available while still meeting the forward current and reverse breakdown voltage requirements will reduce energy usage. Or, the diode can be replaced by a low-resistance fuse followed by a reverse-biased diode connected across the input to the monitor. Under normal operation, only a very small reverse leakage current ($I_R$) flows through the diode. If the polarity of the power source is reversed, the diode conducts in the forward direction, allowing sufficient current flow to blow the fuse and open the circuit. This approach works well if a diode with low $I_R$ is used and the monitor can tolerate a small, reverse input voltage equal to $V_F$ for the amount of time it takes for the fuse to open.

Because clamping diodes are normally reverse biased, diodes with very low $I_R$ should be used for that purpose. However, low $I_R$ usually comes at the expense of higher $V_F$, so care must be taken to select a diode that will still provide the needed clamping behavior. The same approach should be taken when selecting diodes for OR-ing use, since both $I_R$ and $V_F$ will determine the power loss in that application.

### 3.4 Selecting the Appropriate Methods

When endeavoring to reduce the energy usage of an existing environmental monitoring system, the first step toward determining the appropriate methods to apply is to define the extent of permissible modifications. The answers to the following questions can help focus energy reduction efforts where they are most appropriate for a specific system.

- Can printed circuit board layouts be altered, necessitating the construction of new monitors or the replacement of entire circuit boards in existing monitors? Or, must any hardware modifications be performed on existing circuit boards?
- To what degree can the firmware be modified? Is it feasible to deploy firmware updates on existing monitors?
- Is the monitor run-time configurable, and is it feasible to change and deploy a new configuration to reduce energy usage?

When answering the questions, it is important to keep in mind that all modifications must be thoroughly tested, and the effectiveness of the modifications must be measured and evaluated before performing the modifications on a large number of monitors.

Next, it is essential to perform energy usage measurements in order to understand the energy usage characteristics of the subsystems and components in the monitor and to establish a baseline that can be used to evaluate the effectiveness of the modifications. Absolute accuracy of the estimates is not as important as consistency across the measurements so that the relative contribution of each subsystem or component can be assessed. Where it is not feasible to take measurements, estimates based on component

data sheet information may suffice. In fact, a quick inspection of the supply current values appearing in module and major component data sheets can help focus measurement and estimation efforts.

After the energy usage characteristics of the monitor are understood, the best candidates for reducing energy usage can then be identified. Initial energy usage reduction efforts should target the areas of highest energy usage first since they are where the largest potential for energy savings can be found. However, small reductions that can add up should not be overlooked.

The following guidelines can help find the ways in which the energy reduction methods described previously can be applied.

- An analysis of possible energy savings from processor voltage and clock frequency changes or dynamic scaling would be worthwhile if it is feasible to make the related hardware and firmware changes.
- Look for opportunities to lower the duty cycle of high-power-use components. For example, a sensor module that uses 30% of the total system power and can be placed in a low-power idle mode when measurements aren't being taken is a prime candidate. If extensive firmware modifications and testing can be performed, task scheduling combined with putting the processor in sleep mode between tasks might significantly reduce energy usage.
- If the related hardware modifications are feasible, look for lower-current alternatives for wireless communication and sensor modules, integrated circuits, and voltage references.

- Look for voltage dividers that could use higher resistances to reduce current flow while still providing adequately high stability and low output impedance.
- Look for improvements in circuit design that could prevent power from being wasted. For example, make sure that unused operational amplifier sections are properly biased to reduce energy usage and prevent oscillation. Or, better yet, replace the multi-op-amp device with one having fewer op-amp sections and lower power requirement.
- Look for components that are not needed during normal monitor operation and can be disabled or eliminated. For example, the driver for a serial port that is used only for debugging could be powered through a jumper that is disconnected when the monitor is deployed for normal use.
- Consider making circuit changes that could increase the amount of usable energy supplied by the battery. For example, if the monitor has a low-voltage shutdown feature, perhaps the low-voltage shutdown threshold could be reduced when operating from battery power in order to safely extract more energy from a primary battery or each charge of a secondary battery.

Finally, the order in which the modifications are to be made should be determined. The easiest modifications should be performed first, especially those that provide the greatest energy savings. After the easier modifications are made, it is important to measure the energy usage change in order to validate the original energy usage estimates as well as the reduction estimates. Also, it may be possible to deploy an intermediate version of the monitor in order to benefit sooner from the energy savings and increased operating time. The more difficult or time-consuming modifications

should be performed after the easier modifications are complete and their effects evaluated. This approach helps ensure that the measurement, estimation, and evaluation methodologies are sound before investing additional time and effort.

# CHAPTER FOUR: BATTERIES FOR ENVIRONMENTAL MONITORS

Selecting the appropriate battery[1] is essential to obtaining the desired operating time from an environmental monitor while still meeting other requirements of the monitoring application, such as monitor size, cost, and reliability. This chapter discusses the battery features and characteristics that are pertinent to the selection of a battery for use in an environmental monitor. It begins by presenting the two fundamental classes of batteries—primary and secondary—in the context of their use in environmental monitors. Next, it lists and describes the battery characteristics that are most relevant to selecting a battery for use in an environmental monitor. It then expands the discussion of battery capacity by explaining the effect of discharge rate on the amount of energy a battery can actually deliver. Finally, the chapter concludes with guidelines for selecting the appropriate battery for a monitor and application.

## 4.1 Battery Classification

The batteries used in environmental monitoring systems can be divided into two classes: primary batteries and secondary batteries. Primary batteries are designed to be discharged once then discarded. Their chemical and mechanical construction does not facilitate reversal of the chemical reactions that take place while discharging. Secondary

---

[1] In this thesis, the term "battery" is used in the popular sense: It can refer to a single cell or multiple cells connected together. In a context where the distinction is significant, the term "cell" is used to refer specifically to a single cell.

batteries, however, can be recharged by applying an external voltage to cause current flow in the opposite direction from that of the discharge current. The reverse current flow causes the discharge chemical reactions to be reversed. The general characteristics, advantages, and disadvantages of primary and secondary batteries are discussed in the following subsections.

### 4.1.1 Primary (Non-Rechargeable) Batteries

For over a century, primary batteries have been a reliable source of power for portable devices and devices operated where a power outlet connection is unavailable. The common, cylindrical form has existed as a commodity product since the early 20$^{th}$ century and has undergone substantial improvement over the years. Modern alkaline-manganese dioxide ("alkaline") primary batteries are not as prone to leaking corrosive liquid and have a much longer shelf life and higher energy density than their early predecessors.

Because of their reliability, low unit cost, and high energy density, alkaline batteries are good candidates for use in environmental monitoring systems. However, the recurring cost of battery replacement—both material and labor costs—can become substantial over time. Disposing of spent alkaline batteries generates a waste product that, while generally not considered hazardous, still must be disposed of properly. With environmental monitors, battery replacement requires physical access to a monitor, which is costly when a large number of monitors have been deployed. In some situations, such as in-home monitoring for research purposes, accessing a monitor can be undesirably intrusive.

4.1.2 Secondary (Rechargeable) Batteries

Secondary batteries also have existed for over a century. Since the invention of the widely used lead-acid battery in 1859, secondary batteries have undergone remarkable improvements in energy density, charge retention, durability, and safety. They generally have flatter discharge curves and can supply higher currents than primary batteries, but they usually have lower energy density and poorer charge retention. Recent advancements in lithium-based secondary batteries have provided significant improvements in energy density and charge retention. Lithium-ion (Li-ion) batteries have become a very popular choice for portable electronic systems, including environmental monitoring systems.

Secondary batteries are often used to power wireless environmental monitors, especially if solar power or another method of energy harvesting is available to recharge the battery. They are also used in monitors that are easily accessed for recharging, such as monitors that are temporarily placed in one location to collect data then retrieved, recharged, and moved to another location.

Although secondary batteries are popular because of lower long-term cost and less material waste, they have drawbacks. While they usually have a lower overall cost than primary batteries, they nearly always have much higher initial cost. Careful charge and discharge management is needed to maximize their lifetime and avoid hazardous operating conditions. With environmental monitoring systems, charging can be overlooked or insufficient, and the batteries will self-discharge during storage. These factors can potentially make secondary batteries less reliable than primary batteries.

## 4.2 Battery Characteristics

Each type of battery has many different characteristics that define its behavior and its appropriateness for a particular application. The characteristics that are most relevant to selecting a battery for use in an environmental monitoring system are discussed in this section.

### 4.2.1 Cell Voltage

The characteristic voltage of a cell is dependent on the cell's chemistry—the materials used for its electrodes and the electrolyte along with the chemical reactions that take place. A cell's actual voltage depends on other factors as well, especially temperature and state of charge. Because of differences in material quality and manufacturing processes, the initial or full-charge voltage of a particular type of cell can vary between manufacturers and even between manufacturing lots.

### 4.2.2 Capacity

The capacity of a battery usually refers to the amount of electrical charge a battery can deliver over its service life (primary battery) or between charges (secondary battery). The capacity rating is stated in ampere-hours (Ah) or milliampere-hours (mAh) at a specified rate of discharge until a specified end voltage is reached. A battery's actual capacity can be affected by various factors including rate of discharge, temperature, and age.

Capacity can also be expressed as the amount of energy a battery can deliver, which is usually measured in watthours (Wh). When measured this way, a battery's capacity can be estimated as the product of its charge capacity and its average output

voltage or measured by integrating the power delivered by the battery over the discharge period.

The choice of using Ah (charge capacity) or Wh (energy capacity) to quantify a battery's capacity can depend on which measure is most convenient for estimating operating time. For a nominally constant-current discharge, as might be encountered with a linear voltage regulator employing a variable-resistance element in series with the load, the Ah measure allows simple calculation of the estimated operating time. In contrast, the Wh measure is more convenient with a constant-power discharge caused by a switching regulator.

### 4.2.3 Energy Density

The energy density of a battery can refer to its gravimetric energy density or its volumetric energy density. A battery's gravimetric energy density is calculated by dividing its energy capacity by its mass and is usually expressed as Wh per gram or kilogram. Volumetric energy density, usually given as Wh per liter or cubic centimeter, is similarly calculated by using a battery's volume instead of its mass. In either case, the battery's casing, terminals, and other components are included in the mass or volume. The capacities and energy densities of several popular sizes of primary cells are shown in Table 1.

**Table 1: Capacity and Energy Density of Duracell Standard Alkaline Cells**

| Size | Model No. | Capacity (Ah) | Capacity (Wh) | Discharge Rate (mA) | Volume ($cm^3$) | Energy Density ($Wh/cm^3$) |
|---|---|---|---|---|---|---|
| AA | MN1500 | 2.85 | 3.38 | 27.9 | 8.4 | 0.402 |
| C | MN1400 | 7.80 | 9.36 | 60.0 | 26.9 | 0.375 |
| D | MN1300 | 15.0 | 18.0 | 120.0 | 56.4 | 0.319 |
| The figures shown above are based on information appearing in [35]. The rated capacity assumes a constant-resistance load, an average current flow shown in the Discharge Rate column, and a final (discharged) cell voltage of 0.8 V at 21°C. The discharge rates shown here were calculated as the average discharge voltage (1.2 V) divided by the load resistance stated in the datasheet. | | | | | | |

4.2.4 Discharge Voltage Curve

A battery's discharge curve is the voltage across the battery's terminals plotted over time as the battery discharges while powering a load. The shape of the discharge curve can be relatively flat then drop off sharply near the end of the battery's service life, indicating that the battery's voltage remains relatively stable as the battery is discharged. A flat discharge curve is characteristic of many secondary battery types as a result of their low internal resistance. In contrast, primary cells typically have a higher internal resistance, causing the discharge curve to have a steeper slope.

4.2.5 Lifetime

The lifetime of a primary battery has two aspects: the shelf life and the service life. Shelf life is the length of time a battery retains a useful amount of charge while in storage. It is dependent on the battery's self-discharge rate which, in turn, is usually highly dependent on temperature, with elevated temperatures substantially reducing a battery's shelf life. Service life is the length of time a battery can supply sufficient voltage and current to operate the intended device. It is dependent on the battery's

capacity and the discharge conditions, especially temperature and discharge rate. Due to the effect of discharge rate on available capacity, the relationship between discharge rate and service life is usually non-linear.

The service life and shelf life of a secondary battery between charges can be thought of in the same way as with a primary battery. However, it is common to think of a secondary battery's lifetime as the number of charge-discharge cycles it can endure before it can no longer retain sufficient charge to provide the needed service life. This aspect of lifetime is especially important in applications where the battery is regularly subjected to charge-discharge cycles, such as when it is recharged daily using solar power, because it determines the interval at which a secondary battery must be replaced.

### 4.3 Effect of Discharge Rate on Available Capacity

As a cell is discharged, chemical reactions take place at the interface between the electrodes and the electrolyte. At the negative electrode—the anode—an oxidation reaction takes place that supplies electrons to the connected circuit. At the positive electrode—the cathode—a reduction reaction occurs that accepts electrons from the connected circuit. The electrolyte is an ionic conductor that facilitates the chemical reactions at the electrodes and the transport of ions between the anode and the cathode.

Since oxidation and reduction take place on the surface of the electrodes, time is required to allow the reaction products to diffuse or migrate away from the electrode surface so that unreacted material can become available. Also, time is required for the ions to be transported through the electrolyte. If the diffusion or transport rate is insufficient to keep up with the reaction rate, which is proportional to current flow, polarization within the cell will occur. Polarization opposes current flow and consumes

part of the energy that would otherwise be delivered by the cell, dissipating the energy as heat [36].

In addition to polarization losses, the internal resistance $R$ of the cell also causes power to be lost in the form of heat. This power, which is often referred to as $I^2R$ loss, is calculated using Ohm's law as $P = I^2R$, and is proportional to the square of the current $I$ flowing through the cell. As the current increases, the $I^2R$ loss greatly increases, causing power to that would otherwise be delivered to a load to be wasted as heat instead.

The losses within a cell are proportional to the current density in the cell. Consequently, the effect of a particular discharge rate on available capacity is greater on a small cell than on a large cell [37]. For this reason, it is possible to obtain an increase in service life that is greater than a proportional increase in cell size. For example, Table 1 shows that a D-size cell has 5.3 times the capacity of an AA-size cell, but because of the lower current density in a D cell, the increased service life from a D cell will likely be more than 5.3 times greater than the service life from an AA cell under the same load. This dependency between available capacity and discharge rate is sometimes called the rate capacity effect.

### 4.4 Selection Criteria for Environmental Monitors

When selecting a battery for an environmental monitoring system, the answers to the following questions will help identify the characteristics that a battery should have for a specific monitoring system and application.

1. Which is a preferable cost structure for the battery: a one-time, high initial cost or low initial cost followed by recurring costs?

2. How reliable does knowing that the battery is fully charged need to be?
3. What nominal input voltage does the system require, and what input voltage range can the system tolerate?
4. What are the system's average and peak current requirements?
5. How long must the system operate between battery replacement or recharging?
6. Are there size or weight limits that must be considered?

### 4.4.1 Battery Type

The answers to questions 1 and 2 will indicate the type of battery that should be used. If recharging the battery is feasible, whether through human intervention or the use of energy harvesting, and a high initial cost is preferred over the recurring cost of battery replacement, then a secondary battery is probably the best candidate. Given the current state of battery technology, Li-ion, lithium polymer, and nickel metal-hydride types should be compared to determine which will provide the required voltage, capacity, energy density, charging rate, and discharge curve characteristics for the lowest cost.

A primary battery may be a more cost-effective solution if large capacity is required (high-capacity secondary batteries tend to be very expensive) or the environmental monitor's energy requirements are low enough that battery replacement would be very infrequent. A primary battery is also a good choice if not having a fully charged battery when expected would cause substantial problems.

### 4.4.2 Battery Voltage

The type and number of cells that make up a battery determine its nominal voltage. However, the actual voltage presented to the monitor will vary over a range that depends on the battery's temperature and charge state as well as the amount of current it is supplying. The maximum voltage is the open-circuit (no-load) voltage produced by a new primary battery or a fully charged secondary battery. It can be significantly higher than the nominal voltage. The monitor must be able to tolerate an input voltage that is at least as high as the maximum expected battery voltage plus some headroom to accommodate variances between manufacturers and production lots.

The minimum battery voltage is determined by the monitor's under-voltage lockout (UVLO) threshold, which must be set to a voltage that is appropriate for the battery being used. With primary batteries, the voltage should be low enough so that almost all of the battery's available energy is delivered to the monitor before the monitor shuts down. With secondary batteries, the voltage should not be lower than the minimum discharge voltage recommended by the battery manufacturer. Discharging a battery below that voltage can cause irreversible damage to one or more of its cells and greatly degrade the battery's performance and lifetime.

### 4.4.3 Battery Capacity

Specifying an appropriate battery capacity depends on the answers to questions 4, 5, and 6. Size and weight are big concerns, especially in portable environmental monitoring systems. The more energy that is needed, the larger and heavier the battery must be. The amount of energy that the battery is required to supply over its service life depends on the operating time requirements—the interval between battery recharging or

replacement—and the monitor's energy requirements. The amount of energy a battery is designed to supply is indicated by its rated capacity. However, if the discharge rate is high, the battery's available capacity may be much lower than its rated capacity due to the rate capacity effect.

With secondary batteries, if the battery's rated capacity is specified for a discharge current that is equal to or greater than the current required by the monitor, the required capacity in Ah can be reasonably approximated by multiplying the average current required by the monitor by the number of hours that the monitor must operate before the battery requires recharging. The result should be increased by at least 20% to accommodate differences between batteries and battery aging.

The capacity of primary batteries is often given for a specific load resistance rather than current flow. Unfortunately, this causes problems when determining if a primary battery will have sufficient capacity to power an environmental monitor for a specific period of time. Low-power applications, such as environmental monitors, frequently employ switching regulators to provide the constant voltages needed by the monitor's circuitry. Those regulators present a constant power load, not a constant resistance load, meaning that the input current increases as the input voltage decreases. The resulting increase of $I^2R$ loss in the battery as the battery discharges affects the battery's usable capacity in a very non-linear fashion. This makes capacity estimation difficult. The following steps outline a pragmatic approach to determining the required primary battery configuration, including the number of cells and cell capacity:

1. Determine the number of series-connected cells that are required to supply a voltage that is just below the monitor's minimum operating voltage when the

cells have reached their end voltage (i.e., voltage at which a cell is considered to have delivered almost all of its energy) specified by the battery manufacturer. For example, if the cell end voltage is 0.8 V and the minimum operating voltage is 6.0 V, the number of cells required to maximize energy extraction from the battery is $\text{ceil}(6.0 \div 0.8) = 8$ cells.

2. Verify that the total open-circuit voltage supplied by a battery having the number of cells determined in step 1 will not exceed the monitor's maximum allowable input voltage when the battery is new. If the battery voltage is too high, consider modifying the monitor to tolerate a higher voltage so that battery's capacity can be fully utilized. Otherwise, reduce the number of cells appropriately.
3. Multiply the average monitor input current by the number of hours that the monitor must operate before the battery is replaced to estimate the required battery Ah capacity. Increase the estimate by 50% to accommodate capacity degradation due to variations in battery quality and the period of time a battery may have spent in storage.
4. Using the Ah capacity rating given by the manufacturer, select the cell size that is rated to have a capacity equal to or greater than the capacity determined in step 3.
5. Assemble a test battery out of new, unused cells. Perform an operating time test by powering the monitor with the battery and measuring how long the monitor can run until its minimum operating voltage is reached.

6. If the operating time is insufficient, consider taking one or more of these actions:
    a. Use the next largest cell size.
    b. Connect two identical batteries in parallel to increase capacity and reduce the current density in the cells. Reducing the current density will mitigate some of the rate capacity effect.
    c. Modify the monitor to reduce its average and/or peak input current. Reducing the average current has the added advantage of increasing available battery capacity due to the rate capacity effect. Reducing the peak current can allow the battery voltage to remain above the minimum for a longer period of time when the battery is nearly discharged.

# CHAPTER FIVE: EXTENDING IHAQ MONITOR OPERATING TIME

The case study undertaken for this thesis, which is described in Sections 1.3 and 1.4, encompasses extending the operating time of the IHAQ monitor in order to meet the operating time requirements of the NCS. This chapter describes the analysis and modifications performed to reduce the monitor's energy usage and increase its energy supply. It begins with a brief description of the monitor's hardware and firmware. It then presents an analysis of the monitor's energy usage, including measurements at the system and subsystem levels and estimates based on circuit analysis and data sheet information. Then, the potential energy savings are identified, and the needed hardware, firmware, and operating configuration changes are described. The chapter concludes with a description of an external battery that greatly extends the monitor's operating time.

## 5.1 IHAQ Monitor Hardware and Firmware

### 5.1.1 The Fusion Platform

The "Mr. Fusion" (referred to here simply as "Fusion") wireless sensor platform created by HSIL is a flexible, modular wireless sensor platform that is well suited for environmental monitoring applications. Fusion features a flexible hardware and firmware architecture that facilitates development of environmental monitors customized for specific applications. Its modular architecture supports the selection of sensors most suited for a particular purpose. The architecture also allows the sensors to be upgraded independently as technology improves, without the need to redesign the entire monitor.

The Fusion hardware platform includes a powerful 32-bit microcontroller; real-time clock with battery backup; an SD card for data storage; $I^2C$, SPI, and UART interfaces for communicating with sensors; ZigBee, WiFi, and cellular modules for wireless communication; USB and UART ports for debugging and data transfer; and user interface components including pushbutton switches, a multi-frequency buzzer, and an LCD display. Figure 6 is a top and bottom view of a Fusion motherboard, and Figure 7 is a block diagram showing major system components. The Fusion firmware architecture includes support for task scheduling, wireless networking, data logging, status and error message logging, and many different sensor hardware combinations. A diagram describing the firmware's layered architecture appears in Figure 8. Operation of a Fusion system, including measurement intervals and networking, is configurable on a unit-by-unit basis using a file stored on an SD card.

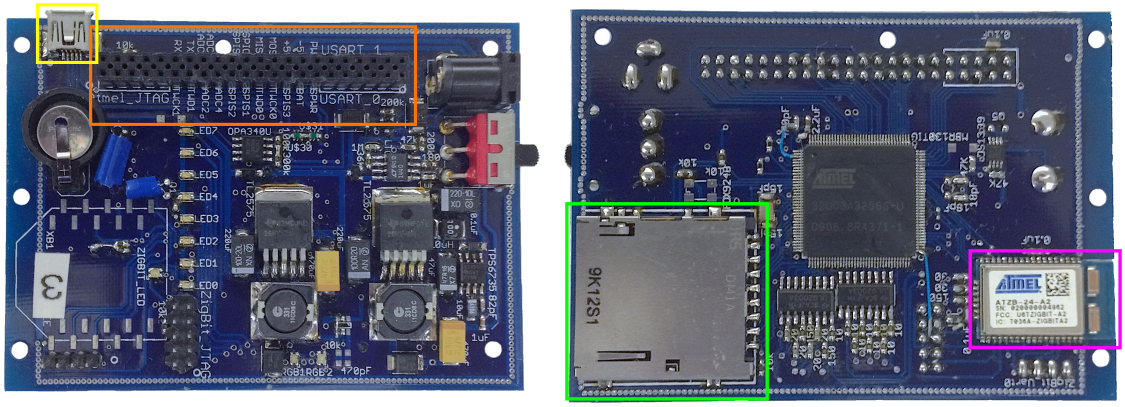


**Figure 6 Fusion Motherboard**

The left image is a top view, and the right image is a bottom view. The connecter highlighted with an orange box supplies these connections to one or more plug-in sensor boards: UART ports, SPI and $I^2C$ buses, GPIOs, ADC inputs, and three regulated DC voltages. The USB port for debugging output and access to the SD card as a mass-storage device is highlighted in yellow. The SD card holder is highlighted in green, and the wireless ZigBee networking module in magenta.

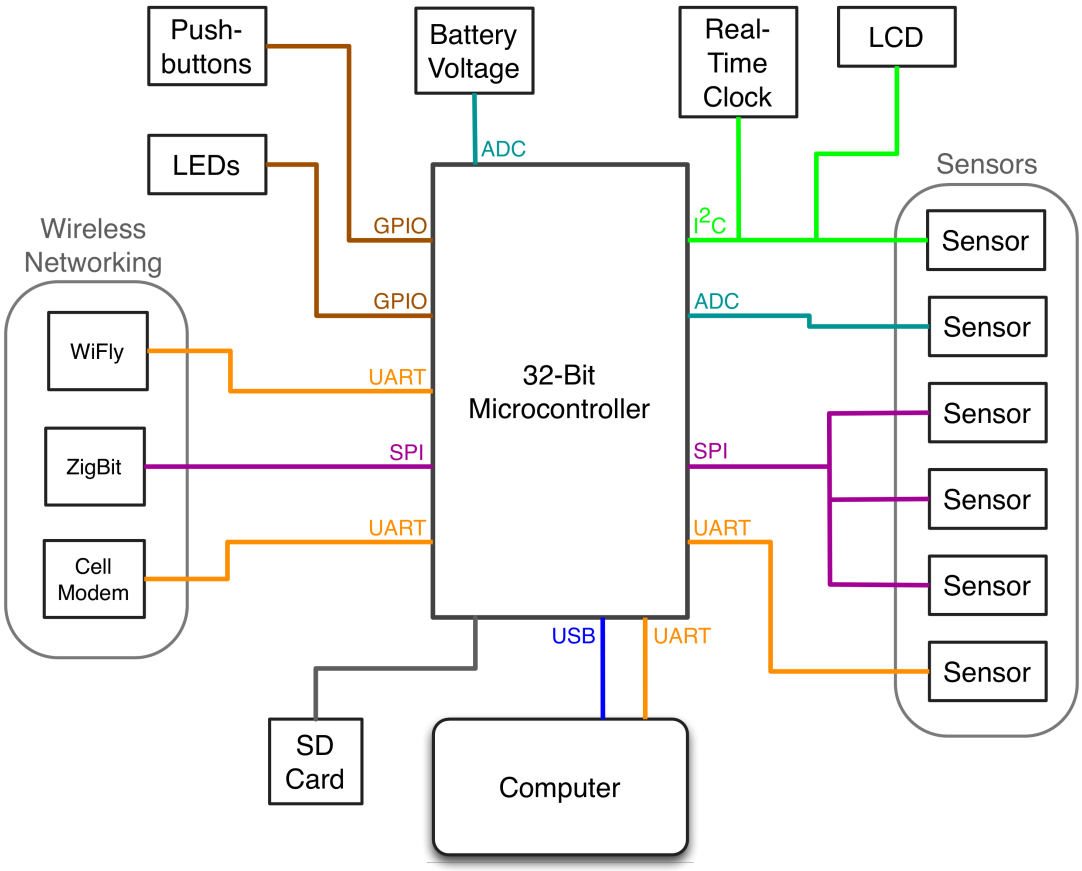


**Figure 7 Block Diagram of Fusion System**

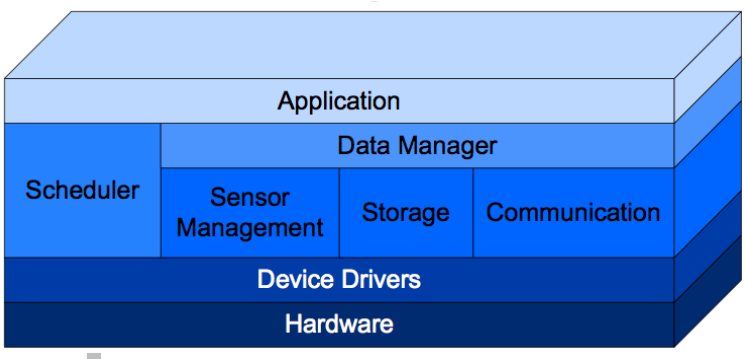


**Figure 8 Fusion Firmware Architecture [15]**

5.1.2 In-Home Air Quality Monitor

An existing aircraft cabin environment monitor built on the Fusion platform provided much of the environmental monitoring capability required for the NCS. The monitor featured data storage and wireless networking capabilities and included sensors for temperature, humidity, pressure, CO concentration, $CO_2$ concentration, and sound level. With the addition of a custom airborne particulate sensor, a 1400 mAh lithium-ion (Li-ion) internal rechargeable battery and charging circuit, and an enclosure suitable for placement in a home, the IHAQ monitor was created. The IHAQ monitor is small, self-contained, and is easy to set up and maintain by NCS field technicians. It can be powered from an AC power outlet connection or from its internal battery. A block diagram of the IHAQ monitor appears in Figure 9 [38], and a detailed description is given in [15]. Figure 10 is a photo of the monitor sitting on top of the enclosure for the external battery described in Section 5.5.

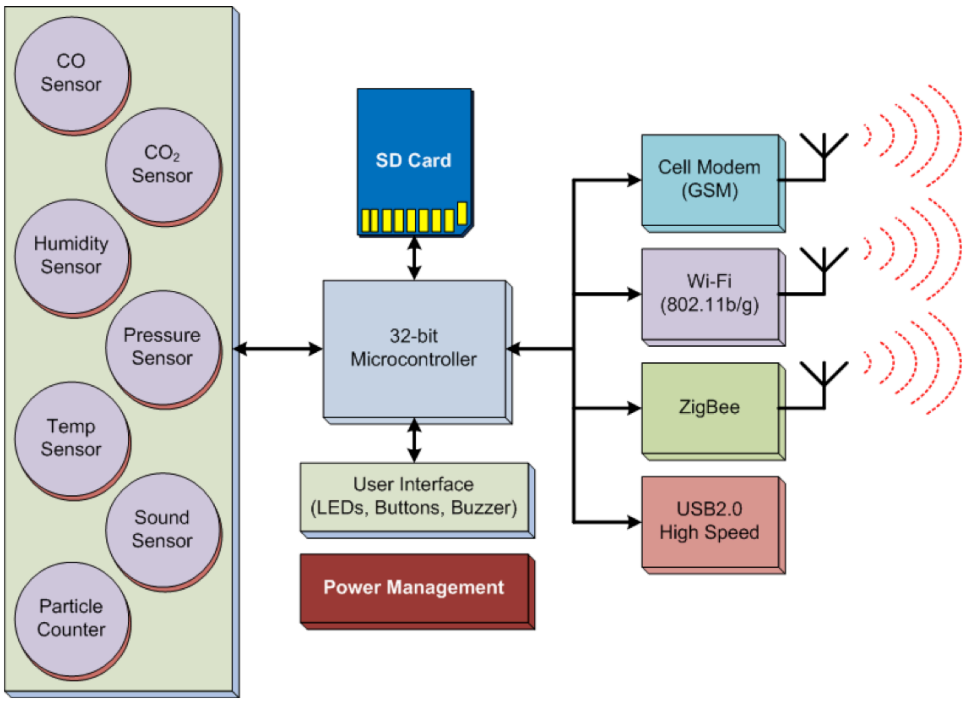


**Figure 9 IHAQ Monitor Block Diagram [38]**

**Figure 10 IHAQ Monitor Atop the External Battery Enclosure.**

## 5.2 Monitor Energy Usage Evaluation

### 5.2.1 Energy Usage Measurements

Direct measurement of the energy used by each IHAQ monitor subsystem (individual sensors, voltage regulators, the microcontroller, wireless modules, etc.) would be very difficult due to the quantity and location of power distribution traces on the monitor's multi-layer printed circuit boards. Instead, the monitor was operated with circuit boards and several easily disconnected components removed in various combinations, and the input voltage and current supplied to the monitor were measured simultaneously for each combination. The principle of superposition was then applied to estimate the input current required from the battery to operate the various subsystems. With the input voltage being held constant, power was then calculated. A photograph showing the circuit boards and the interconnecting cables appears in Figure 11. The block diagram in Figure 12 more clearly depicts the functions of the circuit boards and the connections between them.

An Agilent Infiniium MSO7104A oscilloscope recorded simultaneous voltage and current measurements at the monitor's power input jack. Figure 13 shows a diagram of the measurement apparatus. The instantaneous current measurements recorded by the oscilloscope were averaged over an appropriate period of time to calculate the average current.

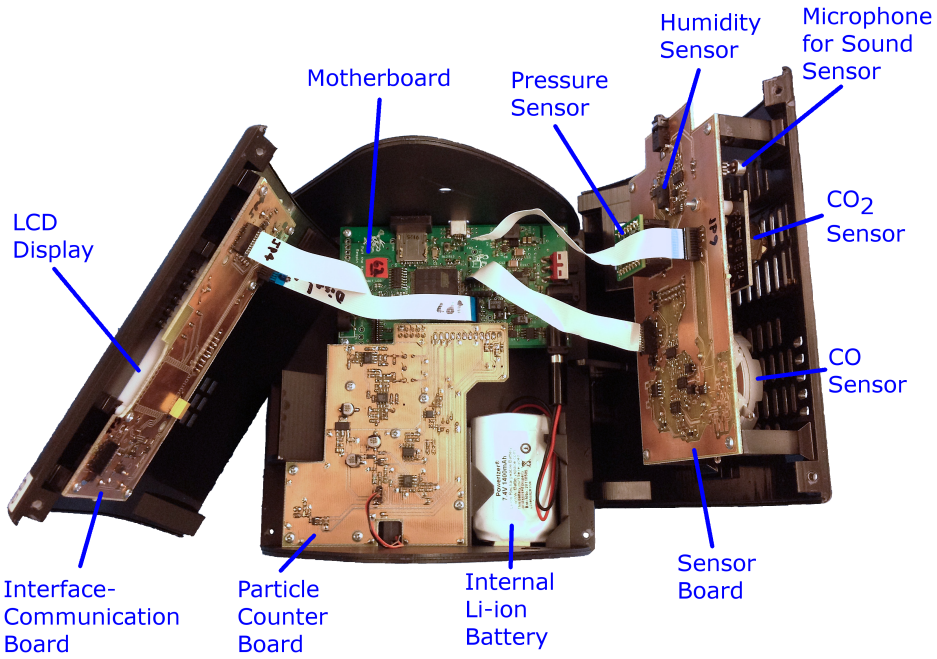


**Figure 11 IHAQ Monitor Internal View Showing Boards and Interconnections**

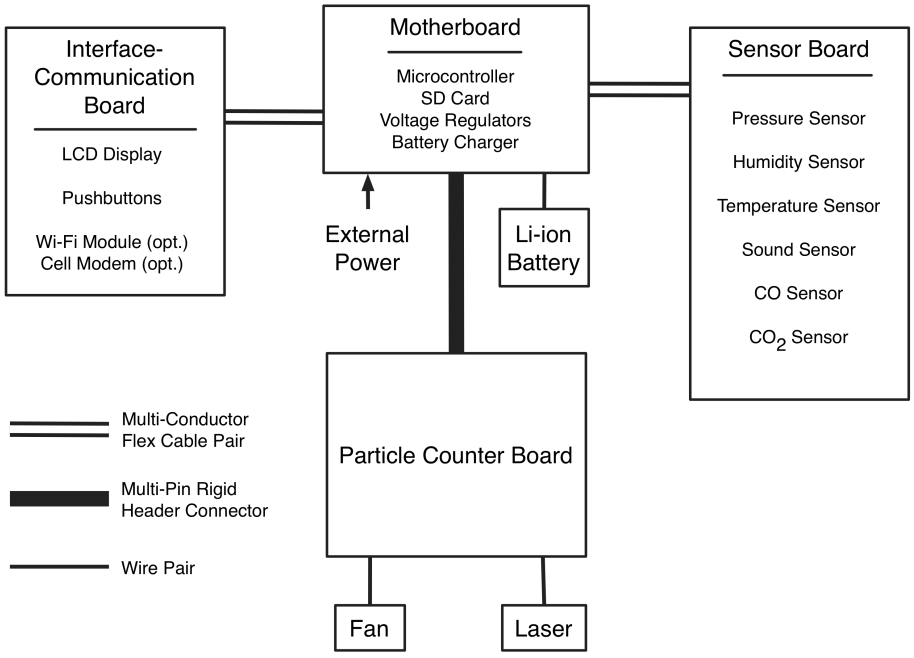


**Figure 12 IHAQ Monitor Board Interconnection Diagram**

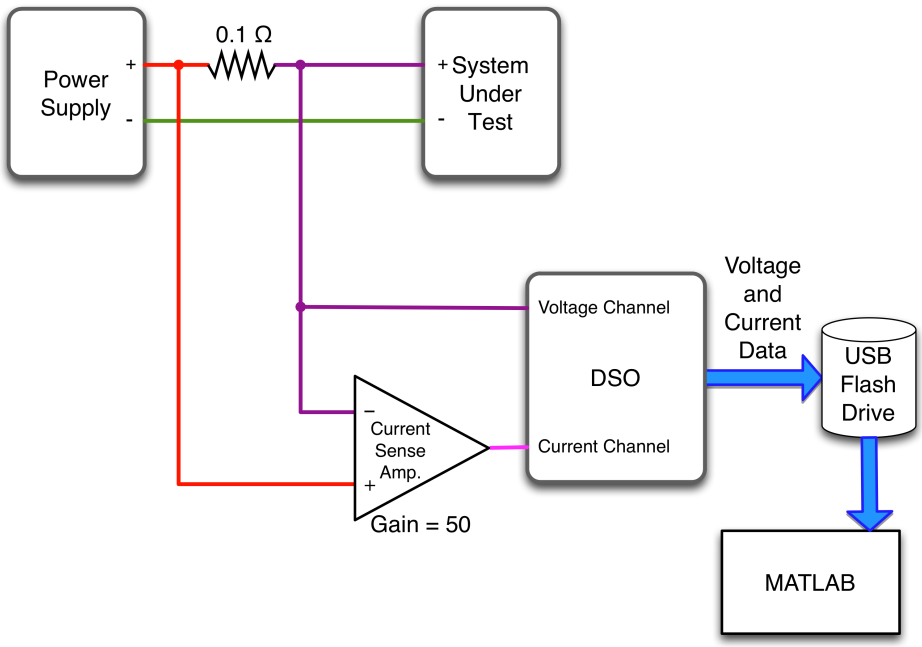


**Figure 13 Diagram of Apparatus Used to Measure IHAQ Monitor Input Current**

5.2.2 Energy Usage Estimates Based on Measurements

The estimated current and power requirements of the monitor's subsystems without energy usage reduction—i.e., a baseline—appear in Table 2. The total estimated average input current is 126.9 mA, which is within approximately 2% of the 124.3 mA average input current measured during a battery operating time test using the same monitor configuration. The small difference between the estimated and measured total input currents suggests that the individual subsystem estimates are accurate enough to provide a good understanding of which subsystems consume the most energy and where energy reduction efforts should be concentrated.

**Table 2: Current and Power Estimates Without Energy Usage Reduction (Baseline)**

| Subsystem | Est. Average Input Current at 10.2 V (mA) | Est. Average Power (mW) |
|---|---|---|
| Motherboard (includes voltage regulators, microcontroller, SD card, and the internal battery charge controller) | 41.1 [3] | 419 |
| Internal ZigBit, RGB2, and laser warning LEDs | 3.3 [1] | 34 |
| External ZigBit LED | 2.5 [1] | 26 |
| ZigBit module (communication disabled) | 7.6 [1] | 78 |
| Interface-Communication board (LCD display only, no Wi-Fly or cellular module) | 0.4 [2,3] | 4 |
| Sensor board (excluding T6615 $CO_2$ sensor) | 0.6 [3] | 6 |
| T6615 $CO_2$ sensor (idle mode disabled) | 28.9 | 295 |
| Particle counter (excluding fan and laser) | 0.6 | 6 |
| Particle counter fan | 34.3 | 350 |
| Particle counter laser | 7.6 | 78 |
| System total | 126.9 | 1,296 |

[1] Estimate is based on the average of input currents measured using the apparatus described in section 7.1.2.
[2] Estimate is based on component data sheet values.
[3] See Table 3 for additional detail.

5.2.3 Energy Usage Estimates Based on Data Sheet Information

In an attempt to gain a more detailed understanding of the IHAQ monitor's energy usage at the sensor and subsystem level, energy usage estimates were also calculated using DC circuit analysis and component data sheet information. These estimates are listed in Table 3, and they show that, apart from the T6615 $CO_2$ sensor and the particle counter, the remaining sensors use very little energy. A much larger amount

of energy is used in the three voltage regulators. Not surprisingly, considerable energy is consumed by the microcontroller.

**Table 3: Current Estimates Using Data Sheet Information**

| Circuit Board | Subsystem | Est. Average Input Current at 10.2 V (mA) |
|---|---|---|
| Motherboard | Voltage regulators | 11.8 |
| | Microcontroller | 16.1 |
| | ZigBit module (in power-save mode) | 0.0023 |
| Interface-Comm. | Display | 0.38 |
| Sensor | Citytech CO sensor | 2.6 |
| | Sound sensor | 3.0 |
| | Pressure sensor | 0.0046 |
| | Humidity sensor | 0.076 |

### 5.3 Identification of Potential Energy Savings

Apart from the motherboard, the particle counter's fan and the T6615 $CO_2$ sensor consume the most energy. Since the T6615 has a reduced-power idle mode feature, and firmware code was already in place to control the duty cycle of the fan and laser, initial energy reduction efforts were focused on those two items. Several LEDs that are not visible from outside the enclosure and unneeded wireless networking modules were also identified as candidates for additional energy savings.

Table 4 shows the estimated current and power requirements when the T6615 is taken out of idle mode for only 8 seconds each minute, the particle counter's fan and laser are turned on for only 20 seconds each minute, the ZigBit wireless networking

module is held in reset, and the internal LEDs are disabled. With these changes, the estimated average system input current is 68.9 mA, representing a reduction of 45.7%. The estimate is slightly more than 1% higher than the 68.2 mA average input current measured during a battery operating time test performed with the same low-power configuration, indicating that the estimation methodology is a useful tool for predicting energy usage under different configurations.

**Table 4: Current and Power Estimates With Energy Usage Reduction**

| Subsystem | Est. Average Input Current at 10.2 V (mA) | Est. Average Power (mW) |
|---|---|---|
| Motherboard (includes voltage regulators, microcontroller, SD card, and the internal battery charge controller) | 41.1 | 419 |
| Interface-Communication board (without Wi-Fly or cellular module) | 0.4 [1] | 4 |
| Sensor board (excluding T6615 $CO_2$ sensor) | 0.6 | 6 |
| T6615 $CO_2$ sensor (idle mode enabled) | 12.3 | 125 |
| Particle counter (excluding fan and laser) | 0.6 | 6 |
| Particle counter fan | 11.4 | 116 |
| Particle counter laser | 2.5 | 26 |
| System total | 68.9 | 702 |

[1] Estimate is based on component data sheet values.

## 5.4 Modifications to the Monitor System

### 5.4.1 Hardware Modifications

The energy usage reduction efforts were focused on reducing the monitor's energy usage without changing circuit board layouts or adding more than a few

components or wire jumpers. Within this constraint, only one minor hardware modification is related to reducing the monitor's energy usage. Two other modifications are required for full compatibility with an external battery. However, almost all of the energy usage reduction and operating time increases described in this thesis can be achieved without any hardware modifications. Also, an unmodified monitor can be powered with an external battery, albeit without the monitor system shutdown control enhancements that increase battery life and reduce the risk of data loss.

The energy-use reduction modification consists of disabling several LEDs that are not visible during normal system operation. The monitor design includes internal and external LEDs that are connected in parallel and provide the same status indications. The internal LEDs are used during initial system setup and troubleshooting; they are not visible from outside the monitor's enclosure. Removing or otherwise disabling the internal LEDs located on the motherboard and the laser operation warning LED on the particle counter board reduces average battery current by approximately 3 mA, which is 5.5% of the average total battery current under the lowest energy usage configuration presented in this report. The externally visible LEDs located on the Interface-Communication board are not affected by disabling the internal LEDs.

Two additional hardware modifications provide compatibility with an external battery and its controller, and they modify the monitor's under-voltage lockout (UVLO) behavior to maximize battery life. The first of these two modifications allows the monitor's firmware to disable charging of the internal Li-ion battery when the monitor is powered by an external battery. Figure 14 contains a schematic of the battery charging circuit showing the modification. The firmware can set high the general-purpose input-

output (GPIO) pin connected to CHRG_SHDN, which causes the charge controller's active-low SHDN_BAR input signal to be set low. When that signal is low, the charge controller enters a low-power standby mode and does not charge the connected Li-ion battery.

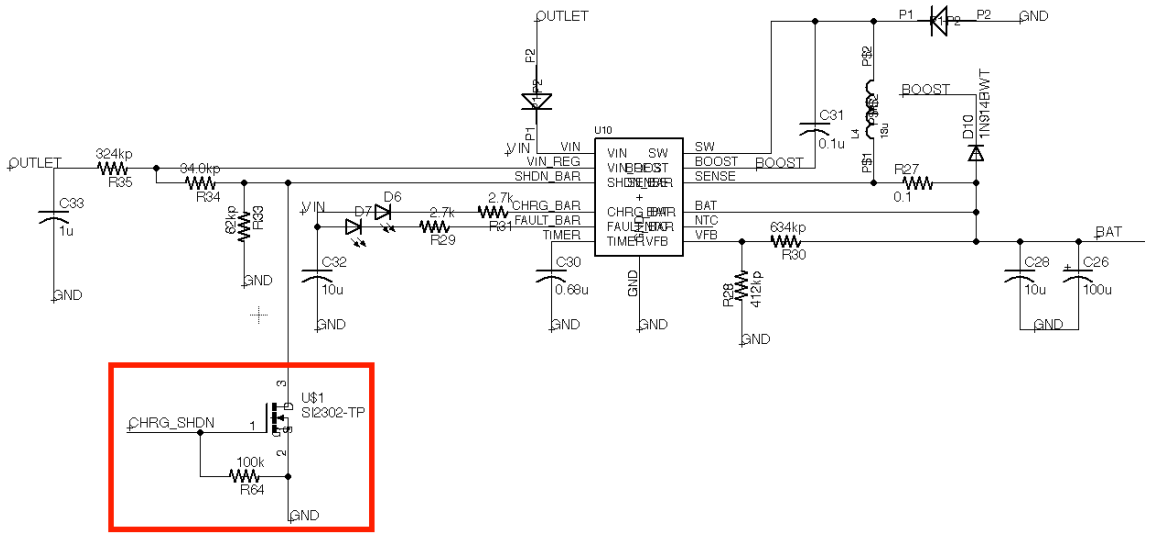


**Figure 14 Schematic Showing CHRG_SHDN Modification**

The modification is highlighted by the red box.

The second modification slows the monitor's UVLO response so that it does not trigger on the voltage sags caused by the large current demand spikes of the T6615 $CO_2$ sensor. Slowing the response allows the external battery to continue powering the system when the battery is near the end of its service life and the load spikes cause the battery voltage to briefly drop below the UVLO threshold voltage. To slow the response, a 100 µF capacitor (highlighted in Figure 15) was added at the input of the comparator that provides the POWER_GOOD signal to the voltage regulators. When the average input

voltage is near the shutdown threshold, the capacitor keeps the input voltage above the threshold during the approximately 500 ms voltage sag caused by the T6615's load spike.

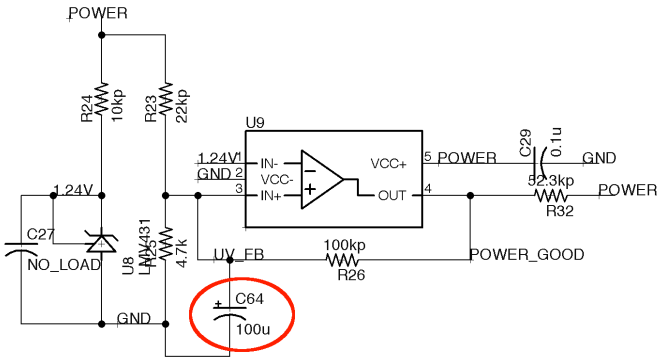


**Figure 15 Schematic Showing the UVLO Delay Modification**

The added capacitor is circled in red.

## 5.4.2 Firmware Modifications

Because updating an existing monitor's firmware is considerably easier than performing hardware modifications, less restriction was placed on the scope of energy-reduction firmware modifications than on the scope of hardware modifications. Four significant firmware modifications were made to the Fusion code base. Each modification consisted of changes to one or more source code files. The modified code is automatically included in present and future Fusion firmware versions, and it is backward compatible with existing Fusion systems.

### 5.4.2.1 Add Support for $CO_2$ Sensor Idle Mode

The first modification adds support for the Telaire T6615 $CO_2$ sensor's idle mode. With this modification, the sensor can be placed in idle mode between recorded

measurements, which suppresses the 0.96 second, 72.3 mA (average) load spikes that occur every 3.45 seconds. In idle mode and between load spikes, the sensor draws only 8.8 mA from the battery. A configuration file setting specifies the amount of time that the sensor is taken out of idle mode before each $CO_2$ measurement is read and recorded.

#### 5.4.2.2 Control CHRG_SHDN Signal from Configuration File

The second modification allows the CHRG_SHDN signal to be controlled by a configuration file setting. When the signal is asserted, charging of the monitor's internal Li-ion battery is disabled. During monitor system startup, CHRG_SHDN is asserted as soon as possible by the firmware's initialization code. After the configuration file has been opened and its contents read into memory, the value of the ENABLE_CHARGE flag read from the file is checked. If the flag is set, CHRG_SHDN is de-asserted. Otherwise, CHRG_SHDN remains asserted, thus preventing the internal battery from being charged.

#### 5.4.2.3 Modify Fan Operation to Improve Measurement Temporal Accuracy

Support for cycling the particle counter's fan and laser was already present in the firmware. However, the fan and laser were turned on by the firmware at the beginning of the 60-second measurement interval rather than at the end of the interval. When the fan duty period was set to 20 seconds, this behavior caused a 40-second delay between the actual particle counts and the timestamp of the particle concentration measurement written to the data log file. The delay would be 55 seconds if the fan duty period were set to 5 seconds. The third firmware modification causes the fan and laser to operate at the end of a measurement interval rather than at the beginning. Counting particles for the

duration of the specified fan duty period immediately prior to recording a particle concentration measurement increases the temporal accuracy of the measurements.

#### 5.5.2.4 Coordinate High-Current Loads

The fourth modification encompasses adding a mechanism for coordinating the operation of high current demand sensors to reduce the magnitude of supply current peaks. The mechanism consists of a mutual exclusion lock (mutex) that prevents more than one high-current operation from occurring at a time. Each participating sensor firmware module must acquire an exclusive lock on the mutex before turning on a high-current device, and it must release the lock after turning off the device. If a module is unable to lock the mutex because the mutex is already locked by another module, it must wait until it can successfully acquire a lock before proceeding with its intended high-current operation. Support for locking and unlocking the mutex was added to the Fusion sensor support framework code.

The mutex is used in the T6615 $CO_2$ sensor module and the particle counter module to prevent the sensor's supply current spikes from occurring while the particle counter fan is running. The sensor's firmware module locks the mutex to take the sensor out of idle mode, and the particle counter module locks the mutex to run the fan. This scheme prevents a load spike from the $CO_2$ sensor from occurring while the fan load is present, thus suppressing the large current spikes and corresponding voltage sags that trigger UVLO and cause the monitor to be shut down when the battery is near but has not yet reached the end of its service life. In addition, reducing the peak current demand increases the usable capacity of an external primary battery.

### 5.4.3 Configuration File Modifications

While most of the hardware and firmware modifications provide the ability to reduce the monitor's energy usage, it is necessary to change several configuration file settings to actually implement the reductions. This approach allows the same monitor unit to be used for deployments where an AC power outlet connection is available and high data quality or short measurement intervals are required and in situations where long-term battery operation is needed. The monitor can be reconfigured for either type of operation simply by inserting an SD card containing the appropriate configuration file. The configuration settings related to energy-use reduction are listed in Table 5.

**Table 5: Configuration File Settings for Low-Power Operation**

| Parameter | Normal Value | Low-energy Value | See Subsection |
|---|---|---|---|
| SENSOR.CO2T6615.IDLE_MODE_EN | 0 | 1 | 5.4.3.1 |
| SENSOR.CO2T6615.IDLE_OFF_PERIOD | - | 8 | |
| SENSOR.CO2T6615.PPM_INTERVAL | 5 | 60 | |
| SENSOR.PARTICLE.INTERVAL | 60 | 60 | 5.4.3.2 |
| SENSOR.PARTICLE.DUTY | 60 | 20 | |
| ENABLE.CHARGE | 1 | 0 | 5.4.3.3 |
| ENABLE.ZIGBEE | 1 | 0 | 5.4.3.4 |
| DEST.ZIGBIT | 1 | 0 | |
| ENABLE.WIFI | see text | see text | |
| WIFI.HOLD_IN_RESET | 0 | 1 | |

#### 5.4.3.1 T6615 $CO_2$ Sensor Idle Mode

Three of the configuration file changes are related to enabling the T6615 $CO_2$ sensor's idle mode. When the idle mode is enabled, the amount of time that the T6615 is not in idle mode before a measurement is recorded must be specified. Energy usage increases with the amount of time the sensor is not in idle mode. However, measurement

accuracy is affected by the length of time the sensor is in idle mode between measurements, as described in Section 7.3.1. Test results indicate that idle-off periods shorter than eight seconds should be avoided.

The measurement interval must be long enough to allow a substantial amount of idle time as well as accommodate the idle-off period. 60 seconds is a reasonable interval. If the measurement interval is too short or the idle-off period is too long, idle mode will be disabled and an error message will appear in the system log.

#### 5.4.3.2 Particle Counter Fan Duty Cycle

The particle counter fan duty cycle is controlled with the SENSOR.PARTICLE.DUTY parameter, which sets the amount of time that the particle counter fan runs during each particle counting interval that occurs prior to recording a particle concentration measurement. When measurements are recorded once per minute, running the fan for 20 seconds out of each minute produces reasonably accurate measurements with relatively low noise. The effect of the fan duty cycle on measurement data quality is described in Section 7.3.2.

#### 5.4.3.3 Internal Battery Charging

If the hardware and firmware modification allowing the CHRG_SHDN signal to be controlled by the firmware have been made, charging of the internal Li-ion battery while the monitor is on can be disabled by setting ENABLE.CHARGE to 0. However, charging while the monitor is off remains unaffected.

5.4.3.4 Wireless Networking

Additional savings can be realized by disabling unneeded wireless networking modules by holding them in reset. The ZigBit module should be disabled if ZigBee wireless networking is not needed (i.e., if the monitor will not be within range of a ZigBee coordinator). The ZigBit data destination must also be disabled whenever ZigBee networking is disabled.

If the monitor includes a Roving Networks WiFly module but Wi-Fi networking is not needed, the module should be held in reset by setting WIFI.HOLD_IN_RESET to 1. Note that the module must be enabled by setting ENABLE.WIFI to 1 in order for WIFI.HOLD_IN_RESET to have any effect. However, if the monitor does not have a WiFly module, ENABLE.WIFI should always be 0.

5.4.3.5 Load Staggering

When the T6615 idle mode is enabled and SENSOR.PARTICLE.DUTY is not equal to SENSOR.PARTICLE.INTERVAL, the high current demands of the $CO_2$ sensor and the particle counter fan are automatically staggered as described previously. However, if the T6615 idle mode is disabled or the fan is set to run continuously, load staggering will not occur.

## 5.5 External Battery for Longer Operating Time

5.5.1 Battery Type

Because of size constraints, it is not feasible to increase the capacity of the IHAQ monitor's internal Li-ion battery to provide several days or more of operating time. A large, rechargeable external battery was considered, but high cost, long recharging times,

and safety concerns made that solution unattractive. Additionally, inadequate or forgotten recharging of the battery could make long operating times unreliable. Instead, an external battery pack consisting of readily available primary (non-rechargeable) cells was selected.

### 5.5.2 Number of Cells

To provide sufficient voltage to operate the monitor until the cells reach the end of their useful life, the external battery consists of eight cells connected in series. That number of cells was chosen so that the final cell voltage would be such that most of a cell's available energy has been delivered when the battery voltage reaches the monitor's internal UVLO shutdown threshold. The UVLO threshold is set to 6.5 V to protect the internal Li-ion battery from being over-discharged. At 6.5 V, the per-cell voltage in an 8-cell battery would be $6.5 \div 8 = 0.8125$ V. The steep falloff that appears in the discharge voltage curves shown in several battery data sheets and recorded during the battery discharge tests presented in Chapter Seven indicates that almost all of a standard or alkaline battery's usable energy has been delivered by the time the cell voltage reaches 0.8 V. Additional discharge tests were performed with six and ten cells to verify that eight cells is the optimum solution.

The initial voltage of a new, standard or alkaline 8-cell battery is nominally 12 V, which is much higher than the 7.3 V to 8.3 V supplied by the internal Li-ion battery and at which the monitor was designed to operate when on battery power. Although the monitor can withstand input voltages exceeding 18 V, the efficiency of the monitor's switching regulators when operating with a high input voltage becomes a concern. To determine how much the input power would increase at a higher input voltage, the

monitor was operated over a range of input voltages while the input current was measured. Input power was then calculated as the product of simultaneous voltage and current measurements. Figure 16 shows the relationships between input voltage and input current and power. When the input voltage is 12 V, the input power is 13.5% higher than at the 7.8 V average input voltage from the internal Li-ion battery. However, assuming that the average input voltage from an 8-cell battery is 10 V, the input power is only 6.8% higher.

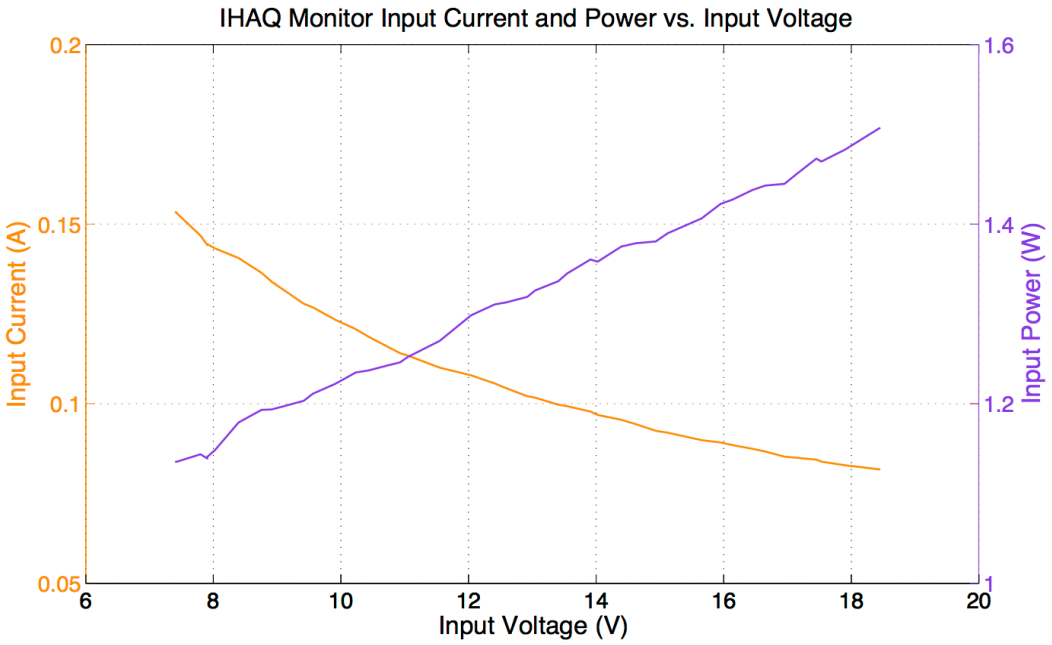


**Figure 16 Monitor Input Current and Power Over a Range of Input Voltages**

The plotted values are 60-second averages of measurements taken at 33 samples per second. Power was calculated as the product of simultaneous voltage and current measurements.

5.5.3 Cell Size

Table 1 shows the capacity and energy density of the Duracell brand of standard alkaline-manganese dioxide AA, C, and D size cells. Among these common cell sizes, AA-size cells have the highest volumetric energy density. However, the stated capacity of the AA cells is based on an average discharge current of 29.7 mA; the cells would have significantly less capacity when supplying an average current of 55 mA to 125 mA required by the monitor. Also, multiples of eight AA cells in a series-parallel connection would be required to provide operating times of two days or longer. For a week of continuous operation, 48 AA cells would be required. The battery holder arrangement would be unwieldy and would likely exceed the volume of the eight D cells that could provide approximately the same operating time.

To facilitate operating times longer than a week in the simplest cell configuration, size D cells were chosen. A battery pack consisting of eight D cells has a size footprint that closely matches that of the monitor, allowing the pack to be used as a base that increases the height of the monitor by approximately two inches but does not significantly increase its width and depth.

# CHAPTER SIX: PRIMARY CELL BATTERY CONTROLLER

The IHAQ monitor was designed to be powered by an internal Li-ion battery or an external power supply connected to an AC power outlet. The monitor's low-voltage shutdown behavior is tailored for the discharge curve of a Li-ion battery, and the monitor automatically recharges the battery whenever external power is connected. These behaviors are not compatible with the external primary battery that was added to extend the monitor's operating time. To overcome the incompatibility, the primary-cell battery controller (PCBC) was created.

This chapter begins with a detailed explanation of the incompatibility between the external battery and the IHAQ monitor. It then describes how the PCBC's low-voltage shutdown and charge-prevention behaviors overcome the incompatibility. Next, the PCBC's specifications and circuit design are set forth followed by a detailed description of the low-power design methodology that was used. Finally, estimates and measurements of the PCBC's own energy usage are presented.

## 6.1 Primary-Cell Battery Controller (PCBC) Overview

The IHAQ monitor was designed to operate from an AC power outlet or an internal rechargeable battery, and it includes battery management hardware designed for a two-cell, 7.4 V Li-ion battery. The internal battery is automatically recharged, if necessary, whenever the monitor is connected to a power outlet. When the monitor is powered from an outlet, the battery is available to provide backup power to keep the

monitor operating in the event of a power failure. Whether the internal battery is being used as a backup energy source or as the primary means to power the monitor, the monitor's UVLO circuit protects the Li-ion battery from over-discharge.

Although these features make the IHAQ monitor well suited for use where AC power is available or the monitor is required to operate for only 8 to 16 hours using battery power, they create two significant incompatibilities with an external battery pack consisting of primary cells. First, the monitor's UVLO hysteresis between the shutdown and startup voltage thresholds, which is tailored for the characteristics of a Li-ion battery, is too small for a battery that has a higher internal resistance and presents wide no-load to full-load voltage swings. The small hysteresis range allows multiple, incomplete system restart attempts when such a battery reaches the end of its service life. Second, the automatic recharging feature would use current from an external battery to recharge the internal battery. Charging one battery from another is inefficient, and the high charging current would quickly drain the external battery, possibly to the point that the operating time from the battery is less than what is required. To resolve these incompatibilities, the external battery pack that was designed for use with the IHAQ monitor includes a custom primary-cell battery controller (PCBC) that addresses both of these issues.

### 6.2 Low-Voltage Shutdown Control

The PCBC prevents potentially damaging monitor system restart attempts caused by the large full-load to no-load voltage swing of a nearly depleted standard or alkaline battery. When the battery voltage drops below the monitor's low-voltage threshold, the monitor's internal UVLO circuit turns off the monitor, thus disconnecting the load from the battery. With the load removed, the battery voltage rapidly increases. The no-load

voltage of an eight-cell standard or alkaline battery quickly exceeds the voltage-good threshold, causing the UVLO circuit to turn on the monitor. The monitor then attempts to restart and resume operation. However, because the battery is almost depleted, the next load spike causes the voltage to drop below the low-voltage threshold, and the monitor is once again turned off. This sequence of events is depicted in Figure 17a. The off-on-off cycle will repeat (Figure 17b), perhaps many dozens of times, until the monitor enters what can be described as a quivering state where the hardware is receiving some power but is non-functional, as illustrated in Figure 17c. Before that state is reached, the rapid cycling of power can lead to incomplete writes to the SD card, which can damage the card's file system and lead to loss of data.

The PCBC prevents the repeated on-off cycling by disconnecting the monitor from the battery when the average battery voltage drops below the monitor's low-voltage threshold for a period of time slightly shorter than the monitor's internal UVLO delay period. It also disconnects the monitor when the load current drops close to zero and the battery voltage is below the 9 V warning threshold, which indicates that the monitor's internal UVLO has probably triggered. Both types of shutdown actions are depicted in Figure 18. Once the PCBC disconnects the monitor from the battery, it will not reconnect it until the battery is replaced or the PCBC's reset button is pressed.

(a)

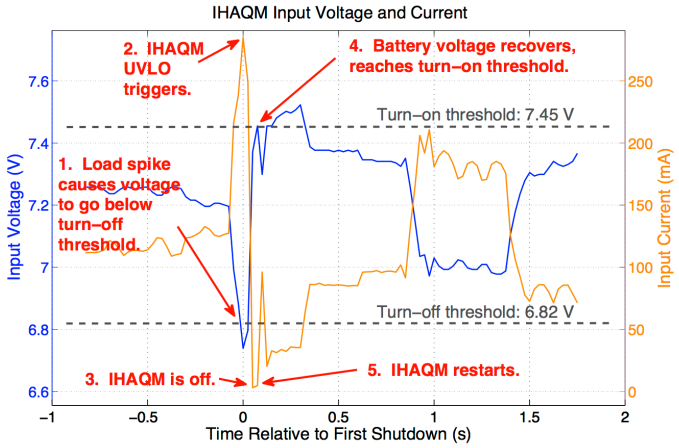


(b)

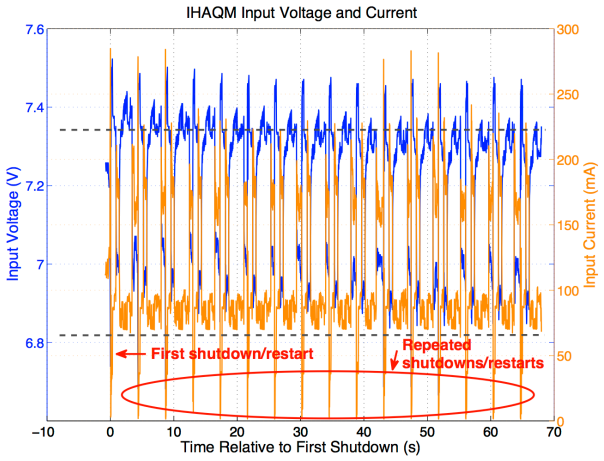


(c)

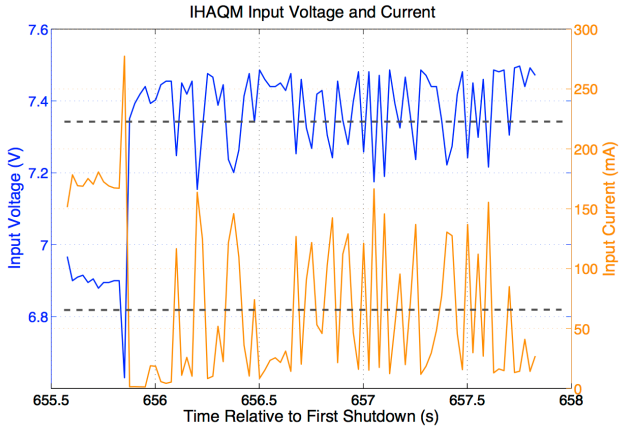


**Figure 17 IHAQ Monitor UVLO Behavior With an External Battery**

(a) chronicles the shutdown and restart behavior. (b) shows the multiple shutdowns and restarts that occur at approximately the $CO_2$ sensor's internal measurement interval. (c) shows the quiver mode during which the monitor is non-functional but still using power.

(a)

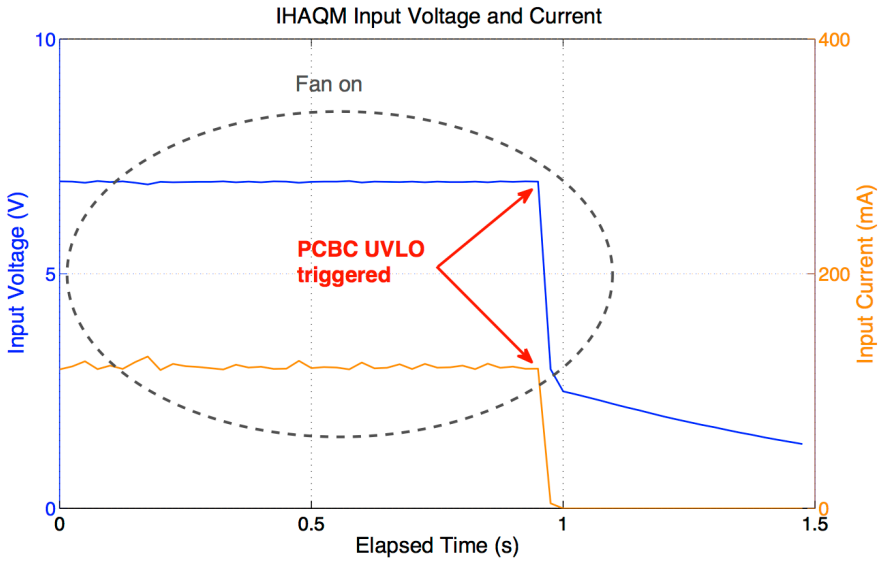


(b)

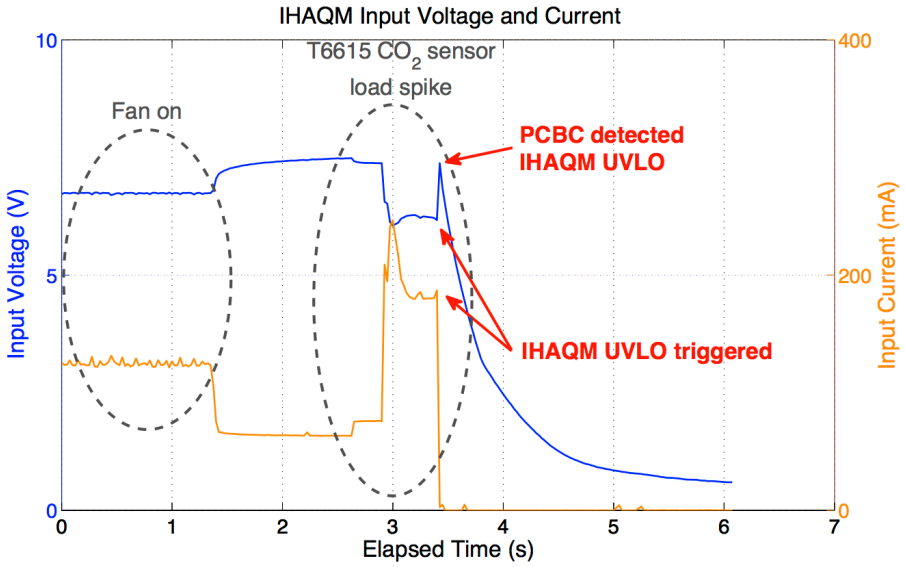


**Figure 18 PCBC UVLO Behavior**

In (a), the PCBC low-voltage threshold was reached, resulting in the battery pack output being turned off. In (b), the monitor's UVLO was triggered first. The PCBC then turned off the battery pack output when it detected that the load had disappeared. The data for both plots were collected during operating time tests in which 8 standard AA cells were used. The voltage was measured at the PCBC output (the input to the monitor).

### 6.3 Internal Battery Charging Prevention

When the IHAQ monitor is configured for use with an external battery, a configuration setting inhibits internal battery charging. However, the setting takes effect only when the monitor is powered on and running; it cannot affect charging behavior when the monitor is turned off. So, if the external battery is connected to the monitor but the monitor is not turned on, charging of the internal battery can take place. If the internal battery is not already fully charged, the high charging current will rapidly decrease the service life of the external battery.

The PCBC prevents charging of the monitor's internal Li-ion battery when the external battery is connected and the monitor is not promptly turned on. When the PCBC detects the steady, high current flow that is characteristic of charging the internal battery, it disconnects the monitor from the external battery if the condition persists for more than about five seconds. It disconnects the monitor immediately if it detects a current flow above the upper limit of its measurement range (approximately 500 mA). In either case, the PCBC's audible alarm sounds. Pressing the PCBC's reset button restores the connection from the battery to the monitor and gives the technician another chance to turn the monitor on, thereby disabling charging of the internal battery.

### 6.4 PCBC Specifications and Circuit Description

The PCBC is contained on a small circuit board, shown in Figure 19, which is located inside the external battery enclosure. It employs a microcontroller, current sense amplifier, and a load switch to monitor and control the output from the battery. The

controller turns off the battery pack output when an under-voltage or over-current condition occurs. The PCBC provides a visual indication of battery voltage (greater or less than 9 V), output state (load or no load detected), and shutdown reason (under voltage or high current) via LEDs. The LED color and flashing patterns and their meanings are listed in Table 7. An audible alarm signals that an over-current condition has occurred. The PCBC specifications, including voltage and current thresholds, are listed in Table 6.

**Table 6: PCBC Specifications**

| Rating or Threshold | Value |
|---|---|
| Minimum battery voltage for operation | 2.8 V |
| Absolute maximum battery voltage | 14.7 V |
| Supply current | 66 µA avg. [1] |
| Low-voltage warning threshold | 9.01 V |
| Low-voltage shutdown threshold | 6.89 V |
| Low-voltage shutdown delay | 594 ms. [2] |
| Load-detection current threshold | 19.6 mA |
| Delayed overcurrent shutdown threshold and period | 249 mA, 4.6 s [3] |
| Immediate overcurrent shutdown threshold | 500 mA |

All voltage, current, and time values are nominal and can vary due to component variances.

[1] See Section 6.6.
[2] The delay accommodates voltage sags caused by the T6615 $CO_2$ sensor load spikes.
[3] Current from 249 mA to 499 mA persisting for more than 4.6 s causes shutdown.

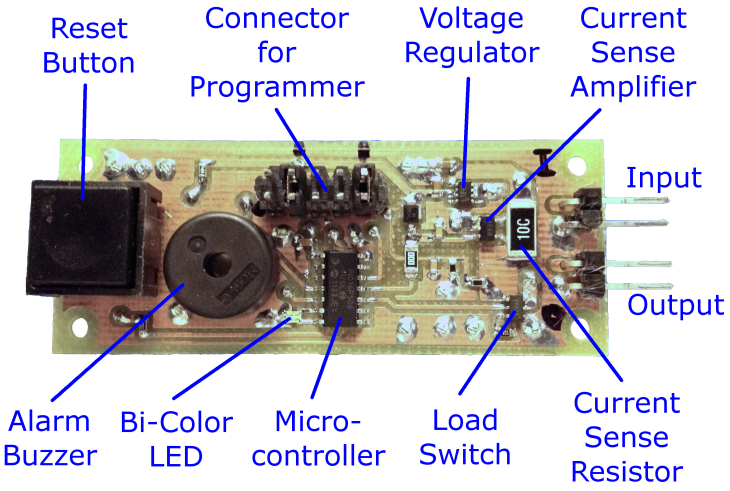


**Figure 19 PCBC Circuit Board**

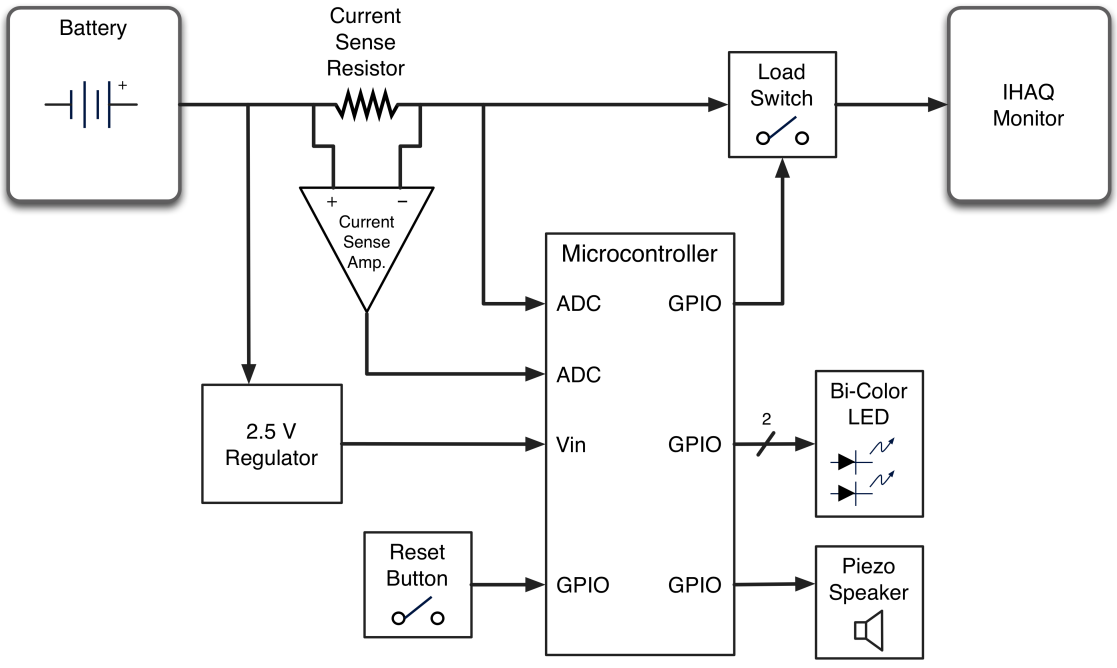


**Figure 20 PCBC Block Diagram**

Figure 20 shows a functional block diagram of the PCBC. At the heart of the PCBC is a PIC16F506 8-bit microcontroller featuring an 8-bit ADC, 12 I/O pins, a built-in clock oscillator, a very low power sleep mode, and a configurable watchdog timer (WDT) that can wake the processor out of sleep mode. A low dropout, low quiescent current LT3008 voltage regulator provides a constant 2.5 V supply voltage to the microcontroller over the full range of battery voltage. A pushbutton switch, a piezo speaker, and two LEDs connected to the microcontroller's GPIO pins comprise a simple user interface. An SI3681BDV low on-resistance, high-side load switch connected to another GPIO pin controls the battery pack output.

The microcontroller measures the battery voltage via one of its ADC inputs. The battery voltage is level-shifted into the ADC's input voltage range via a voltage divider. The resistors used in the divider were selected to minimize energy usage while giving a level conversion ratio that accommodates a battery with up to 8 standard or alkaline cells. The full range of the ADC is used, providing 51.4 mV resolution.

For current measurements, the output of a MAX9634 high-precision current sense amplifier is connected to another ADC input. The input of the amplifier is connected across a high-precision, 0.1-ohm shunt resistor that is in series with the load (the monitor). The common-mode voltage present between the amplifier's inputs and ground provides the supply voltage for the amplifier. The amplifier's voltage gain of 50 allows measurement of currents up to approximately 500 mA with 1.96 mA resolution. Half of the ADC input voltage range is utilized for the current range expected during normal monitor operation, leaving sufficient headroom to detect the higher current present when the monitor's internal battery is being charged.

The amplifier's maximum output, which is internally clamped to 6 V, could appear if the battery pack's output is short-circuited. Considering the low supply voltage used with the microcontroller, 6 V greatly exceeds the maximum ADC input voltage, which should be no more than 0.3 V above the supply voltage. To prevent damage to the microcontroller, a diode is placed between the ADC input and the microcontroller's supply voltage input. The MBRM120E Schottky diode was selected for its combination of low forward voltage and very low reverse leakage current. The diode allows the supply voltage to increase if the amplifier's output voltage exceeds the normal supply voltage, thus maintaining an acceptable difference between the ADC input voltage and the supply voltage. When this occurs, the firmware can still detect that the current is above the shutdown threshold and take immediate action to disconnect the load.

The firmware controls the battery pack output via an SI3681BDV load switch. The load switch employs an n-channel MOSFET to provide level conversion between the GPIO signal from the microcontroller and the gate of a high-current, low on-resistance p-channel MOSFET that switches the load. To turn on the output, the firmware puts the GPIO pin connected to the load switch into the high state.

**Table 7: PCBC LED Indications**

| LED Color | LED Flash Interval (s) | Meaning | Output On/Off |
|---|---|---|---|
| Green | 4 | Battery voltage > 9.0 V, no load detected | On |
| Yellow | 4 | 6.9 V < Battery voltage ≤ 9.0 V, no load detected | On |
| Green | 2 | Battery voltage > 9.0 V | On |
| Yellow | 2 | 6.9 V < Battery voltage ≤ 9.0 V | On |
| Red | 1 | Battery voltage ≤ 6.9 V for 594 ms or longer | Off |
| Red | 1, double flash | Monitor UVLO detected | Off |
| Red | 0.2 | Over-current condition detected | Off |
| Due to microcontroller WDT tolerance, the flash intervals can vary by -50% to +100%. However, the relationships between the intervals will be maintained (e.g., the intervals will be 8 s, 4 s, 2 s, and 0.4 s if the variance is +100%). | | | |

## 6.5 PCBC Low-Power Design Methodology

### 6.5.1 Overview

The PCBC is a good example of a device for which minimizing energy usage was considered from design inception. Apart from providing the needed functionality, the most important design criterion for the PCBC is that it not reduce battery service life through its own energy usage. To minimize the energy used by the PCBC, low-power design techniques were employed from the initial concept through building and debugging the first prototype. The techniques included selecting low-power devices, selecting a microcontroller operating voltage and clock frequency that would minimize power consumption, minimizing current flow through passive components such as resistors in voltage dividers, and designing the firmware to take advantage of the microcontroller's sleep mode as much as possible.

### 6.5.2 Microcontroller Operating Voltage Selection

The PIC16F506 microcontroller will operate with a supply voltage $V_{dd}$ from 2.0 V to 5.5 V. For the PCBC, 2.5 V was selected as the supply voltage to reduce power use while still providing adequate functionality. With a clock frequency of 4 MHz, the supply current at 2.5 V is typically only 250 µA while at 5 V, the current would be 625 µA.

Although the supply current at 2.5 V is greater than the supply current of 175 µA at 2.0 V, the higher voltage offers several advantages. Operating the microcontroller at 2.5 V provides sufficient voltage output from its GPIO pins to directly drive a red or green LED. With $V_{dd}$ = 2.5 V, the GPIO output of $V_{dd} - 0.7 = 1.8$ V causes adequate current flow through the LEDs used in the PCBC yet does not require a current-limiting resistor, thus saving energy and reducing component count. The GPIO output voltage is also sufficient to drive the load switch and the piezoelectric speaker. Additionally, the ADC input voltage range of 0 V to $V_{dd} + 0.3 = 2.8$ V accommodates the output of the current sense amplifier such that currents up to approximately 500 mA can be measured without the need for level conversion.

### 6.5.3 Microcontroller Clock Frequency Selection

The microcontroller could be clocked at 32 kHz, and the data sheet figures show that the required supply current is much lower at that speed. However, to operate at 32 kHz, an external resonator would be needed, and firmware instruction execution would take much longer, which would result in greater energy usage. Using its 4 MHz internal clock, the microcontroller can execute instructions 125 times faster than with a 32 kHz

clock, but the supply current is only 16 to 18 times higher at 4 MHz. This suggests that the overall energy usage could be lower at the higher clock frequency.

An energy-use comparison of the two clock frequencies is very revealing. For the comparison, let $N = 250$ be the number of instructions that are executed each time the PCBC wakes up to check the input voltage and output current, and assume that one instruction is executed every four clock cycles (as is the case with the PIC16F506). For clock frequency $f = 4$ MHz, the length of time $T_{awake}$ that the processor would be awake for each check is

$$T_{awake} = \frac{4N}{f} = \frac{4(250)}{4\times10^{6}} = 250\ \mu\text{s}. \tag{6.1}$$

With a 4 MHz clock, the required supply current $I_{dd}$ is 250 µA. The energy $E$ required for each voltage and current check would then be

$$E = V_{dd}I_{dd}T_{awake} = (2.5)(250\times10^{-6})(250\times10^{-6}) = 0.156\ \mu\text{J}. \tag{6.2}$$

With a clock frequency $f = 32$ kHz, the processor would be awake for

$$T_{awake} = \frac{4(250)}{32\times10^{3}} = 31.2\ \text{ms}. \tag{6.3}$$

At that clock speed, the required supply current is only 15.4 µA, but the total energy required for each voltage and current check would be

$$E = (2.5)(15.4\times10^{-6})(31.2\times10^{-3}) = 1.21\mu\text{J}. \tag{6.4}$$

Based on these first-order calculations, almost eight times more energy would be needed with the 32 kHz clock.

Clock frequencies up to 20 MHz are possible, but frequencies over 8 MHz would require an external resonator or oscillator. Adding a resonator or oscillator would increase component count, and an oscillator would increase energy usage. Also, the microcontroller's device reset timer (DRT) period is set to 18 ms when an external oscillator is used but is only 1.125 ms when an external RC circuit or the internal oscillator is used. The longer DRT period is needed with an external oscillator to allow the oscillator to stabilize before instruction execution begins. The DRT period becomes very significant when the microcontroller goes through a sleep/wake cycle frequently, which is the case in the PCBC. The DRT is triggered when the WDT expires while the microcontroller is in the low-power sleep state, and it does not allow instruction execution to resume until the DRT period expires. Because the PCBC makes extensive use of sleep mode and WDT wakeups, much time and energy would be wasted while out of low-power sleep mode, waiting for the 18-ms DRT period to expire after each wakeup.

The internal oscillator can operate at 4 MHz or 8 MHz, is accurate enough for the PCBC, and requires no external components. Additionally, the PIC16F506 data sheet does not specify any additional current flow when the internal oscillator is enabled. 8 MHz is on the borderline of allowable clock frequencies when the PIC16F506 is operated at 2.5 V, so 4 MHz was chosen.

### 6.5.4 Minimizing Current through Passive Components

To minimize current flow, high resistances are used in the voltage divider that level shifts the battery voltage for the microcontroller's ADC input. Because the effective impedance of the voltage divider is much higher than the maximum impedance specified for the ADC, a capacitor was added across the ADC input to minimize voltage

sag during the ADC conversion process. The resulting RC low-pass filter does not adversely affect the measurements.

The PCBC includes a reset switch accessible from outside the external battery enclosure. The switch allows the battery output to be re-enabled easily if a high-current shutdown is triggered when the battery is first connected to the monitor. The reset switch circuit is designed so that only a very low leakage current (typically 1 μA) flows through the associated GPIO pin when the switch is not pressed.

At $V_{dd} - 0.7 = 1.8$ V, the current flow through each LED is much less than the 20 mA maximum specified in the LED data sheet but still adequate to produce a bright light. The LED data sheet's I-V graphs show that approximately 1 mA will flow through the red LED and 2.5 mA will flow through the green LED when the forward voltage is 1.8 V. However, even with the reduced current flow, the LEDs would consume more energy than all the other PCBC components combined if they were illuminated continuously. To reduce the energy consumption while still providing an easily discernable visual indication, the LEDs are flashed briefly rather than illuminated steadily. With a flash repetition rate of only 0.5 Hz (one flash every 2 seconds, the rate used during normal PCBC operation) and a flash duration of approximately 25 ms, the duty cycle is only 1.25%. Assuming a total LED current of 3.5 mA when illuminating both LEDs, the average current flow through the LEDs would be only 44 μA.

### 6.5.5 Firmware Design

As with the hardware, the PCBC firmware was designed to minimize energy usage. Except when sounding the high-current alarm buzzer, which can occur for only 10 seconds before the PCBC enters a shutdown state, energy-wasting timing loops are not

used. Rather, the timing for various intervals is performed using the microcontroller's low-power sleep mode and WDT. During startup, the firmware configures the WDT to have a nominal timeout period of 25 ms. When a delay is required, such as the delay between LED flashes, the firmware maintains the microcontroller in sleep mode between measurement tasks and counts the number of times that the microcontroller wakes up in response to a WDT timeout. When the count reaches the threshold defined for the delay interval, the firmware performs the necessary work. An LED flash is performed by turning on the LED immediately before putting the microcontroller in sleep mode, leaving it on for the duration of one 25 ms WDT timeout period, then turning it off when the microcontroller wakes up. This approach results in a very low, energy-saving LED duty cycle while still providing an easily visible flash.

The firmware was developed using the Microchip MPLAB X integrated development environment and XC8 compiler. Although the operation of the firmware is designed to minimize energy usage, readability and maintainability were of primary concern when selecting the programming language and designing the program code structure. The C programming language was chosen over assembly language to speed development and facilitate code maintenance by someone unfamiliar with the PIC assembly language. To make the code more readable and to facilitate porting the code to other PIC microcontroller models, macros are used for model-specific operations such as setting a GPIO or reading the ADC. The main processing loop uses a state machine structure to clearly express the processing that takes place in each state and the transitions between states. The C language and state machine require more program memory than a linear program flow written in assembly language, but the program still fits in the

microcontroller's flash memory with room to spare and is much easier to understand and maintain. The firmware occupies 803 of the 1024 available 12-bit words of program flash memory. Variable storage consumes 29 of the 67 available bytes of RAM memory.

### 6.6 PCBC Energy Usage

To validate the design and to facilitate development of the firmware, the PCBC was first implemented using a PIC16F887 microcontroller on a commercial development board. The remainder of the PCBC system was constructed on a prototyping board using non-low-power components that were on hand. Although this initial prototype consumed much more energy than the final version constructed with low-power components, it provided a source for timing measurements that were used to estimate the energy usage of the low-power design. After the PCBC was constructed using the selected low-power components and the firmware was debugged and tested on the PIC16F506, the estimate was refined using timing measurements on the new prototype. The actual energy usage was then measured using the capacitor-discharge method.

**Table 8: Data for PCBC Energy Usage Estimation**

| Parameter | Symbol | Source | Value |
|---|---|---|---|
| the watchdog timeout--the interval between wake-ups | $T_{WDT}$ | Meas. | 25.2 ms |
| how long the system is not sleeping after wake-up when Vout is high, no LED flash | $T_1$ | Meas. | 301.5 µs |
| how long the system is not sleeping after wake-up when Vout is high, with LED flash | $T_2$ | Meas. | 325.5 µs |
| the LED flash interval when no load is detected | $T_F$ | F/W | 5.5944 s (stby.)<br>2.7972 s (on) |
| approx. how long the LED is on | $T_L$ | (6.5) | 25.224 ms |
| microcontroller awake duty cycle | $D_W$ | (6.9) | 1.1964% |
| microcontroller sleep duty cycle | $D_S$ | (6.10) | 98.804% |
| LED duty cycle | $D_L$ | (6.11) | 0.45088% (stby.)<br>0.90176% (on) |
| input (battery) voltage | $V_{IN}$ | Meas. | 12.0 V |
| microcontroller supply voltage | $V_{DD}$ | Meas. | 2.5 V |
| maximum supply current (awake) | $I_{DD}$ | IDSV | 412.50 µA |
| maximum WDT current | $I_{WDT}$ | IDSV | 5.1667 µA |
| maximum ADC conversion current | $I_{ADC}$ | IDSV | 166.67 µA |
| maximum power-down (sleep) current | $I_{PD}$ | IDSV | 1.4 µA |
| maximum regulator quiescent current | $I_Q$ | DS | 6 µA |
| maximum regulator gnd. current, PIC awake | $I_{GNDW}$ | IDSV | 32.450 µA |
| maximum regulator gnd. current, PIC asleep | $I_{GNDS}$ | IDSV | 6.3940 µA |
| maximum regulator gnd. current, LED on | $I_{GNDL}$ | IDSV | 50.328 µA |
| LED current, green only | $I_{LED}$ | DS | 1.0000 mA |
| voltage divider current | $I_{DIV}$ | Calc. | 14.286 µA |
| current sense amplifier supply current | $I_{AMP}$ | IDSV | 682.61 µA |
| total PCBC sleep current | $I_{SYSS}$ | (6.6) | 33.929 µA |
| total PCBC awake current, LED not on | $I_{SYSW}$ | (6.7) | 637.75 µA |
| total PCBC awake current, LED on | $I_{SYSWL}$ | (6.8) | 1.6556 mA |
| average PCBC system current | $I_{SYSAVG}$ | (6.12) | 45.860 µA (stby.)<br>50.567 µA (on) |

Source abbreviations: (-.-), equation; Calc., simple calculation; DS, datasheet; F/W, firmware source code; IDSV, interpolated using datasheet values; Meas., measurement

Five figures are shown for most intermediate values to facilitate reproducing the calculations. However, the data sheet values and measurement precision do not provide five significant figures.

6.6.1 Energy Usage Estimate

Table 8 lists the measurements, data sheet values, and calculation results associated with estimating the PCBC's energy usage. The values for $T_1$ and $T_2$ were obtained by measuring with an oscilloscope the periods of pulses representing the periods when the microcontroller is awake (i.e., not in sleep mode). The pulses are generated by turning on a GPIO signal configured for output whenever the microcontroller comes out of sleep mode and turning off the signal just prior to putting the microcontroller in sleep mode. $T_{WDT}$ was determined by measuring the period between pulses. As defined in the firmware, the flash interval $T_F$ is 222 × $T_{WDT}$ seconds in standby mode and 111 × $T_{WDT}$ seconds when a load is detected.

To flash an LED, the LED is turned on just prior to putting the microcontroller in sleep mode and turned off just after the microcontroller comes out of sleep mode in response to a WDT timeout. $T_L$, the period of each LED flash (in seconds), is calculated in Eq. (6.5) as the length of the WDT timeout period plus an estimate of the time spent in the LED-specific code. The estimate is the difference between $T_2$, the length of time the microcontroller is awake when an LED is flashed, and $T_1$, the length of time it is awake when an LED is not flashed.

$$T_L = T_{WDT} + (T_2 - T_1) \tag{6.5}$$

To calculate the microcontroller currents, data sheet values for $V_{DD}$ = 5.0 V and $V_{DD}$ = 2.0 V were used to interpolate the currents at $V_{DD}$ = 2.5 V. The regulator ground currents were interpolated from data sheet values defined for the corresponding load current range. For example, $I_{GNDW}$ was interpolated from the range of ground currents for

a load current between 100 µA and 1 mA. The current sense amplifier supply current $I_{AMP}$ was interpolated from data sheet values for $V_{IN}$.

The current for each microcontroller power mode—sleep, awake with LED off, awake with LED on—are calculated using Eq. (6.6) through Eq. (6.8). The duty cycle of each mode must be known to calculate the overall average current. The duty cycles are calculated using Eq. (6.9) through Eq. (6.11). Using the individual current values and the duty cycle values, the average PCBC supply current is given by Eq. (6.12).

$$I_{SYSS} = I_{PD} + I_{GNDS} + I_{WDT} + I_Q + I_{DIV} + I_{AMP} \tag{6.6}$$

$$I_{SYSW} = I_{DD} + I_{ADC} + I_{GNDW} + I_{WDT} + I_Q + I_{DIV} + I_{AMP} \tag{6.7}$$

$$I_{SYSWL} = I_{DD} + I_{ADC} + I_{LED} + I_{GNDL} + I_{WDT} + I_Q + I_{DIV} + I_{AMP} \tag{6.8}$$

$$D_W = \frac{T_1}{T_{WDT}} \tag{6.9}$$

$$D_S = 1 - D_W \tag{6.10}$$

$$D_L = \frac{T_L}{T_F} \tag{6.11}$$

$$\begin{aligned} I_{SYSAVG} = {} & D_W(I_{DD} + I_{ADC} + I_{GNDW}) + (D_S - D_L)(I_{PD} + I_{GNDS}) \\ & + D_L(I_{PD} + I_{LED} + I_{GNDL}) + I_{WDT} + I_Q + I_{DIV} + I_{AMP} \end{aligned} \tag{6.12}$$

Using the data sheet maximum values shown in Table 8, the average PCBC supply current when in standby mode (i.e., the monitor is not connected) is estimated to be 46 µA, and the current in normal mode (i.e., the monitor is connected and turned on) is estimated to be 51 µA. Considering that the minimum monitor input current is approximately 45 mA at 12 V, the estimated supply current required by the PCBC is

approximately three orders of magnitude lower and therefore will have an insignificant impact on monitor operating time.

### 6.6.2 Energy Usage Measurement

To calculate the PCBC power and energy requirements, the average supply current was measured using the capacitor discharge method described in Section 2.4. An electrolytic capacitor with a marked value of 2,200 μF was used. Because electrolytic capacitors typically have a very wide tolerance [27], the actual value of the capacitor was measured using two different methods: charging with a constant-current and discharging through a known resistance.

#### 6.6.2.1 Capacitance Measurement Using Constant Charging Current

The relationship between charge $Q$, voltage $V$, and capacitance $C$, as expressed by

$$Q = CV, \tag{6.13}$$

can be used to determine $C$ if $Q$ and $V$ are known. If a capacitor is charged with a constant current of $I$ amperes (i.e., coulombs per second) for $t$ seconds, then the charge, which is measured in coulombs, is simply $I$ multiplied by $t$. The relationship can be expressed as

$$C = \frac{It}{V}. \tag{6.14}$$

Because the relationship is linear,

$$C = \frac{I\Delta t}{\Delta V} \tag{6.15}$$

also holds, which allows some flexibility with the initial and final voltages.

For the measurements, an HP E3631A regulated power supply provided a nominally constant current, and the apparatus described in Section 7.1.2 measured the voltage, current, and elapsed time. Setting the supply's output voltage to 14 V and output current to 1 mA or 3 mA configured the supply as a constant current source over the desired voltage range. Three tests were performed with each current limit, and the calculated capacitance results of all the tests were averaged. Capacitor leakage current was not considered.

The voltage and current recorded during one of the 3-mA tests are shown in Figure 21a. The current plot shows a large amount of noise, which is probably due to operating the E3631A very close to its lower current limit. The average currents were approximately 0.8 mA during the 1-mA tests and 3.3 mA during the 3-mA tests. The average current for each test was used in the corresponding capacitance calculation. The result from each test is shown in Table 9. The mean capacitance is 2,423 μF, and the range is 109 μF.

**Table 9: Results from Constant-Current Charging Tests**

| Test No. | Avg. $\underline{I}$ (mA) | $\Delta V$ (V) | $\Delta t$ (s) | $C$ (μF) |
|---|---|---|---|---|
| 1 | 3.308 | 13.09 | 9.825 | 2482 |
| 2 | 3.351 | 13.09 | 9.600 | 2458 |
| 3 | 3.342 | 12.94 | 9.575 | 2473 |
| 4 | 0.7950 | 13.13 | 39.23 | 2375 |
| 5 | 0.7990 | 13.14 | 39.03 | 2374 |
| 6 | 0.8050 | 13.13 | 38.70 | 2373 |

6.6.2.2 Capacitance Measurement Using Discharge Through A Known Resistance

When a capacitor discharges through a resistance *R*, the time-varying voltage *v*(*t*) is given by

$$v(t) = V_0 e^{-\frac{t}{\tau}}, \tag{6.16}$$

where $\tau = RC$, *t* is the elapsed time since the discharge started, and $V_0$ is the initial voltage when $t = 0$. Since $v(\tau) = V_0 e^{-1} = 0.3679 V_0$, it is only necessary to find the value of *t* when the voltage across the capacitor is 36.79% of its initial value in order to determine the capacitance. Figure 21b depicts this graphically. Setting $\tau$ equal to the value found for *t*, C can then be calculated with

$$C = \frac{\tau}{R}. \tag{6.17}$$

To determine the capacitance using this method, the capacitor was charged until the voltage across its terminals reached approximately 13 V, then the power supply was disconnected and the capacitor allowed to discharge through a resistor. To supply the charging current, the E3631 power supply was configured for a maximum output of 13 V and its output current was limited to 10 mA. The resistor, which had been measured at 15.789 kΩ, remained connected to the capacitor during charging and discharging. An oscilloscope measured and recorded the voltage across the capacitor. Four tests were performed, but in one of the tests, the voltage failed to reach the desired level during charging so the results were discarded. The results of the three successful tests appear in Table 10. Using these results, the mean capacitance is 2500 μF and the range is 17 μF.

To evaluate the effect of the oscilloscope probe resistance and the capacitor's self discharge due to leakage current, the test was repeated without the resistor connected. The dashed orange curve in Figure 21b shows the result. The very small voltage decrease over the time period $\tau$ suggests that the error resulting from the probe current and capacitor leakage current is not significant.

**Table 10: Results of the Capacitor Discharge Through Known Resistance Tests**

| Test No. | $V_0$ (V) | $v(\tau)$ (V) | $\tau$ (s) | $C$ (µF) |
|---|---|---|---|---|
| 1 | 12.633 | 4.6474 | 39.605 | 2508 |
| 2 | 12.629 | 4.6459 | 39.334 | 2491 |
| 3 | 12.629 | 4.6459 | 39.502 | 2502 |

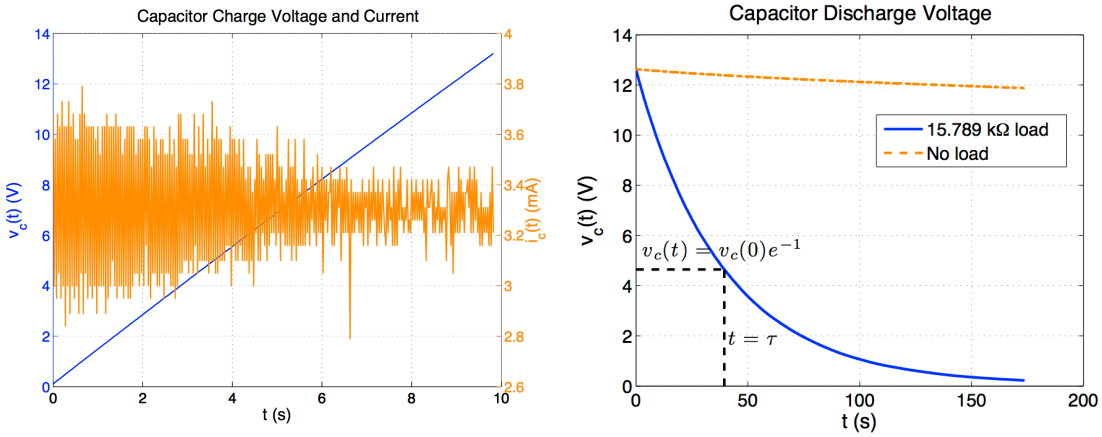


(a) (b)

**Figure 21 Voltage Across Load-Test Capacitor While Charging and Discharging**

6.6.2.3 Energy Usage Measurement Using Capacitor Discharge Method

Applying the relationship in Eq. (6.15) and using the mean capacitance value of 2448 μF that was obtained by averaging the results of the four charging tests and the three discharging tests, the average PCBC supply current can be calculated with

$$I = \frac{C\Delta V}{\Delta t} \ . \tag{6.18}$$

The apparatus and procedure used for the capacitor discharge tests to determine the capacitor's value were also used to determine the energy usage of the PCBC. The PCBC was connected to the capacitor in place of the resistor. $\Delta V$ and $\Delta t$ were measured as the capacitor supplied current to operate the PCBC. Three 200-second tests were performed to take advantage of a faster sampling rate by the oscilloscope, and two 500-second tests were performed to measure the voltage until the PCBC ceased functioning due to the supply voltage being too low. The results appear in Table 11, and a graph of the voltages measured in one of the 500-second tests is shown in Figure 22. The sampling rate for the 200-second tests was 2,500 samples per second, and the rate for the 500-second tests was 1,000 samples per second. Current was calculated using the time and voltage deltas for an entire operating mode period. Average power $P$ was calculated with

$$P = \frac{C(V_1^2 - V_2^2)}{2\Delta t} \ , \tag{6.19}$$

where $V_1$ is the voltage at the start of the period and $V_2$ is the voltage at the end of the period for which the average power was being calculated.

The mean current value of 64.9 μA shown in the "$V \geq 9$" column of Table 11 corresponds to the average PCBC supply current when operating in the standby-normal mode. It can be compared to the 46 μA estimate in Section 6.6.1. Considering that the estimate is based on data sheet maximum values, the measured current is substantially higher than expected. The reason for this is not clear. However, the measured current is still almost three orders of magnitude less than the monitor current, so the impact of the PCBC on monitor operating time should be negligible.

Three distinct slopes can be seen in the voltage plot in Figure 22, indicating that the average current depends on the PCBC's operating mode. Since no load was connected to the PCBC during the tests, it operated in standby modes until the voltage dropped below the low-voltage turn-off threshold, at which it operated in shutdown mode. The steeper slope when the voltage is between the warning and turn-off voltage thresholds is due to flashing both the red and green LEDs to produce yellow. In the visible stair-step pattern, the sharp drops correspond to LED flashes and the relatively flat steps correspond to the time between flashes. This indicates that the LEDs consume substantially more power than the rest of the PCBC. The stair-step pattern is not visible after the low-voltage shutdown has been reached because the faster flashing rate of the red LED in shutdown mode causes the line to appear smooth at the resolution of the graph.

One might expect power to be much higher in warning or shutdown mode as suggested by the higher current, the voltage line slope, and because two LEDs are flashed in warning mode or one LED is flashed rapidly in shutdown mode. However, the average power consumed in those two modes is less than the power consumed in normal

mode because less power is lost in the 2.5-V series regulator at the lower battery voltages. This also explains why the average warning-mode power is lower in the 500-second tests: The 500-second tests allowed longer operation in warning mode thus operation at a lower battery voltage is included in the average.

**Table 11: PCBC Current and Power Measurement Results**

| Test No. | Duration | $V \geq 9$ | | $6.8 \leq V < 9$ | | $V < 6.8$ | |
|---|---|---|---|---|---|---|---|
| | | I (µA) | P (µW) | I (µA) | P (µW) | I (µA) | P (µW) |
| 1 | 200 s | 66.9 | 726 | 74.9 | 621 | - | - |
| 2 | 200 s | 64.6 | 700 | 77.9 | 650 | - | - |
| 3 | 200 s | 63.5 | 689 | 80.4 | 672 | - | - |
| 4 | 500 s | 64.6 | 701 | 73.1 | 585 | 106 | 511 |
| 5 | 500 s | 65.2 | 707 | 75.3 | 602 | 104 | 505 |
| Mean | | 64.9 | 705 | 76.3 | 626 | 105 | 508 |
| Range | | 3.4 | 37 | 7.3 | 87 | 2 | 6 |

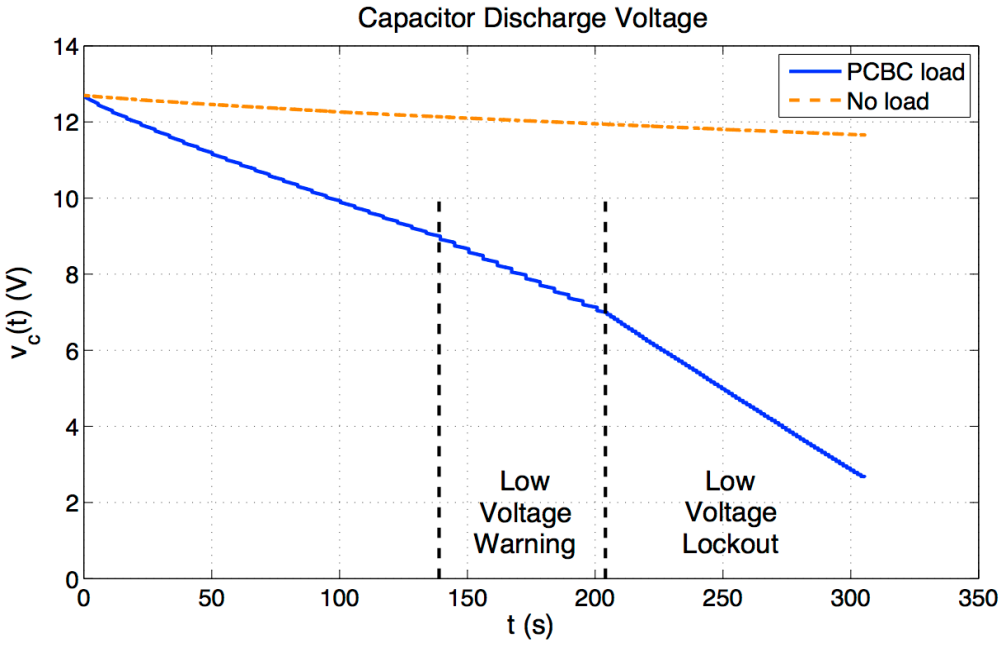


**Figure 22 Voltage Across Discharge-Test Capacitor While Powering the PCBC**

# CHAPTER SEVEN: RESULTS

The effects of the modifications to the IHAQ monitor and the performance of the external battery were evaluated through a series of operating-time tests. This chapter describes the tests and presents the results. An analysis of the effects of the energy-reduction modifications on measurement data quality is also given.

## 7.1 Operating Time Test Description

### 7.1.1 Overview

To evaluate the effects of the hardware, firmware, and configuration changes on the battery-powered operating time of the IHAQ monitor and to determine if the external battery could provide sufficient operating time to meet the eight-day goal, numerous battery discharge tests were performed. Test details are listed in Table 12. The tests are grouped into the following four categories:

I. Tests performed using eight inexpensive, standard (non-alkaline) AA-size cells to evaluate the relative effects of hardware and firmware changes

II. Tests that measure the operating times obtainable with an eight D-size alkaline cell battery pack

III. Tests that measure the operating times obtainable using only the monitor's internal Li-ion battery

IV. Tests of various numbers, sizes, and types of cells to evaluate different external battery pack configurations.

Low-capacity AA-size cells were used for all of the category I tests to reduce testing time while still giving results that are generally representative of primary battery behavior. The results show the relative effects of hardware modifications and different monitor configurations. However, they do not show the actual operating time that would be obtained with the external 8 D-cell battery or the internal Li-ion battery.

The category II tests provide the operating time measurements that can be used to predict the additional operating time provided by the external battery pack. These tests were performed with the configurations and cell types that are recommended for use when an IHAQ monitor is deployed in a home. The category III test results can be used to predict operating time provided by the internal Li-ion battery. Because the monitor normally includes an internal battery, the actual operating time that could be expected with an external battery is roughly the sum of the operating time provided by the internal battery and the time provided by the external battery, assuming that the internal battery is fully charged when operation commences.

The category IV tests were performed using a variety of common cell sizes and two different cell types—standard or alkaline—to measure the relative operating times that can be achieved with different external battery configurations. The number, size, and type of cells used in each test are shown in Table 12. Inexpensive, “dollar store” Sunbeam-brand cells were used, so the results likely represent the minimum operating time that can be expected for each battery configuration.

**Table 12: Operating Time Test Parameters and Results**

| Test No. | Description | H/W Mod | Fan Duty % | $CO_2$ Idle | Zig-Bit | Battery | Avg. Pwr (mW) | Op. Time (hrs.) | Plot Color | Plot Fig. |
|---|---|---|---|---|---|---|---|---|---|---|
| Category I Tests | | | | | | | | | | |
| 1 | Std. config. (baseline) | None | 100 | No | Yes | 8 AA | 1,143 | 5.7 | Orange | 26, 27 |
| 2 | Semi-low-power | All | 33 | No | No | 8 AA | 757 | 10.6 | Light green | 26 |
| 3 | Semi-low-power | All | 33 | Yes | Yes | 8 AA | 754 | 10.9 | Red | 26 |
| 4 | Low power | LEDs | 33 | Yes | No | 8 AA | 664 | 11.8 | Dark blue | 26 |
| 5 | Low power | LEDs, UVLO dly. | 33 | Yes | No | 8 AA | 663 | 12.6 | Violet | 27 |
| 6 | Low-power | All | 33 | Yes | No | 8 AA | 662 | 13.0 | Dark green | 26, 27, 30 |
| 7 | Very low power | All | 8.3 | Yes | No | 8 AA | 559 | 16.3 | Light blue | 26 |
| Category II Tests | | | | | | | | | | |
| 8 | Std. config. (baseline) | None | 100 | No | Yes | 8 D | 1,233 | 110.4 | Dark blue | 28 |
| 9 | Low power | LEDs | 33 | Yes | No | 8 D | 685 | 221.6 | Dark green | 28 |
| 10 | Low power #63 | None | 33 | Yes | No | 8 D | 722 | 216.1 | Purple | 28 |
| 11 | Very low power | All | 8.3 | Yes | No | 8 D | 558 | 282.1 | Light blue | 28 |
| Category III Tests | | | | | | | | | | |
| 12 | Std. config. (baseline) | LEDs | 100 | No | Yes | Li-ion | - | 8.3 | Orange | 29 |
| 13 | Std. config. | LEDs | 100 | No | Yes | Li-ion | - | 8.3 | Light green | 29 |
| 14 | Low power | LEDs | 33 | Yes | No | Li-ion | - | 14.9 | Dark green | 29 |
| 15 | Very low power | LEDs | 8.3 | Yes | No | Li-ion | - | 16.7 | Violet | 29 |
| 16 | Very low power | LEDs | 8.3 | Yes | No | Li-ion | - | 16.8 | Light blue | 29 |
| Category IV Tests | | | | | | | | | | |
| 17 | Low power | All | 33 | Yes | No | 8 std. AAA | 664 | 4.7 | Dark red | 30 |
| 18 | Low power | All | 33 | Yes | No | 8 alk. AAA | 653 | 15.2 | Dark blue | 30 |
| 19 | Low power | All | 33 | Yes | No | 6 alk. AA | 615 | 19.7 | Purple | 30 |
| 20 | Low power | All | 33 | Yes | No | 8 std. C | 655 | 31.6 | Gold | 30 |
| 21 | Low power | All | 33 | Yes | No | 8 alk. AA | 661 | 34.3 | Violet | 30 |
| 22 | Low power | All | 33 | Yes | No | 10 alk. AA | 696 | 41.9 | Light green | 30 |
| 23 | Low power | All | 33 | Yes | No | 8 std. D | 655 | 65.2 | Pink | 30 |

### 7.1.2 Test Apparatus

For external battery operating time tests, separate HP34401A multimeters triggered from a common source measured the external battery voltage and current. A single HP 33120A arbitrary waveform generator provided triggering pulses to both multimeters at 40 Hz, resulting in a synchronized sampling rate of 40 voltage and current samples per second. The multimeters transmitted the measurements via RS-232 to a custom data acquisition program. The program parsed the measurement strings from the multimeters, added time stamps, calculated power for each pair of voltage and current measurements, and wrote the data to a file. MATLAB scripts were used to read and process the files, produce plots, and calculate statistical information. For plotting, the data were smoothed with a moving-average filter to produce values representing the average voltage over a one-minute period. A diagram of the test apparatus showing electrical connections and data flow can be found in Figure 23.

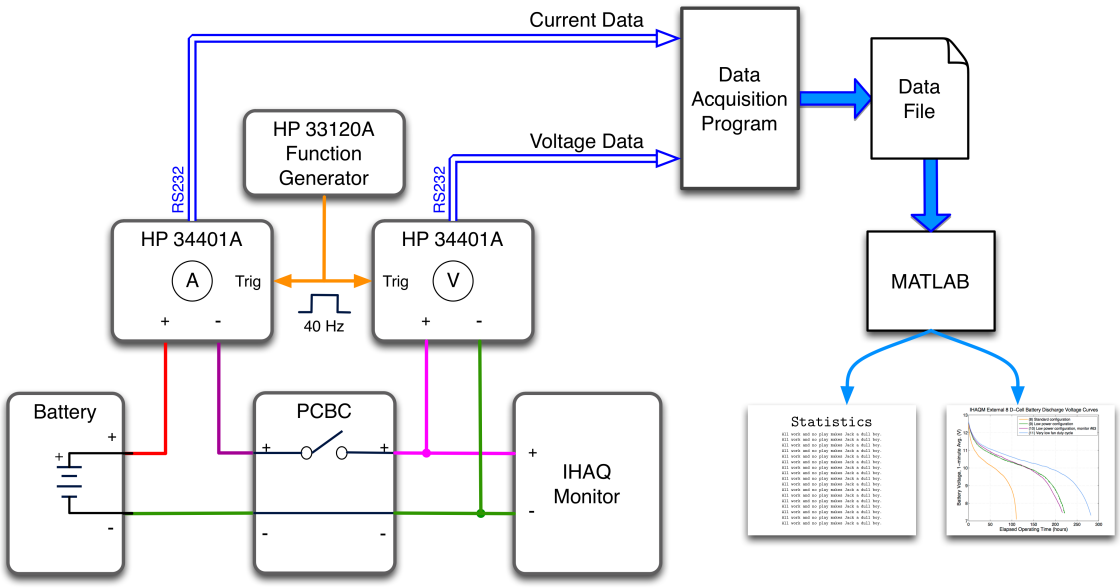


**Figure 23 Operating Time Test Apparatus**

To determine if the 40-Hz sampling rate would be sufficient to accurately measure the monitor's input voltage and current, the spectral content of a signal representing the monitor's input current was examined. The signal was recorded using an oscilloscope to sample the voltage drop across the resistor shown in Figure 13. The recorded signal was then processed in MATLAB to produce a Welch power spectral density (PSD) estimate.

To capture a signal representing normal monitor operation, the input current signal was sampled at 1000 samples per second for 500 seconds. During that period of time, the T6615 $CO_2$ sensor was active and the particle counter fan operated for 20 seconds out of every 60 seconds. The PSD estimate of the signal, which is shown in Figure 24, indicates that the most of the energy in the signal is at DC or very low frequencies. To verify that the input current did not contain significant energy above 500

Hz, another sample was taken over a period of 1 second at 250,000 samples per second. The sample captured continuous operation of the particle counter fan and a single, complete load spike caused by the $CO_2$ sensor. (A $CO_2$ sensor load spike can be seen in Figure 3.) The resulting PSD estimate in Figure 25 indicates that the input current does not contain significant energy at frequencies above those shown in Figure 24.

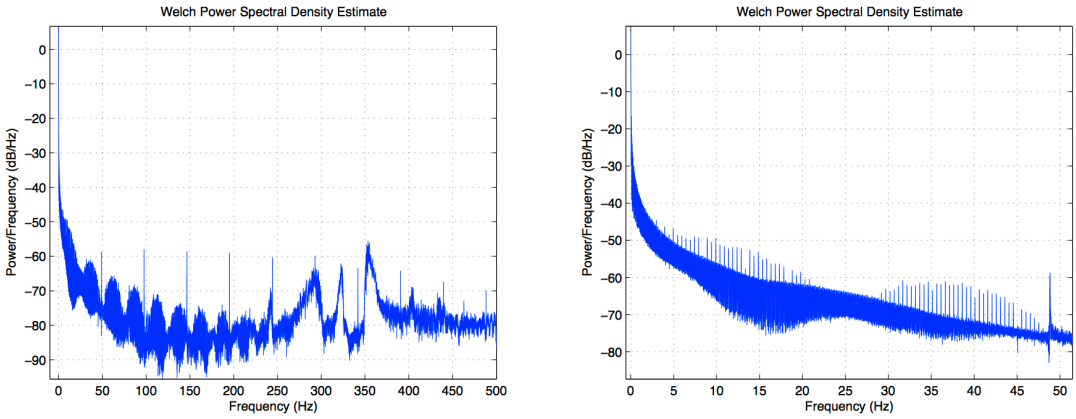


**Figure 24 Welch PSD Estimate of IHAQ Monitor Input Current (to 500 Hz)**

The sampling rate was 1000 samples per second, and the sample length was 500 seconds. The graph on the right is a close-up view of the 0 to 50 Hz range.

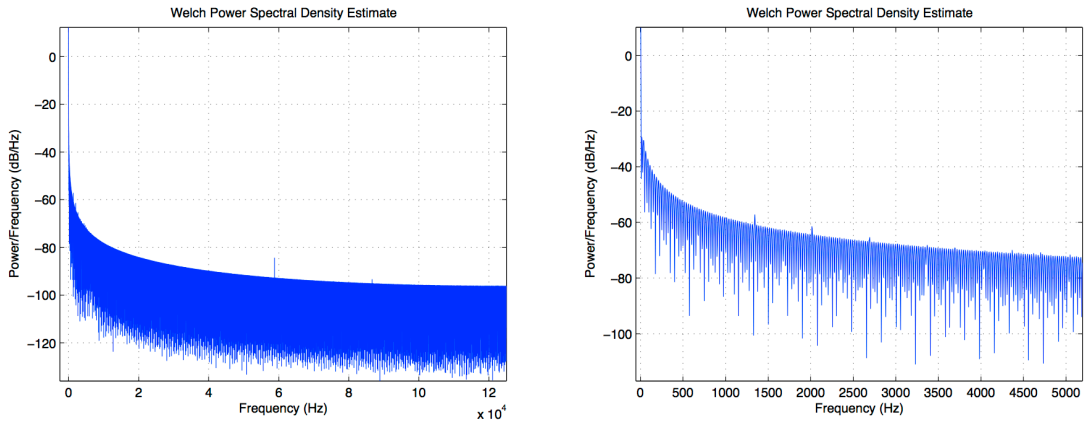


**Figure 25 Welch PSD Estimate of IHAQ Monitor Input Current (to 125 kHz)**

The sampling rate was 250,000 samples per second, and the sample length was 1 second. The labels on the frequency axis of the left graph are in units of 10 kHz. The graph on the right is a close-up view of the 0 to 5 kHz range.

### 7.1.3 Internal Battery Operating Time Measurement

Measurements taken by the IHAQ monitor's internal battery voltage sensor were used to measure operating time and plot the battery discharge voltage curve when the monitor was powered by its internal Li-ion battery. Prior to each internal-battery operating time test, the monitor's internal charging circuit was allowed to charge the battery until the circuit's charging indicator LED extinguished, indicating that the battery had reached full charge. Then, the monitor was turned on and allowed to run until UVLO occurred. MATLAB scripts were used to read the battery voltage measurements recorded in the monitor's data log file, plot the discharge voltage curves, and calculate the operating time. Battery current was not measured.

7.1.4 Test Conditions

The same physical IHAQ monitor unit, which is designated as unit 62, was used for all category I, II, and IV tests unless otherwise noted. An internal Li-ion battery was not installed in the monitor, so the external battery operating times do not include any additional time that could be provided by the internal battery. Unlike newer models, unit 62 has the City Technology A3CO CO sensor, not the Figaro brand sensor. However, energy usage estimates based on data sheet information indicate that similar battery life should be expected with the Figaro sensor. All category III tests were performed with unit 79. The internal LEDs in unit 79 were disabled but the UVLO delay modification was not done. Unit 79 has the Figaro CO sensor and a WiFly module. The WiFly module was held in reset during all tests.

In all tests where the T6615 idle mode was enabled, the sensor was taken out of idle mode 8 seconds before each $CO_2$ measurement was taken. The 33% fan duty cycle (20 seconds on, 40 seconds off) used in most of the low-power tests is somewhat arbitrary and is based on an assumption that 20 seconds of fan operation each minute would allow airflow to stabilize and provide sufficient time for accurate particle counting. An 8.3% fan duty cycle (5 seconds on, 55 seconds off) was chosen for the very low power tests because it is the lowest duty cycle identified that produces particulate concentration measurements without spike artifacts.

## 7.2 Operating Time Test Results

### 7.2.1 Relative Effects of Configuration Changes

Figure 26 shows the results of five tests that demonstrate the effects of several different monitor configurations on operating time.

Tests 2 (light green) and 3 (dark red) show that enabling ZigBee networking or not using the T6615 idle mode have about the same effect on operating time. The long operating time of test 7 (light blue) demonstrates how reducing the fan duty cycle can substantially increase operating time. However, as described in Section 7.3.2, a very low fan duty cycle has a detrimental effect on measurement data quality.

(a)

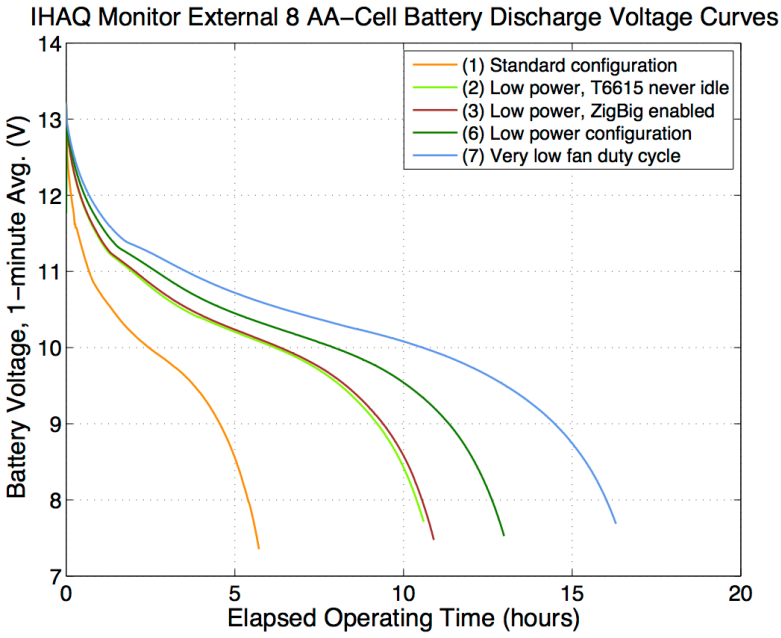


(b)

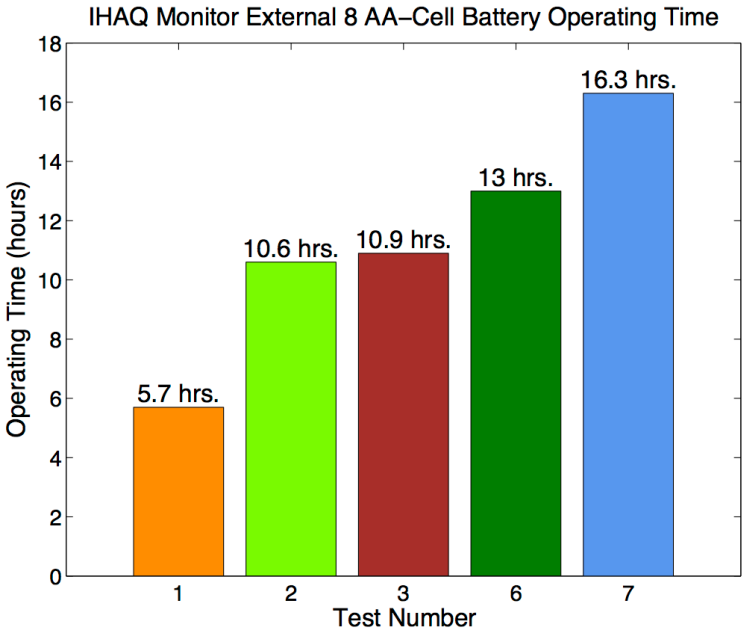


**Figure 26 The Effects of Different Configurations on Operating Time**

(a) shows the battery voltages over time, and (b) shows an operating-time comparison. Test details appear in Table 12.

### 7.2.2 Relative Effects of Hardware and Firmware Modifications

Figure 27 shows the effects of the hardware modification that delays the monitor's internal UVLO and the firmware modification that staggers high-current operations. Delaying the UVLO action to accommodate current spikes and their accompanying voltage drops appears to have increased the operating time by 6.8%. Preventing simultaneous high-current operations—the $CO_2$ sensor being out of idle mode or the particle counter fan and laser running—allowed the input voltage to remain above the UVLO shutdown threshold longer despite a lower average battery voltage, thus providing an additional 3.4% increase in operating time. The higher final voltage of test 4 indicates that the modifications increase operating time by allowing the average battery voltage to be lower before the UVLO threshold is reached.

Although the average power during tests 4, 5, and 6 was practically the same, the discharge curve of test 4 is notably different. It is possible that the reduction of peak current in test 6 could have resulted in an increase in the battery's available capacity due to the rate capacity effect, but the nearly identical discharge curve of test 5, which was performed without peak-current reduction, suggests that was not the case. The lower voltage curve and shorter operating time of test 4 may have been due to differences in the batteries themselves. The batteries were all the same brand and were purchased at the same store, but the batteries used in test 4 were purchased approximately one week prior to those used in tests 5 and 6. Perhaps the batteries were from different manufacturing lots and were subject to process variations or had significantly different ages. If the

batteries used in test 4 indeed had less capacity, the overall increase in running time provided by the two modifications would be approximately 5.7%, not 10.2%

### 7.2.3 Operating Time Obtained with an 8 D-Cell External Battery

The operating times that can be achieved with an external battery pack comprised of eight D-size alkaline cells are depicted in Figure 28. Duracell model MN1300 standard-life alkaline cells were used for all the tests except test 10, while enercell (Radio Shack) model 23-852 standard-life alkaline cells were used for test 10. The results of the tests clearly show that the eight-day continuous operation goal has been exceeded. Tests 9 and 10 were performed using the same configuration on different monitors and with different brands of cells, demonstrating the repeatability of the results. Note that tests 9 and 10 were performed without the PCBC, the UVLO delay modification, and the peak current reduction modification, so an even longer operating time is expected in the future when the same low-power configuration is used.

(a)

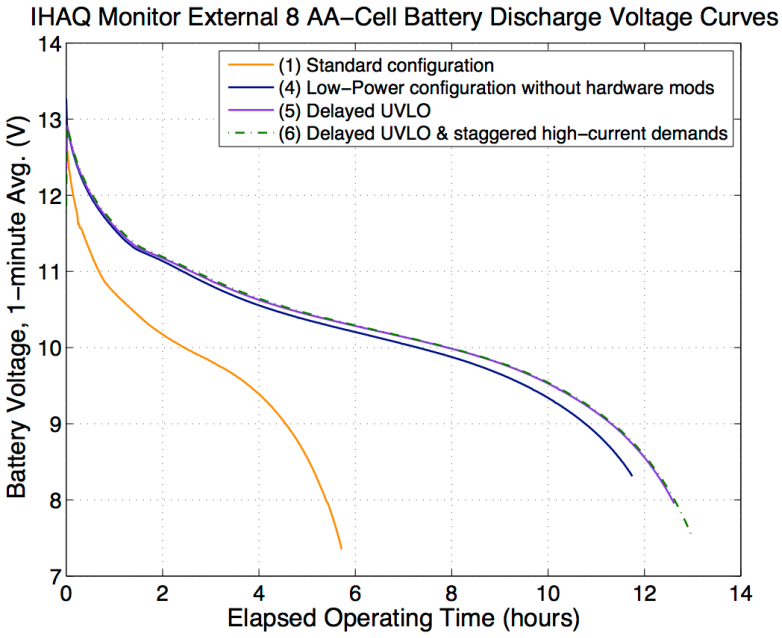


(b)

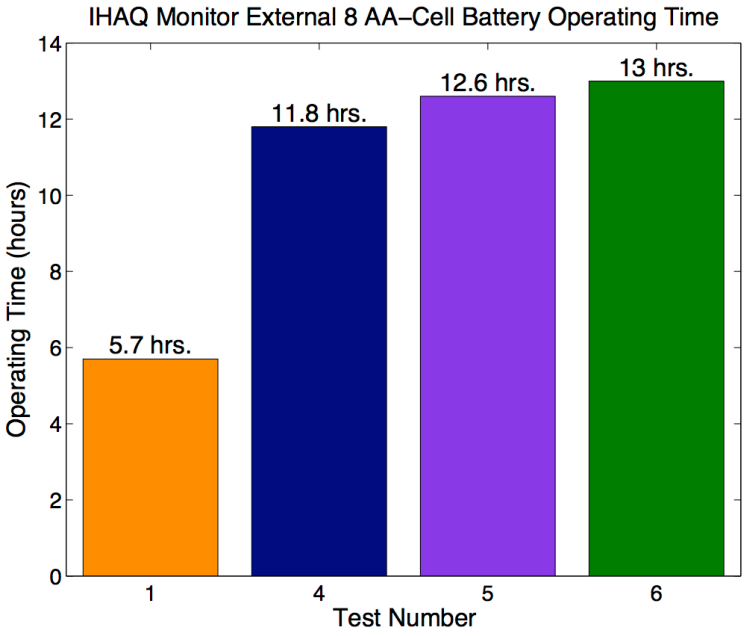


**Figure 27 The Effects of Hardware Modifications on Operating Time**

(a) shows the battery voltages over time, and (b) shows an operating-time comparison. Test details appear in Table 12.

(a)

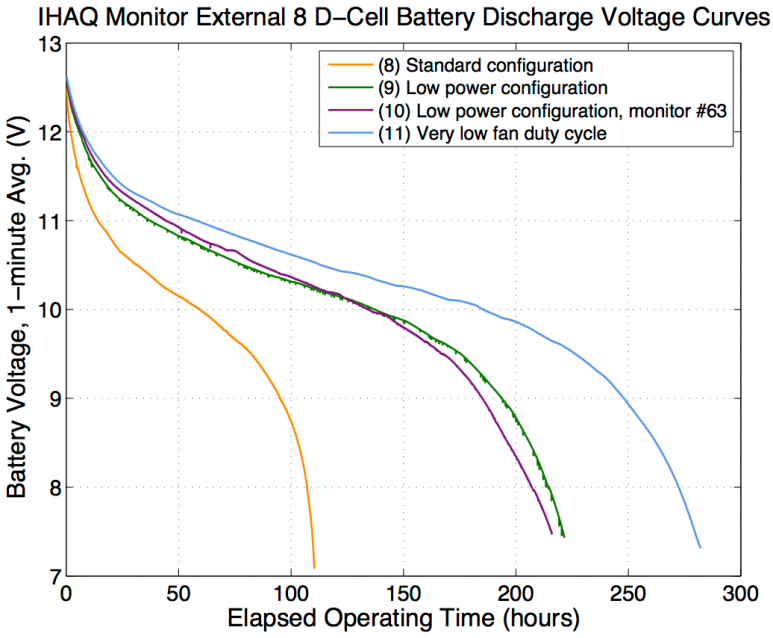


(b)

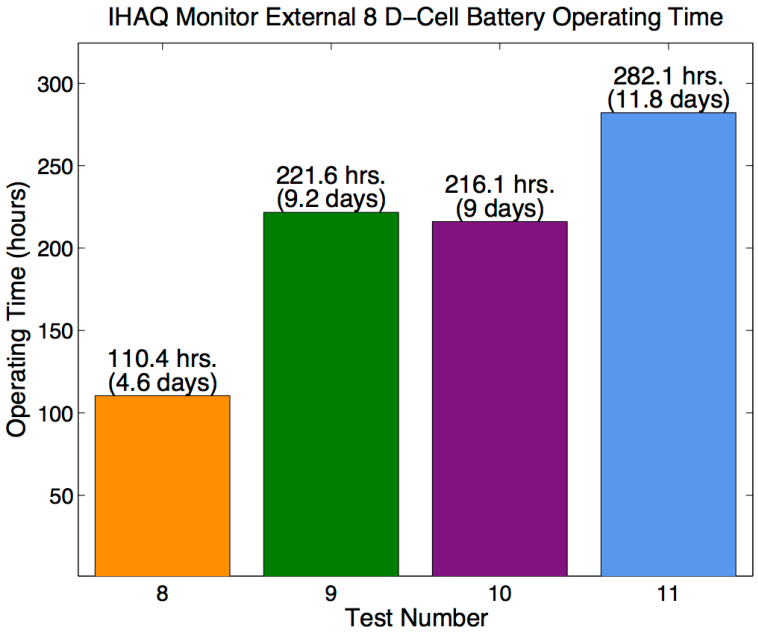


**Figure 28 Operating Times Obtained with an External, 8 Alkaline D-Cell Battery**

(a) shows the battery voltages over time, and (b) shows an operating-time comparison. Test details appear in Table 12.

7.2.4 Operating Time Obtained with the Internal Li-ion Battery

The operating times obtained with the internal Li-ion battery are shown in Figure 29. Tests using the standard and very-low-power configurations were performed multiple times to verify repeatability. The differences in initial voltage at the start of the tests are proportional to the elapsed time from the end of the previous charging cycle to the start of the test. The differences appear to have an insignificant impact on operating time.

The relative operating time increases obtained with the Li-ion battery are significantly less than those obtained with an external, primary battery. With a standard or alkaline battery, the low-power configuration (20 s fan-on period) ran 2.1 times longer than the baseline configuration and the lowest power configuration (5 s fan-on period) ran 2.9 times longer. However, with the Li-ion battery, the low-power configuration ran only 1.8 times longer than the corresponding Li-ion baseline and the lowest power configuration ran only 2.0 times longer.

The smaller operating time increases obtained with the Li-ion battery are likely due to differences in battery behavior with regard to the relationship between discharge rate and available energy. The average power values appearing in Table 12 show that the baseline configuration (test 1) consumes 1.7 times more power than the low-power configuration (test 6) and 2.0 times more than the lowest power configuration (test 7). The power differences are very similar to the Li-ion operating time differences, suggesting that the Li-ion battery's available capacity did not increase as the discharge rate decreased. In contrast, it is well documented that substantially more energy can be obtained from a standard or alkaline cell by decreasing the discharge rate (i.e., decreasing

the current flow through the cell), even at the relatively low discharge rates of all the monitor configurations.

### 7.2.5 Operating Times Obtained with Different External Batteries

As expected, the category IV tests show that larger cells provide longer operating time than smaller cells. For each increase in cell size (i.e., AAA to AA, AA to C, C to D), operating time more than doubles, and the increase is more pronounced with the smaller cell sizes. For example, with standard cells, increasing cell size from AAA to AA lengthens operating time by a factor of 2.77, but increasing size from C to D lengthens operating time by a factor of only 2.06. The higher current density in the smaller cells likely causes a substantial decrease in available capacity of those cells. With alkaline cells, the operating time increase is only 2.26 times when going from AAA to AA cells, suggesting that the current density may have a smaller effect on the available capacity of alkaline cells.

The tests also show that alkaline cells provide much longer operating time than standard cells. The alkaline AAA cells lasted 3.23 times longer than the same brand of standard AAA cells, and the alkaline AA cells lasted 2.64 times longer than the standard AA cells. Comparing the results of tests 9 and 23, the Duracell alkaline D cells lasted 3.40 times longer than the Sunbeam standard D cells.

The results of tests 19, 21, and 22 confirm that 8 cells provide a good balance between battery size and operating time. Increasing the number of cells from 6 to 8 gives a 33% increase in capacity but 74% longer operating time. The large operating time increase is due to discharging the cells more completely before low-voltage shutdown occurs. Increasing from 8 to 10 cells is a 25% capacity increase that gives only a 22%

operating time increase, indicating that most of each cell's available energy has been delivered by the time the cell voltage reaches approximately 0.8 V—the point at which low-voltage shutdown occurs with the 8-cell battery. The smaller increase in operating time compared to the capacity increase may be due to reduced efficiency of the voltage regulators when operating at a higher input voltage.

(a)

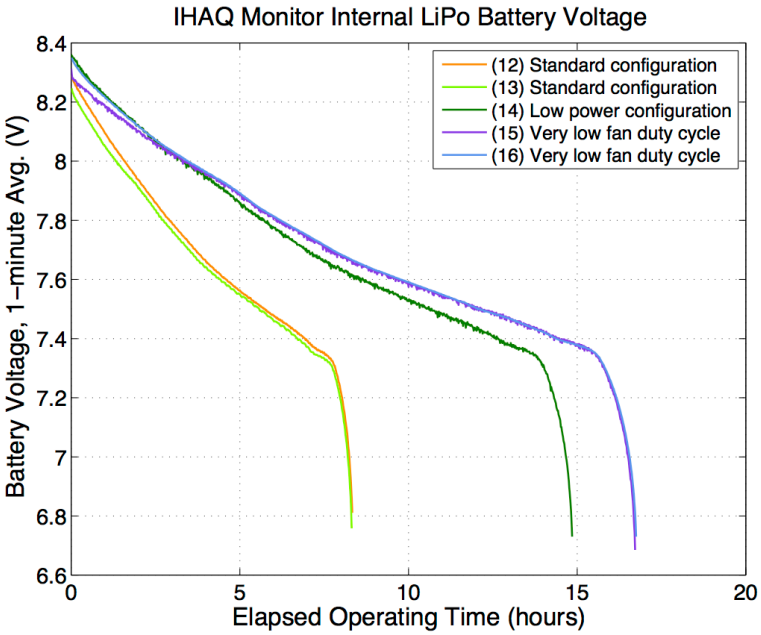


(b)

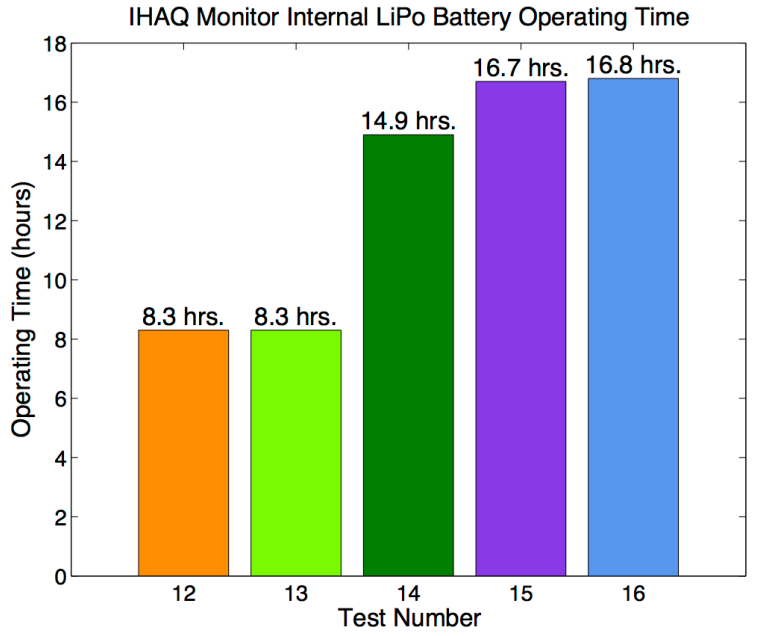


**Figure 29 Operating Times Achieved with the Internal Li-ion Battery**

(a) shows the battery voltages over time, and (b) shows an operating-time comparison. Test details appear in Table 12. Voltages were measured using the monitor's built-in battery voltage sensor at a rate of one sample every 5 or 60 seconds, depending on monitor configuration. The voltages recorded at 5-second intervals were smoothed with a moving-average filter to produce the one-minute average values shown on this plot. The voltages recorded at 60-second intervals are not averages.

(a)

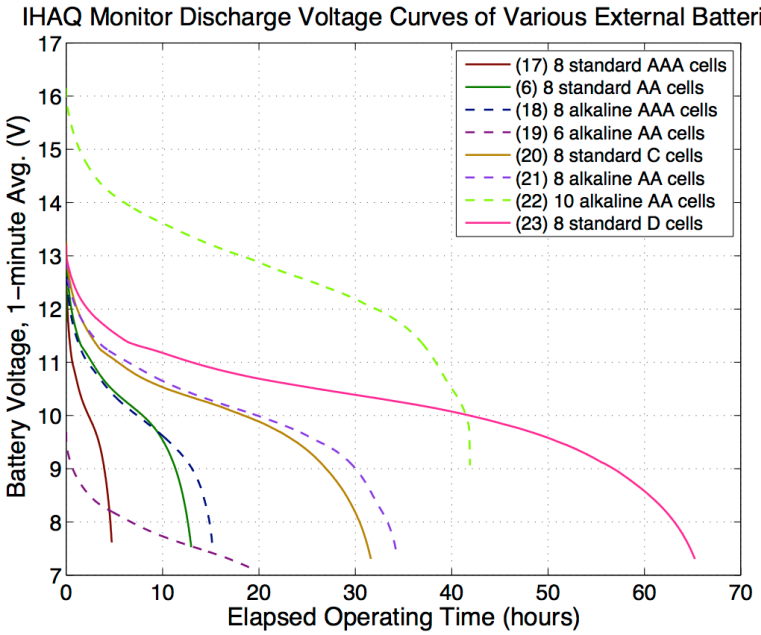


(b)

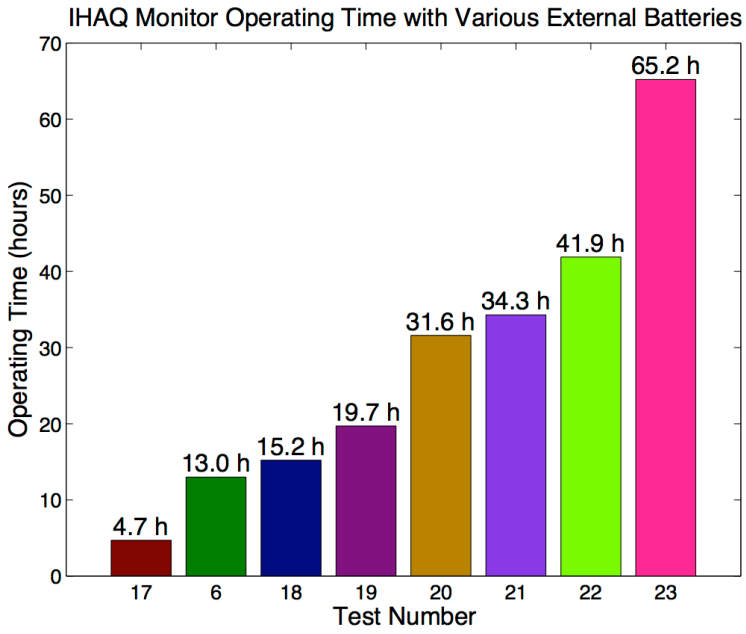


**Figure 30 Operating Times with Various External Battery Configurations**

(a) shows the battery voltages over time, and (b) shows an operating-time comparison. Test details appear in Table 12. All the tests shown in this figure were performed with the same low-power configuration on monitor #62.

## 7.3 Evaluation of Energy Usage Reduction on Data Quality

The quality of the data produced by an environmental monitor can be evaluated in terms of measurement accuracy, precision, and noise. Energy usage reduction modifications made to a monitor can affect all three. Because the modifications to the IHAQ monitor involved putting the $CO_2$ sensor into idle mode most of the time and reducing the duty cycle of the particle counter fan and laser, the data quality analysis efforts focused on measurements from those sensors.

Apart from increasing the measurement interval of the remaining sensors from 5 to 60 seconds, those sensors were not directly affected by the modifications. Visual inspection of graphs comparing the data from a modified monitor to data from unmodified monitors indicated that the accuracy and precision of those sensors were not materially affected. However, the longer interval between measurements could affect noise reduction via averaging performed during data analysis because fewer measurements would be available over a given time period.

### 7.3.1 T6615 $CO_2$ Sensor

The T6615 $CO_2$ sensor documentation states that the sensor must be brought out of idle mode for several measurement cycles (each cycle lasts approximately 3.4 seconds) to maintain accuracy [39]. To verify this claim, five IHAQ monitors were operated in an uncontrolled environment for approximately one week, and the $CO_2$ sensor idle-off period of one of the monitors was set to various different values in order to evaluate the effect of the sensor's idle mode on data quality. The idle-off configuration changes were made to monitor unit 79 while units 60, 66, 72, and 77 served as controls. To facilitate comparison of the results, the 30-minute period having the least variation in measurement

mean was identified in the data from each idle-off configuration, and the measurement data from that period were used to calculate the mean and variance for each monitor.

The results of the tests indicate that the $CO_2$ sensor's accuracy is indeed affected by putting the sensor in idle mode. However, contrary to the claim in the sensor's documentation, allowing the sensor to operate for several measurement cycles after bringing the sensor out of idle mode does not eliminate or even substantially reduce the effect. A positive offset appears in the measurement data when idle mode is used, and the magnitude of the offset is proportional to the amount of time that the sensor spends in idle mode. Figure 31 shows that the offset generally increases as idle time increases. The differences in measurement variance shown in Figure 32 suggest that increasing the idle time may also affect measurement noise or precision, but the relationship is not clear due to the decreases in variance with 52 and 56-second idle periods.

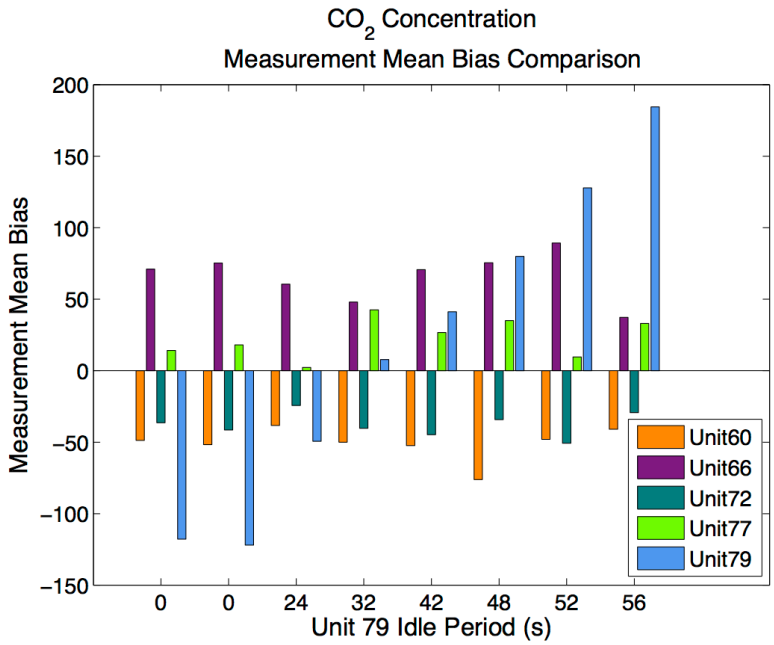


**Figure 31 Effect of $CO_2$ Sensor Idle Time on Measurement Mean Bias**

A zero-second idle period represents a baseline when the sensor's idle mode was disabled. Two baseline tests were performed to evaluate repeatability. The large negative bias present for unit 79 when its idle period is zero is likely due to sensor calibration error.

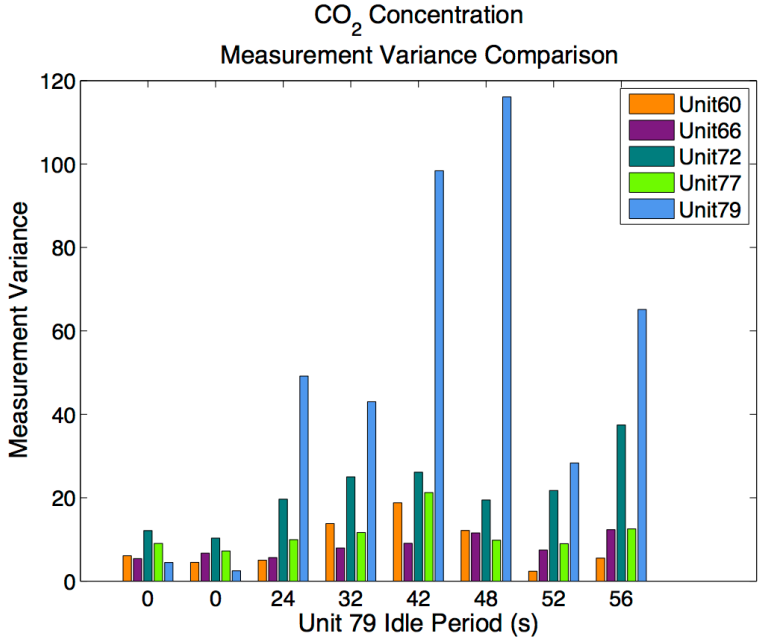


**Figure 32 Effect of $CO_2$ Sensor Idle Time on Measurement Variance**

During several tests in which a long idle period was used, an abrupt downward shift observed in the reported $CO_2$ concentration suggested that the sensor had automatically recalibrated itself due to the action of its automatic background calibration (ABC) feature. If the sensor is able to automatically recalibrate to compensate for being placed in idle mode, measurement accuracy may not be affected by energy reduction modifications after the recalibration takes place. Otherwise, it will be necessary to document the relationship between idle time and measurement offset so that the offset can be cancelled out during data analysis. Manually recalibrating the sensor to correctly report $CO_2$ concentration during idle-mode operation is not possible because the sensor cannot be placed in idle mode while it is in calibration mode.

### 7.3.2 Particle Counter

Preliminary evaluations of the effects of reduced fan duty cycle on the particle concentration measurements were performed in an uncontrolled environment. In that environment, the ambient particulate concentration varied greatly due to human activity and other factors. The monitor was configured to turn on the fan for a fixed period of time each minute then allowed to operate undisturbed for at least 6 hours. Three other monitors configured for continuous fan operation were placed within one meter of the monitor under test. After comparing the small particle count measurements recorded by the four monitors, it became apparent that shorter fan duty periods introduced increasing amounts of measurement noise. However, the uncontrolled nature of the particulate concentration made quantifying the effect infeasible.

Additional testing was performed in a more controlled environment. Four monitors were placed in a sealed chamber into which a constant flow of nebulizer-generated aerosol particles could be introduced. Unfortunately, the nebulizer did not produce a stable particle concentration throughout the tests. However, the stability over several 20 to 25 minute periods was sufficient to allow reasonably good evaluation of the effects of fan duty cycle on measurement data quality.

During the tests, the monitors designated as 60, 66, and 67 were the controls; their fans ran constantly. The fan duty period of monitor 77 was set such that the fan operated for *n* seconds out of every 60 seconds, where *n* is 1, 2, 5, 10, 20, 30, 40, or 50. All the monitors were configured to record a particle concentration measurement once per minute.

The measurements recorded during two testing sessions are shown in Figure 33 and Figure 34. The intervals over which the small particle concentration measurements were sufficiently stable to permit evaluation of the fan duty effects are noted on the graphs. During the interval from approximately 3.8 to 4.2 hours in Figure 33 and 0.3 to 0.5 hours in Figure 34, the fan of unit 77 was set to run continuously in order to verify that the particle counter was still operating properly.

The graphs in Figure 33 and Figure 34 show that measurement noise and distance from the mean increase as the fan duty period decreases. The effect on measurement accuracy is very pronounced when the fan duty period is shorter than 20 seconds. Figure 35 shows a comparison of normalized root-mean-square error (NRMSE) values between monitors and across the different fan duty periods. (NRMSE is calculated by dividing the root-mean-square error by the measurement range. This facilitates comparison across

different ranges.) The pronounced increase in the NRMSE of unit 77 when the fan duty was set to 50 seconds suggests that merely cycling the fan and laser impacts measurement data quality. However, the measurement variances shown in Figure 36 indicate that measurement noise does not substantially increase until the fan duty period is less than 30 seconds. The jump in NRMSE at the 50-second fan duty period is probably due to an increase in the magnitude of overall offset from the mean, as indicated by the mean bias values appearing in Figure 37. The bias is quite visible in the measurement graphs: As the fan duty period is reduced, the distance between unit 77 and the other units increases, with unit 77 reporting significantly lower values with fan duty periods less than 20 seconds. Still, the measurements are well correlated with those from the other monitors, suggesting that the addition of a fan-period-dependent constant and the application of noise filtering during data analysis could render the measurement data usable even when a very short fan duty period is used.

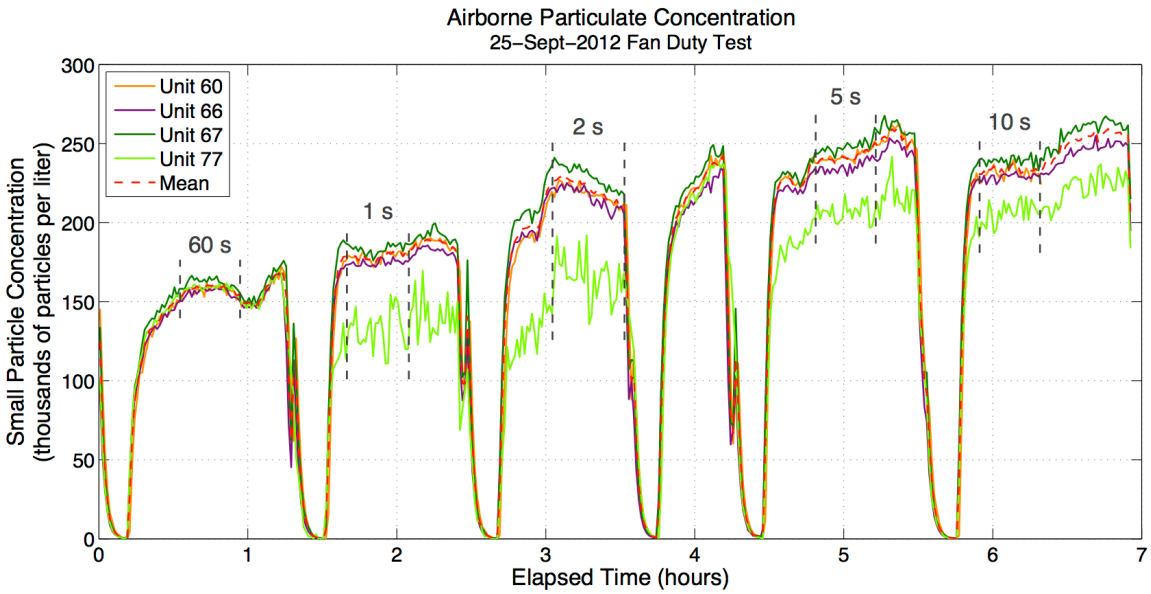


**Figure 33 Particle Counter Measurements from the First Set of Fan Duty Tests**

Each pair of dashed vertical lines denotes an interval over which a fan duty configuration was evaluated. The fan duty period of monitor unit 77 appears above each interval.

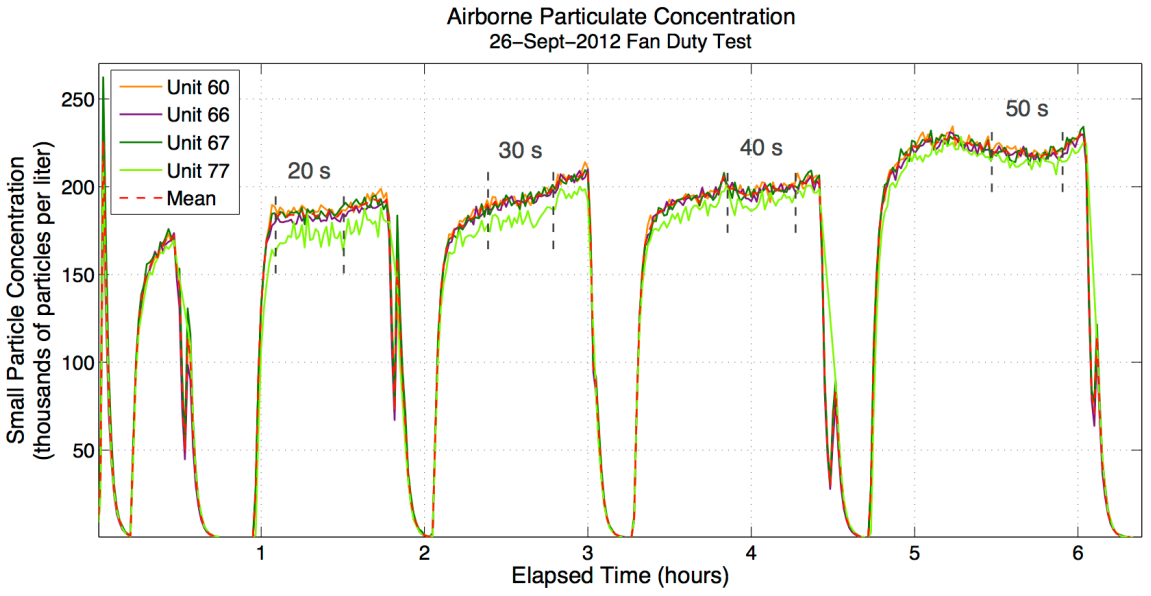


**Figure 34 Particle Counter Measurements from the Second Set of Fan Duty Tests**

Each pair of dashed vertical lines denotes an interval over which a fan duty configuration was evaluated. The fan duty period of monitor unit 77 appears above each interval.

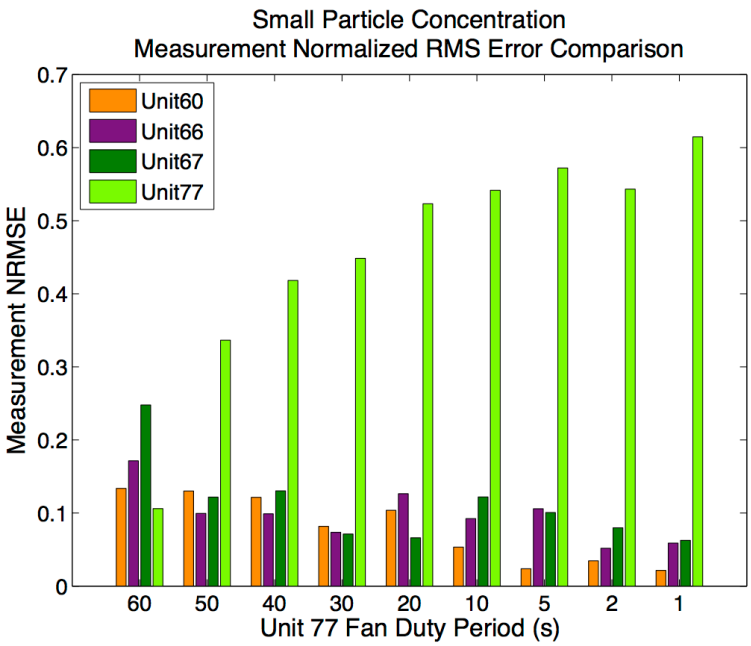


**Figure 35 Effect of Fan Duty Period on Normalized Root-Mean-Square Error**

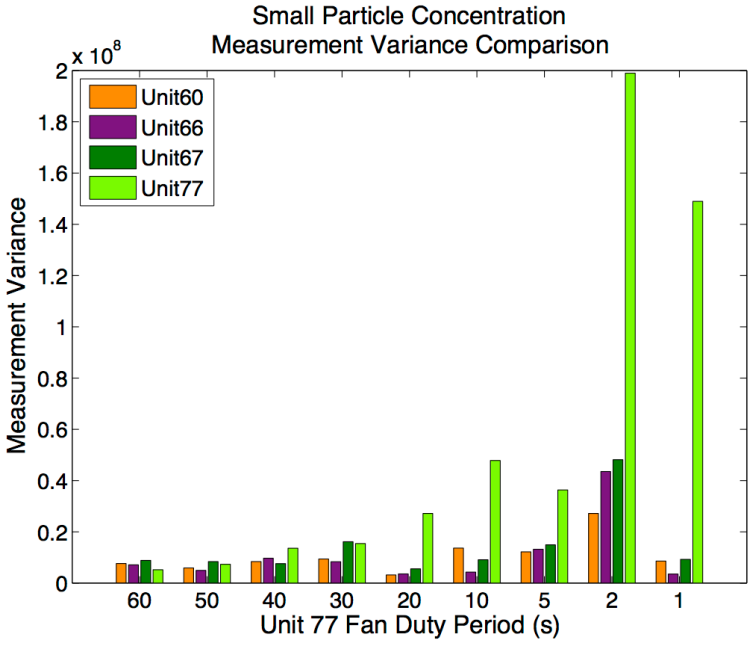


**Figure 36 Effect of Fan Duty Period on Measurement Variance**

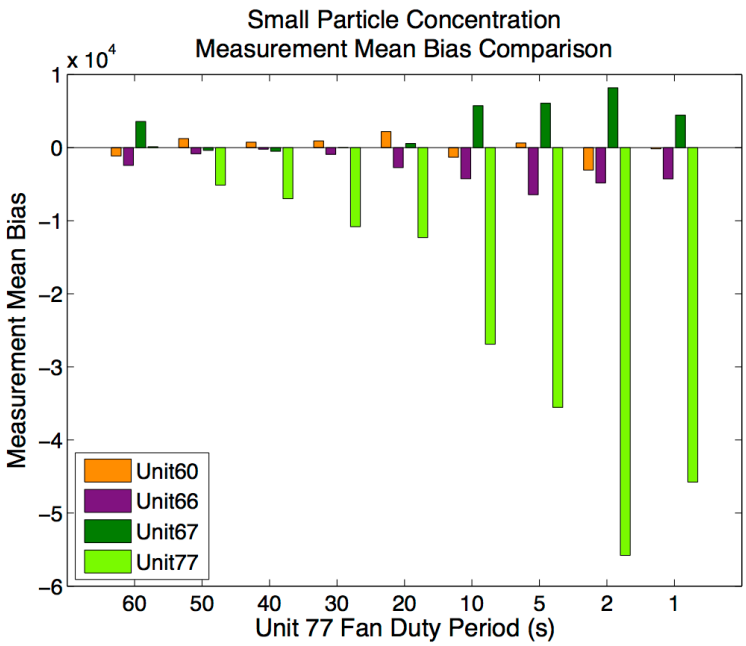


**Figure 37 Effect of Fan Duty Period on Measurement Mean Bias**

# CHAPTER EIGHT: CONCLUSIONS AND FUTURE WORK

## 8.1 Summary of Operating Time Extension Results

Although constrained by the limited scope of allowable hardware modifications, the efforts to extend the operating time of the monitor were quite successful: The operating time of the monitor, when using battery power alone, was more than doubled. When an external battery consisting of eight D-size alkaline cells is used, the monitor can operate continuously for more than nine days. Existing monitors can be configured for such long operating times with only minimal hardware modifications, a firmware update, and changes to several configuration file settings.

Adding an external 8 alkaline D cell battery extended the baseline operating time from 8.3 hours to 4.6 days. Configuration modifications and minor firmware modifications approximately doubled the operating time, giving 14.9 hours with the internal battery and 9.4 days with the external battery. The addition of a primary-cell battery controller solved the issue of multiple system restarts near the end of the external battery's useful life that was caused by insufficient (for a primary battery) hysteresis in the UVLO. The controller also prevents the external battery from charging the internal battery. Several additional modifications to the monitor, such as making sure that high-current sensors do not operate simultaneously, further increased the operating time by

another 10%, thus extending the operating time with top-quality batteries well beyond the 8-day goal and possibly allowing the goal to be met with lower quality batteries.

## 8.2 Future Work

### 8.2.1 Additional Energy Usage Reduction

The subsystem energy usage estimates shown in Table 2 and Table 3 suggest that future energy reduction efforts should focus on the motherboard. Based on data sheet information, the microcontroller only requires 16 mA from the battery. However, putting it in sleep mode could provide significant energy savings, especially if other components could be shut down while the microcontroller is asleep. DC circuit analysis and component data sheet information indicate that the voltage regulator overhead, which includes quiescent and boost currents, is approximately 10 mA. If supercapacitors could be used to power critical components, perhaps the voltage regulators could be shut down during sleep periods. Firmware modifications to support scheduling and coordination of various activities could allow the system to spend a substantial amount of time in a lower power or sleep mode.

### 8.2.2 T6615 $CO_2$ Idle Mode Effect on Sensor Measurement Bias

The measurements from the T6615 $CO_2$ sensor show a positive bias that increases with the amount of time the sensor is idle between measurements. It was noted several times that an abrupt correction was made after a monitor had been operating continuously with the same idle configuration for several days. The correction may have been caused by the sensor's ABC feature, which is normally disabled in the IHAQ monitor. However, the newest revision of the sensor does not respond to the command that turns ABC off, so

the feature may be permanently enabled on those sensors. In any case, a solution to the bias should be found, whether through reliable and predictable ABC correction or through an offset applied during post processing. Replacing the sensor with a model from another manufacturer is another possible solution.

### 8.2.3 Particle Counter Fan Duty Period Effects on Measurement Data Quality

Several observations made during the measurement data quality tests suggest that cycling the fan may not be the primary contributor to increased measurement noise and variance. Cycling the laser may also cause degradation of measurement data quality, or there may be another cause that has not been identified. Additional investigation should be performed to determine if additional modifications to the particle counter could mitigate the effects of reducing the fan and laser duty cycle, thereby possibly facilitating additional energy usage reduction.

### 8.2.4 Operating Time Prediction Model

The results presented in this thesis demonstrate the relationships between the various IHAQ monitor modifications and corresponding increases in operating time. However, a model that predicts operating time or measurement data quality based on monitor configuration was not developed. Because different monitoring applications require different operating times and different levels of data quality, the availability of a model for predicting monitor operating time and expected data quality for different measurement intervals, sensor sets, and batteries would be very useful.

# REFERENCES

[1] M. K. Barnett, “A brief history of thermometry,” *J. Chem. Educ.*, vol. 18, no. 8, p. 358, Aug. 1941.

[2] K. Chintalapudi, T. Fu, J. Paek, N. Kothari, S. Rangwala, J. Caffrey, R. Govindan, E. Johnson, and S. Masri, “Monitoring civil structures with a wireless sensor network,” *IEEE Internet Computing*, vol. 10, no. 2, pp. 26–34, Mar. 2006.

[3] V. Mehta and M. El Zarki, “A bluetooth based sensor network for civil infrastructure health monitoring,” *Wireless Networks*, vol. 10, no. 4, Jul. 2004.

[4] G. Werner-Allen, K. Lorincz, M. Ruiz, O. Marcillo, J. Johnson, J. Lees, and M. Welsh, “Deploying a wireless sensor network on an active volcano,” *IEEE Internet Computing*, vol. 10, no. 2, pp. 18–25, Mar. 2006.

[5] A. Sheth, C. A. Thekkath, P. Mehta, K. Tejaswi, C. Parekh, T. N. Singh, and U. B. Desai, “Senslide: a distributed landslide prediction system,” *SIGOPS Operating Systems Review*, vol. 41, no. 2, Apr. 2007.

[6] R. Szewczyk, E. Osterweil, J. Polastre, M. Hamilton, A. Mainwaring, and D. Estrin, “Habitat Monitoring with Sensor Networks,” *Communications of the ACM*, vol. 47, no. 6, pp. 34–40, Jun. 2004.

[7] V. Raghunathan, C. Schurgers, S. Park, and M. B. Srivastava, “Energy-aware wireless microsensor networks,” *IEEE Signal Processing Magazine*, vol. 19, no. 2, pp. 40–50, Mar. 2002.

[8] A. Mainwaring, D. Culler, J. Polastre, R. Szewczyk, and J. Anderson, “Wireless sensor networks for habitat monitoring,” *Proceedings of the 1st ACM International Workshop on Wireless Sensor Networks and Applications*, pp. 88–97, Sep. 2002.

[9] Sravanthi Chalasani and J. M. Conrad, “A Survey of Energy Harvesting Sources for Embedded Systems,” presented at the IEEE SoutheastCon 2008, 2008, pp. 442–447.

[10] S. Roundy, P. K. Wright, and J. Rabaey, “A study of low level vibrations as a power source for wireless sensor nodes,” *Computer Communications*, vol. 26, no. 11, pp. 1131–1144, Jul. 2003.

[11] “H.R. 4365--106th Congress: Children’s Health Act of 2000,” *GovTrack.us*, 17-Oct.-2000. [Online]. Available: http://www.govtrack.us/congress/bills/106/hr4365/text. [Accessed: 23-Sep.-2012].

[12] P. J. Landrigan, L. Trasande, L. E. Thorpe, C. Gwynn, P. J. Lioy, M. E. D'Alton, H. S. Lipkind, J. Swanson, P. D. Wadhwa, E. B. Clark, V. A. Rauh, F. P. Perera, and E. Susser, “The National Children's Study: A 21-Year Prospective Study of 100 000 American Children,” *Pediatrics*, vol. 118, no. 5, pp. 2173–2186, Nov. 2006.

[13] “The National Children’s Study and Your Community: Working Together for Children's Health.” National Institutes of Health Publication No. 11-5764, pp. 1–8, 13-Sep.-2011.

[14] J. Kiepert, S. M. Loo, D. Klein, and M. Pook, “Wireless Sensor Network for Aircraft Cabin Environment Sensing,” presented at the AIAA-2011-5108 41st International Conference on Environmental Systems, 2011.

[15] J. A. Hall, S. M. Loo, D. Stephenson, R. Butler, M. Pook, J. Kiepert, J. Anderson, and N. Terrell, “A Portable Wireless Particulate Sensor System for Continuous Real-Time Environmental Monitoring,” presented at the AIAA-2012-3441 42nd International Conference on Environmental Systems, 2012.

[16] K. I. Farkas, J. Flinn, G. Back, D. Grunwald, and J. M. Anderson, “Quantifying the Energy Consumption of a Pocket Computer and a Java Virtual Machine,” *Proceedings of the 2000 ACM SIGMETRICS International Conference on Measurement and Modeling of Computer Systems*, pp. 252–263, Jun. 2000.

[17] K. R. Yamamoto and P. G. Flikkema, “Prospector: Multiscale Energy Measurement of Networked Embedded Systems with Wideband Power Signals,” *2009 International Conference on Computational Science and Engineering*, vol. 2, pp. 543–549, 2009.

[18] X. Jiang, P. Dutta, D. Culler, and I. Stoica, “Micro Power Meter for Energy Monitoring of Wireless Sensor Networks at Scale,” *6th International Symposium on Information Processing in Sensor Networks*, pp. 186–195, 2007.

[19] D. Macii and D. Petri, “Accurate Current Measurements for the Estimation of the Power Consumption in Wireless Modules,” *Proceedings of the 2006 IEEE International Workshop on Advanced Methods for Uncertainty Estimation in Measurement*, pp. 92–97, Apr. 2006.

[20] M. Lundberg, J. Eliasson, J. Allan, J. Johansson, and P. Lindgren, “Power Characterization of a Bluetooth-Equipped Sensor Node,” presented at the 2005 Workshop on Real-World Wireless Sensor Networks, Stockholm, Sweden, 2005.

[21] T. Laopoulos, P. Neofotistos, C. Kosmatopoulos, and S. Nikolaidis, “Measurement of Current Variations for the Estimation of Software-Related Power Consumption,” *IEEE Trans Instrum Meas*, vol. 52, no. 4, pp. 1206–1212, Aug. 2003.

[22] T. Trathnigg and R. Weiss, “A Runtime Energy Monitoring System for Wireless Sensor Networks,” presented at the 2008 3rd International Symposium on Wireless Pervasive Computing (ISWPC), 2008, pp. 21–25.

[23] N. Chang, K. Kim, and H. G. Lee, “Cycle-accurate energy measurement and characterization with a case study of the ARM7TDMI,” *IEEE Transactions on Very Large Scale Integration (VLSI) Systems*, vol. 10, no. 2, pp. 146–154, Apr. 2002.

[24] V. Konstantakos, K. Kosmatopoulos, S. Nikolaidis, and T. Laopoulos, “Measurement of Power Consumption in Digital Systems,” *IEEE Trans Instrum Meas*, vol. 55, no. 5, pp. 1662–1670, Oct. 2006.

[25] H. Ritter, J. Schiller, T. Voigt, A. Dunkels, and J. Alonso, “Experimental evaluation of lifetime bounds for wireless sensor networks,” *Proceedings of the Second European Workshop on Wireless Sensor Networks*, pp. 25–32, 2005.

[26] J. Both, “Leakage current properties of modern electrolytic capacitors,” *Tadiran Batteries GmbH*, 29-Sep.-2007. [Online]. Available: http://www.tadiranbatteries.de/pdf/BothEng.pdf. [Accessed: 29-Sep.-2012].

[27] P. Horowitz and W. Hill, *The Art of Electronics*, 2nd ed. Cambridge, MA: Cambridge University Press, 1989.

[28] V.-G. Voiculescu, V.-A. Grosu, L. Milea, P. Schiopu, O. Oltu, and E. Franti, “Impact of frequency scaling on power management of an autonomous weather monitoring embedded system,” presented at the 2011 International Semiconductor Conference (CAS), 2011, vol. 2, pp. 383–386.

[29] "PIC12F510/16F506 Data Sheet," *Microchip, Inc.*, 30-Nov.-2007. [Online]. Available: http://ww1.microchip.com/downloads/en/devicedoc/41268d.pdf. [Accessed: 30-Sep.-2012].

[30] A. Y. Benbasat, "An Automated Framework for Power-efficient Detection in Embedded Sensor Systems," Ph.D. dissertation, School of Architecture and Planning, Massachusetts Institute of Technology, Cambridge, MA, 2007.

[31] "MXR2312G/M Datasheet," *Alldatasheet*, 18-Jan.-2005. [Online]. Available: http://pdf1.alldatasheet.com/datasheet-pdf/view/142388/ETC1/MXR2312G.html. [Accessed: 30-Sep.-2012].

[32] "ADXL212 Datasheet (Rev. 0)," *Analog Devices*, 03-May-2011. [Online]. Available: http://www.analog.com/static/imported-files/data_sheets/ADXL212.pdf. [Accessed: 30-Sep.-2012].

[33] "ADG714/ADG715 CMOS, Low Voltage Serially Controlled, Octal SPST Switches Data Sheet (REV. B)," *Analog Devices*, 19-Nov.-2002. [Online]. Available: http://www.analog.com/static/imported-files/data_sheets/ADG714_715.pdf. [Accessed: 30-Sep.-2012].

[34] "LMV431/LMV431A/LMV431B Low-Voltage (1.24V) Adjustable Precision Shunt Regulators (Rev. F)," *Texas Instruments*, 07-Dec.-2011. [Online]. Available: http://www.ti.com/lit/ds/symlink/lmv431.pdf. [Accessed: 30-Sep.-2012].

[35] "Duracell Alkaline-Manganese Dioxide," *Duracell Global Technical Content Library*, 16-Jun.-1997. [Online]. Available: http://media.duracell.com/media/en-US/pdf/gtcl/Technical_Bulletins/Alkaline%20Technical%20Bulletin.pdf. [Accessed: 03-Oct.-2012].

[36] J. Broadhead and H. C. Kuo, "Electrochemical Principles and Reactions," in *Handbook of Batteries*, 2nd ed, D. Linden, Ed. New York, NY: McGraw-Hill, Inc., 1995, pp. 2.1–2.35.

[37] D. Linden, "Factors Affecting Battery Performance," in *Handbook of Batteries*, 2nd ed, D. Linden, Ed. New York, NY: McGraw-Hill, Inc., 1995, pp. 3.1–3.20.

[38] J. Hall, R. Butler, S. M. Loo, and C. Weisel, "A Multi-Sensor Wireless System for Continuous Real-Time Environmental Monitoring," presented at the 21st Annual Meeting of the International Society of Exposure Science, Baltimore, MD, 2011.

[39] "$CO_2$ Sensor UART Communications Protocol," GE Sensing & Inspection Technologies, Jun. 2008.

APPENDIX

**PCBC Schematic**

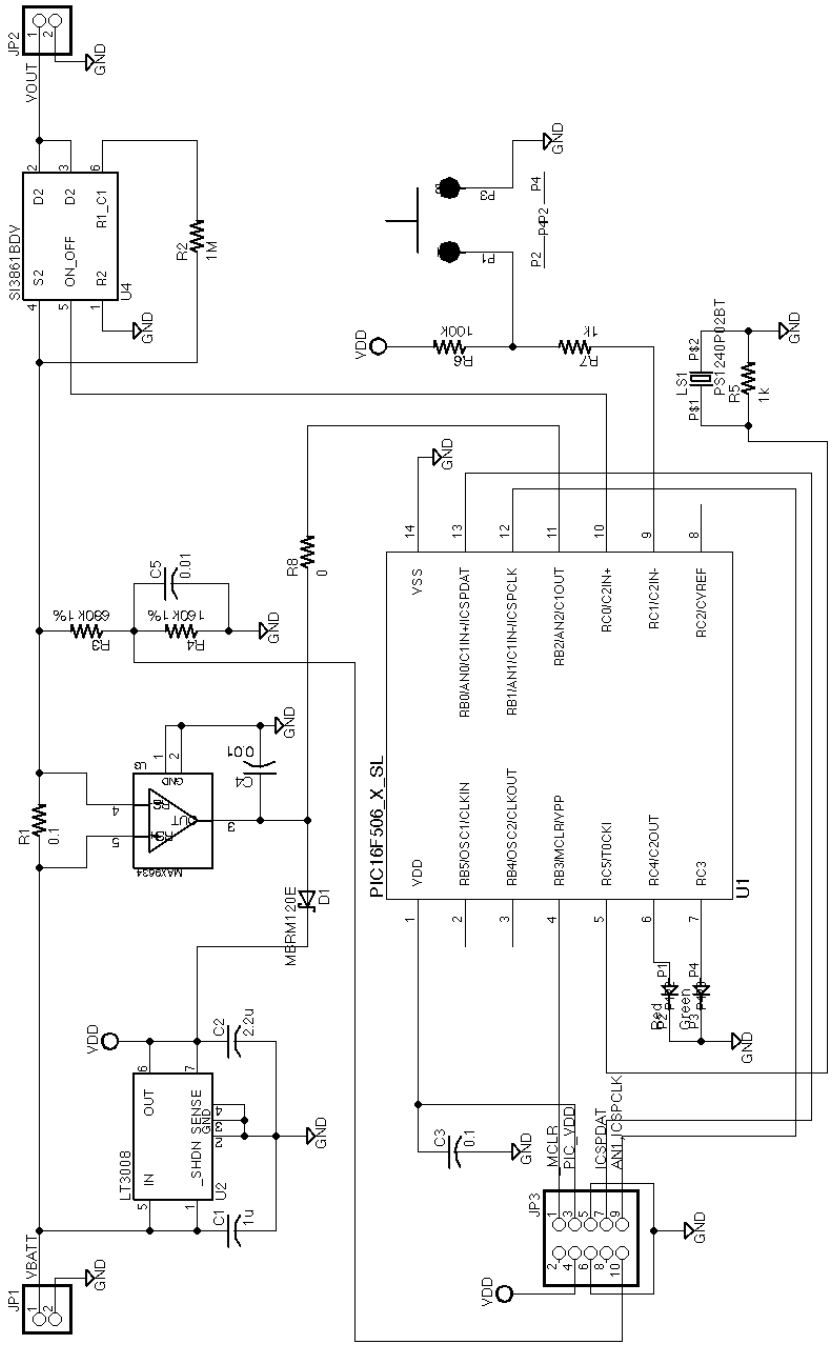

# PCBC Firmware Source Code

## configuration_bits.c

```
#include <xc.h>


#ifdef _16F887

/*
 * PIC16F887 config word 1
 * -----------------------
 *
 * FOSC_INTRC_CLKOUT   INTOSC oscillator: CLKOUT function on RA6/OSC2/CLKOUT pin,
 *                                        I/O function on RA7/OSC1/CLKIN
 * FOSC_INTRC_NOCLKOUT INTOSCIO oscillator: I/O function on RA6/OSC2/CLKOUT pin,
 *                                          I/O function on RA7/OSC1/CLKIN
 *
 * WDTE_OFF     WDT disabled and can be enabled by SWDTEN bit of the WDTCON register
 * WDTE_ON      WDT enabled
 *
 * PWRTE_OFF    power-up timer disabled
 * PWRTE_ON     power-up timer enabled
 *
 * MCLRE_ON     RE3/MCLR pin function is MCLR
 * MCLRE_OFF    RE3/MCLR pin function is digital input, MCLR internally tied to VDD
 *
 * BOREN_ON     BOR enabled
 * BOREN_NSLEEP BOR enabled during operation and disabled in Sleep
 * BOREN_SBODEN BOR controlled by SBOREN bit of the PCON register
 * BOREN_OFF    BOR disabled
 *
 * IESO_ON      Internal/External Switchover mode is enabled
 * IESO_OFF     Internal/External Switchover mode is disabled
 *
 * FCMEN_ON     Fail-Safe Clock Monitor is enabled
 * FCMEN_OFF    Fail-Safe Clock Monitor is disabled
 *
 * LVP_ON       RB3/PGM pin has PGM function, low voltage programming enabled
 * LVP_OFF      RB3 pin has digital I/O, HV on MCLR must be used for programming
 *
 * DEBUG_OFF    In-Circuit Debugger disabled, RB6/ICSPCLK and RB7/ICSPDAT are
 *              general purpose I/O pins
 * DEBUG_ON     In_Circuit Debugger enabled, RB6/ICSPCLK and RB7/ICSPDAT are dedicated
 *              to the debugger
 *
 *
 * PIC16F887 config word 2
 * -----------------------
 *
 * BOR4V_BOR21V Brown-out Reset set to 2.1V
 * BOR4V_BOR40V Brown-out Reset set to 4.0V
 */

// first configuration word
__CONFIG(FOSC_INTRC_CLKOUT & WDTE_OFF & PWRTE_OFF & MCLRE_OFF & BOREN_ON & IESO_OFF &
FCMEN_OFF & LVP_OFF & DEBUG_OFF);

// second configuration word
__CONFIG(BOR4V_BOR21V);
```

```
#elif defined(_16F506)

/*
 * OSC_IntRC_RB4EN      INTRC With RB4 and 1.125 ms DRT
 * OSC_IntRC_CLKOUTEN   INTRC With CLKOUT and 1.125 ms DRT
 * WDT_ON               WDT enabled
 * WDT_OFF              WDT disabled
 * CP_OFF               Code protection off
 * CP_ON                Code protection on
 * MCLRE_ON             RB3/MCLR pin functions as MCLR
 * MCLRE_OFF            RB3/MCLR pin functions as RB3, MCLR tied internally to VDD
 * IOSCFS_ON            8 MHz INTOSC Speed
 * IOSCFS_OFF           4 MHz INTOSC Speed
 */

__CONFIG(OSC_IntRC_RB4EN & WDT_ON & CP_OFF & MCLRE_OFF & IOSCFS_OFF);


#else
#error Device not supported.
#endif
```

## main.c

```
/*
 * @file        main.c
 * @abstract    alkaline battery pack controller for the IHAQ monitor
 * @written     06-13-2012
 * @author      Ross Butler
 * @version     0.0.1
 * @discussion  Monitors the output voltage of an alkaline cell battery pack and
 *              turns it off when the voltage drops lower than a setpoint.
 *              Update 08/23/2012:  Changed threshold values to agree with measurements
 *                                  made on new prototypes and MBRM120ET3G diode.
 */


#include <xc.h>
#include <stdint.h>        /* For uint8_t definition */
#include <stdbool.h>       /* For true/false definition */


// Assuming that each count interval is one 18 ms watchdog timeout period, the
// following mapping gives the relationship between counter initialization value
// and time period (value -> interval in seconds):
//     255->4.59  222->4  167->3  111->2 56->1 18->0.324 12->0.216
// Note that the 16F506's watchdog timeout period can be significantly longer
// than 18 ms.  25 to 36 ms seems to be typical.

#define LED_STANDBY_FLASH_COUNT 222
#define LED_NORMAL_FLASH_COUNT 111
#define LED_LOW_V_FLASH_COUNT 56
#define LED_UVLO_FLASH1_COUNT 8
#define LED_UVLO_FLASH2_COUNT 56
#define LED_HIGH_I_FLASH_COUNT 12

// The count-threshold values below are the number of consecutive readings
// beyond the associated voltage or current threshold that must occur in
// order to indicate that the associated condition has been reached.  The
// voltage and current threshold values are ADC output values.

// Try to avoid seeing load spikes as a low-voltage condition ((34-1)->594ms).
// The Telaire T6615 CO2 sensor in the monitor creates load spikes that last
// approx. 600 ms.  Monitor units that have been modified for delayed low-
// voltage shutdown should tolerate those load spikes.  A low-voltage condition
// longer than that will likely trigger the monitor's internal low-voltage shutdown.
```

```
#define LOW_VBATT_COUNT_THRESHOLD 34
// Give 'em time to resolve the high-current condition ((255-1)->4.6s).  This also
// accommodates the monitor's occasional 200+ mA current peaks.
#define HIGH_I_COUNT_THRESHOLD 255
// Shut down immediately if the output might be shorted.
#define SHORTED_I_COUNT_THRESHOLD 1
// Allow time for power switch debounce and system startup before assuming that
// the attached load is in normal-operation mode.
#define OPERATING_I_COUNT_THRESHOLD 255
// If the current drops below the operating threshold long enough while the
// voltage is below the warning threshold, we'll assume that the monitor's
// undervoltage lockout has been tripped.  Because the battery voltage can recover
// very rapidly after the monitor shuts off thus allowing it to restart almost
// immediately, we'll act immediately on any drop below the threshold.
#define UVLO_COUNT_THRESHOLD 1

// Ideally, the voltage divider for measuring Vbatt should produce 2.5 V to the
// ADC when Vbatt = 13.1 V.  However, testing on the protoboard and the initial
// prototype show that Vbatt = 13.27 V when Vadc = 2.5 V.  So, it appears that
// there is an offset of approx. 0.17 V.  At Vbatt=6.92 V, the offset is more
// like 0.21 V.  The production threholds below take that into consideration
// and were fine tuned to hit the target values.

// 6.9 V (255->13.1V, 138->7.0894-0.21=6.8794V, 136 gives 6.89 V)
#define LOW_VBATT_THRESHOLD 136

// 9.0 V (255->13.1V, 179->9.1957-0.20=8.9957V, 178 gives 9.01 V)
#define WARN_VBATT_THRESHOLD 178

// The reverse leakage current through the MBRM120L clamping diode D1 produces
// around 100 mV at the ADC input when no current is flowing to the load.  That
// voltage is very temperature sensitive!  With the MBRM120E diode, the voltage
// in prototypes 2 and 3 was measured at 5.1 and 1.9 mV, and did not appear to
// be nearly as temperature sensitive.  I_ADC_OFFSET is subtracted from the ADC
// values to compensate somewhat for that offset.  Note that I_ADC_OFFSET will
// need to be changed if a different diode is used.
// (255->2.5V, 11->0.1078V, 1->0.0098V)
#define I_ADC_OFFSET 1

// 250 mA (255->500mA, 127->249mA)
#define HIGH_I_THRESHOLD 127
// full scale (255->500mA)
#define SHORTED_I_THRESHOLD 254
// The monitor can draw around 5 mA when power switch is off
// (255->500 mA, 3->5.882mA, 5->9.8039mA).
#define OPERATING_I_THRESHOLD 5


// the number of seconds to sound the high-current audible alarm
#define HIGH_I_ALARM_SECONDS 10

// device-specific definitions
// ---------- PIC16F887 ----------
#if defined(_16F887)
#define RESET_BUTTON_IS_PUSHED      (!PORTBbits.RB0)
#define ADC_CONV_IS_NOT_DONE        (ADCON0bits.nDONE)
// Use only upper 8 bits of ADC result.
#define ADC_RESULT                  (ADRESH)
#define SET_OUTPUT_TO_LOAD_ON       PORTCbits.RC0 = 1
#define SET_OUTPUT_TO_LOAD_OFF      PORTCbits.RC0 = 0
#define SET_RED_LED_ON              PORTCbits.RC3 = 1
#define SET_RED_LED_OFF             PORTCbits.RC3 = 0
#define SET_GREEN_LED_ON            PORTCbits.RC4 = 1
#define SET_GREEN_LED_OFF           PORTCbits.RC4 = 0
#define SET_BUZZER_ON               PORTCbits.RC2 = 1
#define SET_BUZZER_OFF              PORTCbits.RC2 = 0
#define SET_OSCOPE_OUTPUT_HIGH      PORTCbits.RC5 = 1
#define SET_OSCOPE_OUTPUT_LOW       PORTCbits.RC5 = 0
// The 887's TRIS configuration isn't lost after sleep so no
// need to enable and disable the buzzer to prevent clicks.
#define ENABLE_BUZZER
```

```
#define DISABLE_BUZZER
// Fosc/8, AN1, don't start conversion, ADC enabled
#define ENABLE_ADC_VBATT            ADCON0 = 0b01000101
// Fosc/8, AN1, start conversion, ADC enabled
#define START_ADC_CONV_VBATT        ADCON0 = 0b01000111
// Fosc/8, AN1, don't start conversion, ADC disabled
#define DISABLE_ADC_VBATT           ADCON0 = 0b01000100
// Fosc/8, AN2, don't start conversion, ADC enabled
#define ENABLE_ADC_ILOAD            ADCON0 = 0b01001001
// Fosc/8, AN2, start conversion, ADC enabled
#define START_ADC_CONV_ILOAD        ADCON0 = 0b01001011
// Fosc/8, AN2, don't start conversion, ADC disabled
#define DISABLE_ADC_ILOAD           ADCON0 = 0b01001000
// Need to delay about 5 us for ADC acquisition.  (If 5 is good, 6 is better.)
#define DELAY_FOR_ADC_ACQUISITION   NOP(); NOP(); NOP(); NOP(); NOP(); NOP();
#define LED_BYTE_DISPLAY(byteVal)   PORTD = byteVal
#define SYS_FREQ                    4000000L
#define FCY                         SYS_FREQ/4
// ---------- PIC16F506 ----------
#elif defined(_16F506)
#define RESET_BUTTON_IS_PUSHED      (!PORTCbits.RC1)
#define ADC_CONV_IS_NOT_DONE        (ADCON0bits.nDONE)
#define ADC_RESULT                  (ADRES)
#define SET_OUTPUT_TO_LOAD_ON       PORTCbits.RC0 = 1
#define SET_OUTPUT_TO_LOAD_OFF      PORTCbits.RC0 = 0
#define SET_RED_LED_ON              PORTCbits.RC4 = 1
#define SET_RED_LED_OFF             PORTCbits.RC4 = 0
#define SET_GREEN_LED_ON            PORTCbits.RC3 = 1
#define SET_GREEN_LED_OFF           PORTCbits.RC3 = 0
#define SET_BUZZER_ON               PORTCbits.RC5 = 1
#define SET_BUZZER_OFF              PORTCbits.RC5 = 0
#define SET_OSCOPE_OUTPUT_HIGH      PORTCbits.RC2 = 1
#define SET_OSCOPE_OUTPUT_LOW       PORTCbits.RC2 = 0
#define ENABLE_BUZZER               TRISC = 0b11000110
#define DISABLE_BUZZER              TRISC = 0b11100110
// AN2,AN1,AN0 analog inputs, INTOSC/4, AN1, don't start conversion, ADC enabled
#define ENABLE_ADC_VBATT            ADCON0 = 0b11110101
// AN2,AN1,AN0 analog inputs, INTOSC/4, AN1, start conversion, ADC enabled
#define START_ADC_CONV_VBATT        ADCON0bits.nDONE = 1
// AN2,AN1,AN0 analog inputs, INTOSC/4, AN1, don't start conversion, ADC disabled
#define DISABLE_ADC_VBATT           ADCON0 = 0b11110100
// AN2,AN1,AN0 analog inputs, INTOSC/4, AN2, don't start conversion, ADC enabled
#define ENABLE_ADC_ILOAD            ADCON0 = 0b11111001
// AN2,AN1,AN0 analog inputs, INTOSC/4, AN2, start conversion, ADC enabled
#define START_ADC_CONV_ILOAD        ADCON0bits.nDONE = 1
// AN2,AN1,AN0 analog inputs, INTOSC/4, AN2, don't start conversion, ADC disabled
#define DISABLE_ADC_ILOAD           ADCON0 = 0b11111000
// Based on the assembly code examples in the datasheet, the 506
// doesn't need a delay for ADC acquisition.  Testing confirms this.
#define DELAY_FOR_ADC_ACQUISITION
// We don't have an LED byte display with the 506.
#define LED_BYTE_DISPLAY(byteVal)
#define SYS_FREQ                    4000000L
#define FCY                         SYS_FREQ/4
// ---------- unsupported device ----------
#else
#error Device not supported.
#endif

// state machine states
typedef enum stateEnum {
    S_INIT = 0,
    S_IDLE_CHECK_I_AND_V,
    S_OPERATING_CHECK_I_AND_V,
    S_IDLE_SLEEP,
    S_OPERATING_SLEEP,
    S_IDLE_SLEEP_WAKEUP,
    S_OPERATING_SLEEP_WAKEUP,
    S_HIGH_I_ALARM,
    S_SHUTDOWN_FLASH1,
    S_SHUTDOWN_FLASH1_WAKEUP,
```

```
    S_SHUTDOWN_FLASH2,
    S_SHUTDOWN_FLASH2_WAKEUP,
} state;



void initializeOscillator(void)
{
#if defined(_16F887)

    OSCCON = 0b01100000;            // set internal oscillator to 4 MHz
    while (!(OSCCON & 0b00000100)); // wait for INTOSC to be stable

#elif defined(_16F506)

    // When compiling with XC8 under MPLAB X, MOVWF 0x5 is automatically placed
    // at location 0x000.  That instruction writes the OSCCAL value set by
    // MOVLW 0xC (for example) at 0x3FF to the OSCCAL register.  Therefore, we
    // don't need to worry about doing anything explicit in the C code.

#else
#error Device not supported.
#endif

}



void firstTimeInit(void)
{

#if defined(_16F887)

    // Set input pins and all unused pins as inputs.
    TRISA = 0b11111111;         // RA1 and RA2 are ADC inputs
    TRISB = 0b11111111;         // RB0 is reset button input
    TRISC = 0b11000010;         // RC0 (power ctl), RC2 (buzzer), RC3 (red LED),
                                // RC4 (green LED), RC5 (o-scope) are outputs
    TRISD = 0b00000000;         // LEDs on 44-pin demo board are outputs
    TRISE = 0b00001111;

    // Set pins as analog or digital.  Unused pins are set as analog
    // inputs to turn off digital stuff, weak pullups, and other things.
    ANSEL = 0b11111111;         // RA1 (ANS1) is Vbatt input,
                                // RA2 (ANS2) is current sense input
    ANSELH = 0b00101111;        // RB0 (ANS12) is the reset button input

    // Configure the ADC.
    ADCON1 = 0b00000000;        // left-justified result, references are Vss and Vdd

    // PORTB pullups disabled, interrupt on falling edge of INT pin,
    // Timer0 clock source is Fosc/4, Timer0 increment on low-to-high
    // transition of T0CKI, prescaler assigned to WDT, prescaler rate 1:1
    OPTION_REG = 0b10001000;

    // Configure the watchdog timer.
    WDTCONbits.SWDTEN = 1;      // enable watchdog timer
    WDTCONbits.WDTPS = 0b0101;  // 1:1024 prescale gives approx. 33 ms timeout
                                // for a 30-Hz Vbatt and Iload sample rate.

#elif defined(_16F506)

    // Need to turn off the comparators so that we can use RC0 and RC1.
    CM1CON0bits.C1ON = 0;
    CM2CON0bits.C2ON = 0;

#else
#error Device not supported.
#endif
}
```

```
void wakeupInit(void)
{
#if defined(_16F887)
    // Only firstTimeInit is needed for the 887.
#elif defined(_16F506)

    TRISB = 0b11111111;         // AN1 and AN2 are inputs
    TRISC = 0b11100010;         // RC1 (button) is input; RC0 (power ctl), RC2 (o-scope),
                                // RC3 (green LED), RC4 (red LED) are outputs
    // Note:  RC5 stays high-z until the buzzer is needed.
    // This prevents a click each time wakeupInit is called.

    SET_OSCOPE_OUTPUT_HIGH;

    // Disable wake-up on pin change and disable weak pullups.  Don't assign
    // prescaler to WDT so that timeout period is 18 ms (typically, but ranges
    // from 9 ms to 30 ms according to the data sheet), which gives a 55 Hz
    // (111 Hz - 33 Hz) Vbatt and Iload sample rate.
    OPTION = nRBWU | nRBPU;

#else
#error Device not supported.
#endif
}



void soundBuzzerAlarm(uint8_t durationSeconds)
{
    uint8_t i, j, k, m;

    ENABLE_BUZZER;

    while (durationSeconds-- && !RESET_BUTTON_IS_PUSHED) {
        // Generate high/low tones near the response
        // peaks of the piezo buzzer for 1 second.
        for (m=0; m<2 && !RESET_BUTTON_IS_PUSHED; ++m) {
            // Sound a high tone for 250 ms.
            for (i=0; i<10; ++i) {
                if (RESET_BUTTON_IS_PUSHED) break;
                for (j=0; j<122; ++j) {
                    // approx. 10.26 instructions per for loop iteration
                    // delay count 10 (twice) -> approx. 4.873 kHz
                    SET_BUZZER_ON;
                    for (k=10; --k;) CLRWDT();
                    SET_BUZZER_OFF;
                    for (k=10; --k;) CLRWDT();
                }
            }
            // Sound a low tone for 250 ms.
            for (i=0; i<10; ++i) {
                if (RESET_BUTTON_IS_PUSHED) break;
                for (j=0; j<111; ++j) {
                    // delay count 11 (twice) -> approx. 4.430 kHz
                    SET_BUZZER_ON;
                    for (k=11; --k;) CLRWDT();
                    SET_BUZZER_OFF;
                    for (k=11; --k;) CLRWDT();
                }
            }
        }
    }

    DISABLE_BUZZER;
}
```

```
uint8_t main(void)
{
    state currentState;
    state nextState;
    uint8_t ledCount;
    uint8_t lowVCount;
    uint8_t highICount;
    uint8_t shortedICount;
    uint8_t operatingICount;
    uint8_t uvloICount;
    uint8_t adcVbattResult;
    uint8_t adcIloadResult;
    uint8_t shutdownFlash1Count;
    uint8_t shutdownFlash2Count;

    if (STATUSbits.nTO) {                   // power-up or other non-WDT event?
        initializeOscillator();
        firstTimeInit();
        wakeupInit();
        currentState = S_INIT;
    }
    else {
        wakeupInit();
        if (STATUSbits.nPD) {               // WDT wakeup but not from sleep?
            currentState = S_INIT;          // something screwed up so try to start over
        }
        CLRWDT();                           // so we can detect future WDT not from sleep
    }

    while(1) {

        nextState = currentState;
        switch(currentState) {

            case S_INIT:

                // Put the outputs in their initial state.
                SET_RED_LED_OFF;
                SET_GREEN_LED_OFF;
                SET_BUZZER_OFF;
                SET_OUTPUT_TO_LOAD_OFF;
                SET_OSCOPE_OUTPUT_HIGH;
                LED_BYTE_DISPLAY(0);

                lowVCount = LOW_VBATT_COUNT_THRESHOLD;
                highICount = HIGH_I_COUNT_THRESHOLD;
                shortedICount = SHORTED_I_COUNT_THRESHOLD;
                operatingICount = OPERATING_I_COUNT_THRESHOLD;
                uvloICount = UVLO_COUNT_THRESHOLD;
                adcVbattResult = 0;
                adcIloadResult = 0;
                ledCount = 1;

                // Wait for reset button to be released.
                while(RESET_BUTTON_IS_PUSHED) CLRWDT();

                nextState = S_IDLE_SLEEP;

                break;


            case S_IDLE_CHECK_I_AND_V:
            case S_OPERATING_CHECK_I_AND_V:

                // Get an Iload measurement.
                ENABLE_ADC_ILOAD;
                DELAY_FOR_ADC_ACQUISITION;
                START_ADC_CONV_ILOAD;
```

```
while (ADC_CONV_IS_NOT_DONE);
adcIloadResult = (ADC_RESULT > I_ADC_OFFSET)
                 ? ADC_RESULT - I_ADC_OFFSET : 0;
DISABLE_ADC_ILOAD;
LED_BYTE_DISPLAY(adcIloadResult);

// Check if short-circuit condition has occurred.
if (adcIloadResult > SHORTED_I_THRESHOLD) {
    if (!--shortedICount) {
        SET_OUTPUT_TO_LOAD_OFF;
        nextState = S_HIGH_I_ALARM;
        break;
    }
}
else {
    shortedICount = SHORTED_I_COUNT_THRESHOLD;

    // Check if high-current condition has occurred.
    if (adcIloadResult > HIGH_I_THRESHOLD) {
        if (!--highICount) {
            SET_OUTPUT_TO_LOAD_OFF;
            nextState = S_HIGH_I_ALARM;
            break;
        }
    }
    else {
        highICount = HIGH_I_COUNT_THRESHOLD;
    }
}

// Get a Vbatt measurement.
ENABLE_ADC_VBATT;
DELAY_FOR_ADC_ACQUISITION;
START_ADC_CONV_VBATT;
while (ADC_CONV_IS_NOT_DONE);
adcVbattResult = ADC_RESULT;
DISABLE_ADC_VBATT;
//LED_BYTE_DISPLAY(adcVbattResult);

// Check for Vbatt good or low condition.
if (adcVbattResult < LOW_VBATT_THRESHOLD) {
    if (!--lowVCount) {
        SET_OUTPUT_TO_LOAD_OFF;
        shutdownFlash1Count = shutdownFlash2Count =
            LED_LOW_V_FLASH_COUNT;
        ledCount = 1;
        nextState = S_SHUTDOWN_FLASH2;
        break;
    }
}
else {
    lowVCount = LOW_VBATT_COUNT_THRESHOLD;
    SET_OUTPUT_TO_LOAD_ON;
}

if (S_IDLE_CHECK_I_AND_V == currentState) {
    if (adcIloadResult > OPERATING_I_THRESHOLD) {
        if (!--operatingICount) {
            // Attached load appears to be in normal operation
            // mode so transition to the operating state.
            nextState = S_OPERATING_SLEEP;
        }
        else {
            nextState = S_IDLE_SLEEP;
        }
    }
    else {
        operatingICount = OPERATING_I_COUNT_THRESHOLD;
        nextState = S_IDLE_SLEEP;
    }
}
```

```
    else {              // in operating state
        if (adcIloadResult > OPERATING_I_THRESHOLD) {
            uvloICount = UVLO_COUNT_THRESHOLD;
            nextState = S_OPERATING_SLEEP;
        }
        else {          // current has dropped below the operating threshold
            if (adcVbattResult < WARN_VBATT_THRESHOLD) {
                // The load device might have shut down due to low
                // input voltage.  When uvloICount expires, we'll
                // assume that has happened and shut down our output
                // to prevent power-up when the battery voltage
                // recovers.
                if (!--uvloICount) {
                    SET_OUTPUT_TO_LOAD_OFF;
                    shutdownFlash1Count = LED_UVLO_FLASH1_COUNT;
                    shutdownFlash2Count = LED_UVLO_FLASH2_COUNT;
                    ledCount = 1;
                    nextState = S_SHUTDOWN_FLASH2;
                    break;
                }
                else {
                    // Stay in operating state unti uvloICount
                    // expires or something else happens.
                    nextState = S_OPERATING_SLEEP;
                }
            }
            else {
                uvloICount = UVLO_COUNT_THRESHOLD;
                // The load device was probably turned off by the
                // the user so go back into idle mode.
                nextState = S_IDLE_SLEEP;
            }
        }
    }

    break;


case S_IDLE_SLEEP:
case S_OPERATING_SLEEP:

    if (!--ledCount) {
        ledCount = (S_OPERATING_SLEEP == currentState)
                   ? LED_NORMAL_FLASH_COUNT : LED_STANDBY_FLASH_COUNT;
        SET_GREEN_LED_ON;
        // Flash yellow if Vbatt is below the warning threshold.
        if (adcVbattResult < WARN_VBATT_THRESHOLD) SET_RED_LED_ON;
    }

    // After waking from sleep, the 16F887 resumes execution with
    // the instruction following sleep.  However, the 16F506 does
    // not; it starts back at the beginning of the program.  So,
    // we'll set both the current and next state here to accommodate
    // both types of behavior.  This approach is used with all
    // all sleeps in this program.
    currentState = nextState = (S_IDLE_SLEEP == currentState)
                               ? S_IDLE_SLEEP_WAKEUP
                               : S_OPERATING_SLEEP_WAKEUP;

    SET_OSCOPE_OUTPUT_LOW;
    CLRWDT();
    SLEEP();                        // sleep until the watchdog wakes us up
    SET_OSCOPE_OUTPUT_HIGH;

    break;


case S_IDLE_SLEEP_WAKEUP:
case S_OPERATING_SLEEP_WAKEUP:

    SET_GREEN_LED_OFF;
```

```
    SET_RED_LED_OFF;

    nextState = (S_IDLE_SLEEP_WAKEUP == currentState)
                ? S_IDLE_CHECK_I_AND_V
                : S_OPERATING_CHECK_I_AND_V;

    break;


case S_HIGH_I_ALARM:

    SET_RED_LED_ON;

    soundBuzzerAlarm(HIGH_I_ALARM_SECONDS);

    if (RESET_BUTTON_IS_PUSHED) {
        nextState = S_INIT;
    }
    else {
        shutdownFlash1Count = shutdownFlash2Count = LED_HIGH_I_FLASH_COUNT;
        ledCount = 1;
        nextState = S_SHUTDOWN_FLASH2;
    }

    SET_RED_LED_OFF;

    break;


case S_SHUTDOWN_FLASH1:

    if (!--ledCount) {
        ledCount = shutdownFlash2Count;
        SET_RED_LED_ON;
        currentState = nextState = S_SHUTDOWN_FLASH2_WAKEUP;
    }
    else {
        currentState = nextState = S_SHUTDOWN_FLASH1_WAKEUP;
    }

    SET_OSCOPE_OUTPUT_LOW;
    CLRWDT();
    SLEEP();                          // sleep until the watchdog wakes us up
    SET_OSCOPE_OUTPUT_HIGH;

    break;


case S_SHUTDOWN_FLASH1_WAKEUP:

    SET_RED_LED_OFF;

    nextState = (RESET_BUTTON_IS_PUSHED) ? S_INIT : S_SHUTDOWN_FLASH1;

    break;


case S_SHUTDOWN_FLASH2:

    if (!--ledCount) {
        ledCount = shutdownFlash1Count;
        SET_RED_LED_ON;
        currentState = nextState = S_SHUTDOWN_FLASH1_WAKEUP;
    }
    else {
        currentState = nextState = S_SHUTDOWN_FLASH2_WAKEUP;
    }

    SET_OSCOPE_OUTPUT_LOW;
    CLRWDT();
    SLEEP();                          // sleep until the watchdog wakes us up
```

```
                SET_OSCOPE_OUTPUT_HIGH;

                break;


            case S_SHUTDOWN_FLASH2_WAKEUP:

                SET_RED_LED_OFF;

                nextState = (RESET_BUTTON_IS_PUSHED) ? S_INIT : S_SHUTDOWN_FLASH2;

                break;


            default:
                nextState = S_INIT;
        }
        currentState = nextState;
        CLRWDT();                               // kick the dog
    }

    return 0;
}
```